

THÈSE DE DOCTORAT DE L'ÉCOLE POLYTECHNIQUE

Spécialité : PHYSIQUE THÉORIQUE

présentée par

Alexey Lokhov

pour obtenir le grade de

Docteur de l'École polytechnique

Sujet :

*Étude non-perturbative des corrélateurs en
chromodynamique quantique*

Soutenue le 8 juin 2006 devant le jury composé de :

MM.	Ulrich Ellwanger,	rapporteur
	Georges Grunberg,	
	Olivier Pène,	
	Silvano Petrarca,	rapporteur
	Claude Roiesnel,	directeur de thèse
	André Rougé,	
&	Jean - Bernard Zuber,	président du jury

CPHT-T 058.0706

Table des matières

Notations and conventions	4
General introduction	7
1 Continuum and lattice QCD	9
1.1 General features of QCD	9
1.1.1 Definitions and symmetries	9
1.1.2 The Gribov ambiguity	11
1.1.3 Schwinger-Dyson equations	13
1.1.4 Slavnov-Taylor identities	16
1.1.5 Renormalisation group equations	17
1.2 Lattice QCD	18
1.2.1 Lattice QCD partition function	18
1.2.2 Fixing the Minimal Landau gauge on the lattice	20
2 Lattice Green functions	25
2.1 Green functions in Landau gauge	25
2.2 Numerical calculation of the ghost Green functions in Landau gauge	28
2.2.1 Lattice implementation of the Faddeev-Popov operator	28
2.2.2 Numerical inversion of the Faddeev-Popov operator	29
2.2.3 Calculation of the ghost-gluon vertex	31
2.3 Errors of the calculation	32
2.3.1 Estimating the statistical error	32
2.3.2 Handling the discretisation errors	32
2.4 Gribov ambiguity and lattice Green functions	34
2.4.1 The landscape of minima of the gauge-fixing functional	35
2.4.2 Lattice Green functions and the Gribov ambiguity	38
3 The ultraviolet behaviour of Green functions	43
3.1 Λ_{QCD} and perturbative expressions for Green functions	44
3.2 OPE for the Green functions and dominant power corrections	46
3.2.1 The dominant OPE power correction for the gluon propagator	48
3.2.2 The dominant OPE power correction for the ghost propagator	49
3.2.3 Constraints on the Wilson coefficients from the Slavnov-Taylor identity	50
3.3 Data analysis	51
3.3.1 Fitting the gluon and the ghost propagators	52
3.3.2 Fit of the ratio	54

3.3.3	Comparing the results	56
4	The infrared behaviour of Green functions	59
4.1	Review of today's analytical results	60
4.1.1	Zwanziger's prediction	60
4.1.2	Study of truncated SD and ERG equations	61
4.2	Constraints on the infrared exponents and the Slavnov-Taylor identity	61
4.3	Relation between the infrared exponents	63
4.4	Lattice study of the ghost Schwinger-Dyson equation	66
4.4.1	Complete ghost Schwinger-Dyson equation in the lattice formulation	66
4.4.2	Checking the validity of the tree-level approximation for the ghost-gluon vertex	68
4.5	Direct fits of infrared exponents	71
4.5.1	Testing the relation $2\alpha_F + \alpha_G = 0$	71
4.5.2	Lattice fits for α_F and α_G	73
5	Conclusions	77
	References	80

Notations and conventions

a	lattice spacing
$A_\mu = A_\mu^a t^a$	gauge field
$\langle A^2 \rangle$	A^2 -condensate
$\alpha_F (\alpha_G)$	infrared exponent of the ghost (gluon) propagator
$\beta = \frac{2N_c}{g_0^2}$	bare lattice coupling
$\beta(g), \beta_i$	the renormalisation group beta function and its first coefficients
$\gamma(g); \tilde{\gamma}, \tilde{\gamma}_i$	anomalous dimension ; anomalous dimension in a generic MOM scheme and its coefficients
e_μ	a vector in direction μ of norm a
$\tilde{F}^{(2)ab}(p) = \delta^{ab} \frac{\tilde{F}(p)}{p^2}$	ghost propagator
$\tilde{G}^{(2)ab}(p) = \delta^{ab} \frac{\tilde{G}(p)}{p^2} \left(\delta_{\mu\nu} - \frac{p_\mu p_\nu}{p^2} \right)$	gluon propagator
G, Λ	Gribov region and the fundamental modular region
Γ_μ^{abc}	three-gluon vertex
$\tilde{\Gamma}_\mu^{abc}(p, q; r) = -ig_0 f^{abc} p_\nu \tilde{\Gamma}_{\nu\mu}(p, q; r)$	ghost-gluon vertex, p is the momentum of the outgoing ghost, r is the gluon momentum.
g_0, g_R	bare coupling, renormalised coupling
$h = g^2 / (4\pi)^2$	
L	size of the lattice
$\mathcal{M}_{FP}, \mathcal{M}_{FP}^{\text{lat}}$	Faddeev - Popov operator and its discretized version
N_c	number of colours
$p_\mu = \frac{2\pi}{L} a^{-1} n_\mu$	relation between physical and lattice momenta
$t = \ln \frac{\mu^2}{\Lambda_{\text{QCD}}^2}$	
$U(x, x + e_\mu) \equiv U_\mu(x) = e^{ig_0 a A_\mu(x + \frac{a}{2} e_\mu)} \in SU(N_c)$	link variable

V	volume of the lattice
$Z_3 (\widetilde{Z}_3)$	gluon (ghost) field renormalisation factor
$\langle 0 \bullet 0 \rangle$	average with respect to the perturbative vacuum
$\langle \bullet \rangle$	average with respect to the non-perturbative vacuum

Shortenings

b.c	best (Gribov) copy choice
f.c.	first (Gribov) copy choice
ERGE	exact renormalisation group equations
IR	infrared
MOM	momentum subtraction renormalisation scheme (see Figures 2.1, 2.2)
RG	renormalisation group
SD	Schwinger-Dyson equations
ST	Slavnov-Taylor identities
UV	ultraviolet
v.e.v.	vacuum expectation values
ZP	zero-point (kinematic configuration, $\widetilde{\text{MOM}}$ renormalisation schemes)

General introduction

“Of course, you can put a theory on the lattice. But then - it is a mess !”

Giorgio Parisi, les Houches

This PhD dissertation is devoted to a non-perturbative study of QCD correlators in Landau gauge. The main tool that we use is lattice QCD. It allows a numerical evaluation of the functional integrals defining vacuum expectation averages of the theory i.e. Green functions. The advantage of this method is that it gives access to the non-perturbative domain and exactly preserves the gauge-invariance allowing to (numerically) study QCD from its first principles. However, the price to pay is the appearance of diverse discretisation artifacts like breakdown of the Lorentz invariance, a necessity to work with the Euclidean formulation of the theory and, in practice, at finite volume. We discuss in details the methods allowing to handle most of the artifacts. Lattice QCD has been successfully used in phenomenology (mass of the charm quark, B - and D -mesons physics, generalised parton distributions, QCD at finite temperature and its phase diagram, etc.). But it can also be used to study the fundamental parameters (like coupling constant) and properties of the theory itself. This is the main goal of the present dissertation. We concentrated our effort on the study of the two-point correlators of the pure Yang - Mills theory in Landau gauge, namely the gluon and the ghost propagators. We are particularly interested in determining the Λ_{QCD} parameter - the fundamental scale of the pure Yang-Mills theory. It is extracted by means of perturbative predictions available up to NNNLO. The related topic is the influence of non-perturbative effects that shows up as appearance of power-corrections to the low-momentum behaviour of the Green functions. We shall see that these corrections are quite important up to energies of the order of 10 GeV.

Another question that we address is the infrared behaviour of the Green functions (in Landau gauge), at momenta of order and below Λ_{QCD} . At low energy the power-law dependence of some Green functions changes considerably, and this is probably related to confinement. The knowledge of the infrared behaviour of the ghost and gluon propagators in Landau gauge is very important, because many confinement scenarii (for example the Gribov-Zwanziger scenario) give predictions for their momentum dependence at very low energies. *Ab initio* simulations on the lattice is a quasi-unique method for testing these predictions and the only way to challenge the underlying models for confinement.

We try to clarify the laws that govern the infrared gluodynamics in order to un-

derstand the radical nature of the changes of the infrared behaviour of some Green functions. Many questions arise : the Gribov ambiguity, the validity of different non-perturbative relations (like Schwinger - Dyson equations, Slavnov - Taylor identities and renormalisation group equations) at low momenta, self-consistency of the lattice approach in this domain. The lattice approach allows to check the predictions of analytical methods because it gives access to non-perturbative correlators. Our main goal thus is to use lattice Green functions as a non-perturbative input for different analytical relations. This allows to control the approximations that are done within the traditional truncation methods for the non-perturbative relations. Such a mixed numerical-analytical analysis of the complete Schwinger - Dyson equation for the ghost propagator provided us with an interesting alternative to the widely spread claim that the gluon dressing function behaves like the inverse squared ghost dressing function, a claim which is at odds with lattice data. According to our analysis the Landau gauge gluon propagator is finite and non-zero at vanishing momentum, and the power-law behaviour of the ghost propagator is the same as in the free case. However, as we shall see, some puzzles remain unsolved.

Chapitre 1

Continuum and lattice QCD

In this chapter we recall very briefly the most fundamental ideas of QCD (definitions, symmetries, covariant gauge fixing, Gribov ambiguity). As we are interested in a non-perturbative calculation of different correlators, we also introduce diverse non-perturbative relations between Green functions, namely Schwinger-Dyson equations, Slavnov-Taylor identities and exact renormalisation group equations. After this we shall discuss the lattice formulation of the pure Yang-Mills theories, in particular the procedure of the Landau gauge fixing on the lattice.

1.1 General features of QCD

1.1.1 Definitions and symmetries

Nowadays there is no doubt that Quantum Chromodynamics (QCD) is the theory of the strong interaction. The fundamental principle of this theory is local gauge invariance. This principle, together with general principles of locality, Lorentz invariance and renormalisability, imposes important constraints on the form of the Lagrangian. The simplest form in Euclidean four-dimensional space reads

$$\mathcal{L}_{\text{QCD}} = -\frac{1}{4}F_{\mu\nu}^a F^{a\mu\nu} + \sum_{\psi=u,d,s,c,b,t} \bar{\psi}(iD_\mu\gamma^\mu - m_\psi)\psi \quad (1.1)$$

with (g_0 is the bare coupling)

$$F_{\mu\nu}^a = \partial_\mu A_\nu^a - \partial_\nu A_\mu^a + g_0 f^{abc} A_\mu^b A_\nu^c, \quad a = 1..N_C^2 - 1 \quad (1.2)$$

$$D_\mu = \partial_\mu - ig_0 t^a A_\mu^a. \quad (1.3)$$

This Lagrangian is invariant under gauge transformations of the fields

$$\mathcal{A}_\mu(x) \mapsto \mathcal{A}_\mu^{(u)}(x) = u(x)\mathcal{A}_\mu(x)u^\dagger(x) + i[\partial_\mu u(x)]u^\dagger(x) \quad (1.4)$$

$$\psi(x) \mapsto \psi^{(u)}(x) = u(x)\psi(x), \quad (1.5)$$

where $u(x) \in SU(N_C)$ and $N_C = 3$ is the number of colours.

In order to quantise QCD using the functional integration formalism one has to

integrate over the quark and the gauge bosons fields. The Grassmannian integral on the quark fields is Gaussian, that is why we discuss only the integration on the gauge boson fields \mathcal{A} . The fields $\mathcal{A}^{(u)}$ and \mathcal{A} in the equation (1.4) are related by a gauge transformation, and thus they are physically equivalent. So, in order to quantise a gauge theory one performs an integration over gauge transformation equivalence classes - the **orbits** of the gauge fields. This is the Faddeev - Popov procedure. The integration on the orbits is done by choosing a representative element on every orbit, i.e. fixing the gauge with some relation

$$f[\mathcal{A}] = 0. \quad (1.6)$$

The condition f should define the orbit of the field \mathcal{A} in a unique way. Then the generating functional for Green functions reads

$$Z[j, \bar{\omega}, \omega] = \int [\mathcal{D}\mathcal{A}\mathcal{D}\psi\mathcal{D}\bar{\psi}] \Delta_f[\mathcal{A}] \delta(f[\mathcal{A}]) e^{-\int d^4x \mathcal{L}_{\text{QCD}} + \int d^4x (A_\mu^a j_\mu^a + \bar{\omega}\psi + \bar{\psi}\omega)}, \quad (1.7)$$

where all loop integrals are understood to be regularised. We denote the ultraviolet cut-off a^{-1} , $g_0 \equiv g(a^{-1})$. The **Faddeev-Popov determinant** $\Delta_f[\mathcal{A}]$ which appears in this formula is defined by means of invariant integration

$$\Delta_f[\mathcal{A}] \int \mathcal{D}u(x) \prod_x \delta\left(f\left[\mathcal{A}^{(u)}(x)\right]\right) = 1 \quad (1.8)$$

yielding in the general case ¹

$$\Delta_f^{-1}[\mathcal{A}] = \sum_{i: f[\mathcal{A}^{(g_i)}]=0} \det^{-1} \frac{\delta f[\mathcal{A}^{(g_i)}]}{\delta g}. \quad (1.9)$$

Choosing the **Landau gauge** condition

$$f[\mathcal{A}] : \quad \partial_\mu \mathcal{A}_\mu = 0 \quad (1.10)$$

and supposing for the moment that it fixes the gauge in a unique way, one obtains

$$\Delta_{\text{Landau}}[\mathcal{A}] = \det(\Delta + ig_0 \partial_\mu \mathcal{A}_\mu) = \int [\mathcal{D}c\mathcal{D}\bar{c}] e^{-\int d^4x d^4y \bar{c}^a(x) \mathcal{M}_{FP}^{ab}(x,y) c^b(y)}. \quad (1.11)$$

The spurious anticommuting fields c and \bar{c} belonging to the adjoint representation of the gauge group are called **Faddeev-Popov ghosts**, and

$$\mathcal{M}_{FP}^{ab}(x,y) = (\Delta + ig_0 \partial_\mu \mathcal{A}_\mu)^{ab} \delta^{(4)}(x-y) \quad (1.12)$$

is the **Faddeev-Popov operator**. The corresponding formula for the generating functional can be easily generalised by choosing for the gauge condition

$$f[\mathcal{A}] : \quad \partial_\mu \mathcal{A}_\mu = \mathfrak{a}(x), \quad \mathfrak{a}(x) \in \mathfrak{su}(N_C). \quad (1.13)$$

¹when the condition (1.6) does not fix the gauge in a unique way.

In this case Δ_f remains the same as (1.11), and one can integrate on $\alpha(x)$ with some Gaussian weight having a dispersion ξ . This gives for the generating functional

$$Z[j, \bar{\omega}, \omega, \bar{\sigma}, \sigma] = \int [\mathcal{D}A \mathcal{D}\psi \mathcal{D}\bar{\psi} \mathcal{D}c \mathcal{D}\bar{c}] e^{-\int d^4x \mathcal{L}_{eff}[A, \psi, \bar{\psi}, c, \bar{c}] + \Sigma}, \quad (1.14)$$

$$\mathcal{L}_{eff}[A, \psi, \bar{\psi}, c, \bar{c}] = \mathcal{L}_{QCD} - \frac{(\partial_\mu A_\mu)^2}{2\xi} - \bar{c}^a(x) (\delta^{ab} \Delta + ig_0 f^{abc} A_\mu^c \partial_\mu) c^b(x) \quad (1.15)$$

$$\Sigma = \int d^4x (A_\mu j_\mu + \bar{\omega} \psi + \bar{\psi} \omega + \bar{\sigma} c + \bar{c} \sigma). \quad (1.16)$$

The choice $\xi = 0$ corresponds to the Landau gauge. The gauge fixing term in (1.14) can be expressed as a result of Gaussian integration on an auxiliary field $B^a(x)$. This gives another form of the Lagrangian \mathcal{L}_{eff} :

$$\mathcal{L}_{BRST} = \mathcal{L}_{QCD} - \frac{\xi}{2} (B^a)^2 + B^a \partial_\mu A_\mu^a + \bar{c}^a (\delta^{ab} \Delta - ig_0 f^{abc} \partial_\mu A_\mu^c) c^b. \quad (1.17)$$

The QCD Lagrangian written in this form is invariant under **BRST transformations**. If λ is a constant infinitesimal Grassmann number these transformations take the form

$$\begin{aligned} \delta A_\mu^a &= \lambda D_\mu^{ac} c^c \\ \delta \psi &= ig_0 \lambda t^a \psi \\ \delta c^a &= -\frac{1}{2} g_0 \lambda f^{abc} c^b c^c \\ \delta \bar{c}^a &= \lambda B^a \\ \delta B^a &= 0. \end{aligned} \quad (1.18)$$

The virtue of the BRST transformation is its global nature. This simplifies a lot the derivation of the Slavnov-Taylor identities (direct consequence of the gauge invariance). We discuss this question below.

1.1.2 The Gribov ambiguity

A serious theoretical difficulty pointed out by Gribov [1] arises when performing the quantisation of a non-Abelian gauge theory (in covariant gauge) in the case of large field magnitudes. The reason for this is the non-uniqueness of the Landau gauge condition (1.10). Indeed, let us find all the intersections of the gauge orbit with the hypersurface defined by (1.10). Imposing the Landau gauge conditions for both fields \mathcal{A}_μ and $\mathcal{A}_\mu^{(\bar{u})}$ in (1.4) we obtain the following equation for $\bar{u}(x)$:

$$\begin{cases} \mathcal{A}_\mu(x) \mapsto \mathcal{A}_\mu^{(\bar{u})}(x) \\ \partial_\mu \mathcal{A}_\mu = 0 \\ \partial_\mu \mathcal{A}_\mu^{(\bar{u})} = 0 \end{cases} \quad \rightarrow \quad \partial_\mu \left(\bar{u}(x) D_\mu(x) \bar{u}^\dagger(x) \right) = 0. \quad (1.19)$$

Setting at the leading order

$$\bar{u} \simeq \mathbb{I} + i\bar{\alpha}(x), \quad \bar{u}^\dagger \simeq \mathbb{I} - i\bar{\alpha}(x) \quad \bar{\alpha}(x) \in \mathfrak{su}(N_c) \quad (1.20)$$

we obtain the following equation for $\bar{\alpha}$:

$$\partial_\mu (\partial_\mu \bar{\alpha} + i[\mathcal{A}_\mu, \bar{\alpha}]) = 0 \quad \longrightarrow \quad \partial_\mu D_\mu \bar{\alpha} = 0. \quad (1.21)$$

But $\partial_\mu D_\mu$ is nothing else but the Faddeev-Popov operator in the covariant gauge. Thus, any non-trivial zero mode of the Faddeev-Popov operator generates an intersection point of the gauge orbit with the hypersurface (1.10). If this point is not unique, we speak about the so called **Gribov copy**. All these secondary gauge configurations correspond to the same physical field \mathcal{A}_μ , and thus they must be removed from the functional integration measure in the partition function.

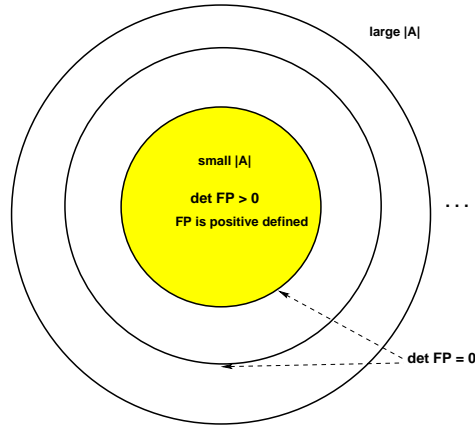


FIG. 1.1 – *The Gribov region.*

A solution to this problem is to supplement the initial gauge-fixing condition (1.10) with some additional requirement. Gribov's solution consists in restricting the integration measure (for the gluonic field) in (1.14) to the domain where (1.21) has a unique solution, see Fig. 1.1. This domain is called the **Gribov region**, and its boundary (where the Faddeev-Popov determinant vanishes) is called the **Gribov horizon**. It has been argued that some of topological solutions like instantons lie on this boundary [2].

Inside the Gribov region all the eigenvalues of the Faddeev-Popov operator are strictly positive². Hence one can realise the Gribov quantisation by using the Minimal Landau gauge. In this gauge one integrates on the fields satisfying the ordinary Landau gauge and belonging to the set of local minima of the integral

$$\int d^4x \left(A_\mu^a(x) \right)^2.$$

As we shall see, this ensures that all the proper values of the Faddeev-Popov operator are positive. The Minimal Landau gauge will be discussed in details in the subsection 1.2.2.

²we recall that in the Euclidean formulation the Faddeev - Popov operator is hermitian.

Nowadays it is known that the Gribov quantisation prescription is not exact - there are secondary solutions to (1.19) for some fields inside the Gribov region. The domain free of them is located inside the Gribov region, and it is called the **fundamental modular region** [3],[4]. This means that the correct quantisation prescription

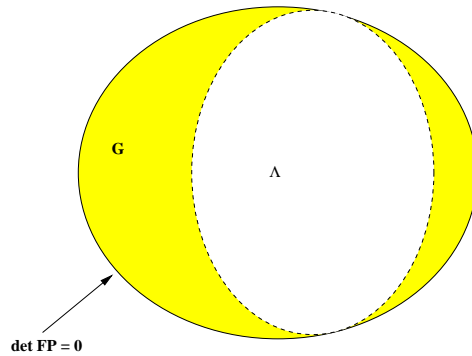


FIG. 1.2 – Gribov region and the fundamental modular region.

consists in restricting the integration in (1.14) to the fundamental modular region Λ instead of the Gribov region G , see figure 1.2. However it is argued in [5] that the expectation values calculated by integration over the Gribov region or the fundamental modular region are equal. So the Gribov quantisation prescription would become in fact exact. We discuss this question in details in the section 2.4.

1.1.3 Schwinger-Dyson equations

The Schwinger-Dyson(SD) equations is a specific class of non-perturbative equations relating Green functions and vertices. They can be easily derived in the functional integration formalism (for a review see [6]). Let $Z[J]$ denote a normalised ($Z[0] = 1$) generating functional (1.14) for the Green functions, and $W[J] = \log Z[J]$ - the one for connected Green functions. Then the effective action, which is a generating functional for one-particle irreducible (1-PI) vertex functions, is obtained by the Legendre transformation

$$\Gamma[\phi^c] = \frac{\delta W[J]}{\delta j_i} j_i - W[J], \quad \phi_i^c = \frac{\delta W[J]}{\delta j_i}, \quad (1.22)$$

where ϕ_i denotes the generic field (A_μ^a, c^a, \dots) and j_i is the corresponding source. Then, introducing the action $S = \int d^4x \mathcal{L}_{eff}$ and using the quantisation prescription based on the integration over the fundamental modular region, the Schwinger-Dyson equations are obtained from the observation that

$$\int_{\Lambda} [\prod_j \mathcal{D}\phi_j] \frac{\delta}{\delta \phi_i} (e^{-S+\phi \cdot j}) \equiv \int_{\Lambda} [\prod_j \mathcal{D}\phi_j] e^{-S+\phi \cdot j} \left(-\frac{\delta S}{\delta \phi_i} + j_i \right) = \int_{\partial \Lambda_i} [\prod_j \mathcal{D}\phi_j] e^{-S+\phi \cdot j} \quad (1.23)$$

Using the Zwanziger's argument [5] (quoted above) on the equivalence of integrations over Λ and G we restrict the integration domain to the Gribov region. It follows

from this that the integral on the boundary vanishes because the Faddeev-Popov determinant present in the integration measure is equal to zero on ∂G (by definition). This allows to write the whole set of the Schwinger-Dyson equations for the Green functions in a compact form

$$\left(-\frac{\delta S[\phi]}{\delta \phi_i} \left[\frac{\delta}{\delta j} \right] + j_i \right) Z[J] = 0. \quad (1.24)$$

We use a generic relation between two smooth functions $f(x)$ and $w(x)$

$$f \left(\frac{d}{dx} \right) e^{w(x)} = e^{w(x)} f \left(\frac{dw(x)}{dx} + \frac{d}{dx} \right) 1, \quad (1.25)$$

that can be applied to (1.24) and yield the equations for the functional W generating the connected Green functions

$$-\frac{\delta S[\phi]}{\delta \phi_i} \left[\frac{\delta}{\delta j} + \frac{\delta W}{\delta j} \right] 1 + j_i = 0. \quad (1.26)$$

Finally, performing a Legendre transformation (1.22), we have

$$-\frac{\delta S[\phi]}{\delta \phi_i} \left[\phi + \frac{\delta^2 W}{\delta j \delta j} \frac{\delta}{\delta \phi} \right] 1 + \frac{\delta \Gamma[\phi]}{\delta \phi_i} = 0, \quad (1.27)$$

corresponding to the full set of Schwinger-Dyson equations for proper functions.

As an example, we derive explicitly the SD equation for the full ghost propagator. Varying S with respect to the antighost field \bar{c}^a we obtain

$$\left\langle -\frac{\delta S}{\delta \bar{c}^a(x)} + \sigma^a(x) \right\rangle_{[j, \bar{\sigma}, \sigma]} = 0. \quad (1.28)$$

Varying the last relation with respect to $\sigma^b(y)$ one obtains

$$\left\langle \frac{\delta S}{\delta \bar{c}^a(x)} \bar{c}^b(y) \right\rangle = \delta^{ab} \delta^{(4)}(x-y) = \left\langle \left(\partial_\mu D_\mu^{ac} c^c(x) \right) \bar{c}^b(y) \right\rangle. \quad (1.29)$$

Denoting the full ghost propagator as

$$F^{(2)ab}(x, y) = \left\langle c^a(x) \bar{c}^b(y) \right\rangle, \quad (1.30)$$

we obtain ($\Delta(x, y) \equiv \delta^{(4)}(x-y)\delta$ is the Laplace operator)

$$\delta^{(4)}(x-y) = \Delta(x, z) F^{(2)}(z, y) + ig_0 \partial_\mu^{(x)} \left\langle \mathcal{A}_\mu(x) c(x) \bar{c}(y) \right\rangle. \quad (1.31)$$

Note that this equation can be obtained in a simpler way only using the definition of the Faddeev-Popov operator. Indeed, the ghost correlator in the background of a

given gauge field configuration $\mathcal{A}_\mu = A_\mu^a t^a$ is given by

$$F_{1\text{conf}}^{(2)}(\mathcal{A}, x, y) \equiv \mathcal{M}_{FP}^{1\text{conf}}(x, y)^{-1}. \quad (1.32)$$

The subscript means here that the equation is valid for a given gauge configuration. Thus one obviously has

$$\delta^4(x - y) \equiv \mathcal{M}_{FP}^{1\text{conf}}(x, z) F_{1\text{conf}}^{(2)}(\mathcal{A}, z, y), \quad (1.33)$$

where a summation on z is understood. Using the explicit formula (1.12) for \mathcal{M}_{FP} we get

$$\delta(x - y) = \Delta(x, z) F_{1\text{conf}}^{(2)}(z, y) + ig_0 \partial_\mu^{(x)} \left(\mathcal{A}_\mu(x) F_{1\text{conf}}^{(2)}(\mathcal{A}, x, y) \right), \quad (1.34)$$

valid for *any* gauge field configuration \mathcal{A} . Performing the functional integration on \mathcal{A} one gets the mean value on gauge configurations

$$\delta(x - y) = \Delta(x, z) \left\langle F_{1\text{conf}}^{(2)}(z, y) \right\rangle + ig_0 \partial_\mu^{(x)} \left\langle \mathcal{A}_\mu(x) F_{1\text{conf}}^{(2)}(\mathcal{A}, x, y) \right\rangle. \quad (1.35)$$

Using $\left\langle F_{1\text{conf}}^{(2)}(z, y) \right\rangle \equiv F^{(2)}(z, y)$ we find the equation (1.31). The translational invariance of the Green functions allows to replace $\partial_\mu^{(x)}$ by $-\partial_\mu^{(y)}$. Performing the Fourier transform on $(x - y)$, we have finally

$$1 = -p^2 F^{(2)}(p^2) - ig_0 p_\mu \left\langle \mathcal{A}_\mu(0) F_{1\text{conf}}^{(2)}(\mathcal{A}, p) \right\rangle. \quad (1.36)$$

This derivation elucidates the trivial dependence of this equation on the functional integral weight with which we calculate the average $\langle \bullet \rangle$ on the gauge fields \mathcal{A} . The form (1.34) allows an explicit discussion of the Gribov copies dependence of the solutions. We address this question below.

Performing the Legendre transformation for the three-point function in (1.31) and introducing the ghost-gluon vertex

$$\tilde{\Gamma}_\mu^{abc}(-q, k; q - k) = g_0 f^{abc} (iq_{\nu'}) \tilde{\Gamma}_{\nu'\nu}(-q, k; q - k) \quad (1.37)$$

and the full gluon propagator $G_{\mu\nu}^{(2)ab}(p)$, we write the Schwinger-Dyson equation for the ghost propagator in Fourier space

$$\left(F^{(2)} \right)_{ab}^{-1}(k) = -\delta_{ab} k^2 - g_0^2 f^{acd} f^{ebf} \int \frac{d^4 q}{(2\pi)^4} F_{ce}^{(2)}(q) (iq_{\nu'}) \tilde{\Gamma}_{\nu'\nu}(-q, k; q - k) (ik_\mu) \left(G^{(2)} \right)_{\mu\nu}^{fd}(q - k), \quad (1.38)$$

given in a diagrammatic form at Figure 1.3. This equation is much simpler than the one for the gluon propagator, because the last involves complete three- and four-gluon vertices (cf. Figure 1.4). Another virtue of (1.38) is that its *form* is explicitly independent of the choice of the integration domain in the functional integral (1.23), because the equality (1.34) holds valid for *individual* gauge configurations.

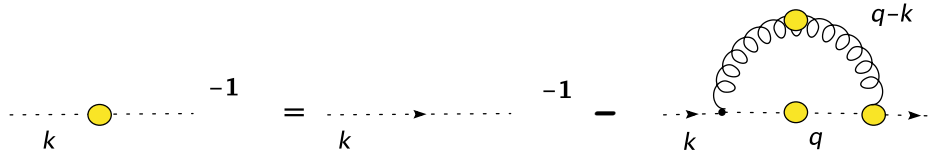


FIG. 1.3 – Schwinger-Dyson equation for the ghost propagator in a pure gauge theory, diagrammatically.

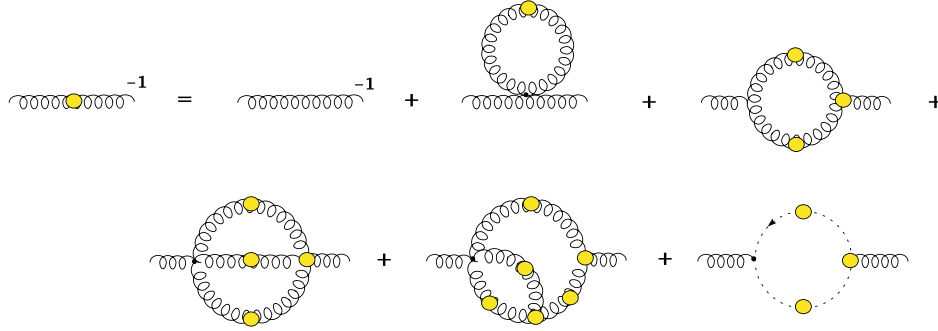


FIG. 1.4 – Schwinger-Dyson equation for the gluon propagator in a pure gauge theory, diagrammatically.

1.1.4 Slavnov-Taylor identities

The Slavnov-Taylor identities ([7],[8]) are Ward identities in the case of a non-Abelian gauge theory. These identities follow directly from the gauge symmetry. We write the generating functional in the case of a general gauge fixing condition (1.6)

$$Z[j] = \int [\mathcal{D}\mathcal{A}] \det \mathcal{M}_{FP} e^{-\int d^4x \left(\mathcal{L}_{\text{QCD}} - \frac{(f^a[A])^2}{2\xi} + j_\mu^a A_\mu^a \right)}, \quad (1.39)$$

and use the fact that the functional integration measure is invariant under the specific gauge transformations

$$\begin{aligned} \delta A_\mu^a &= D_\mu^{ab} \epsilon^b \\ \delta f^a[A] &= \mathcal{M}_{FP}^{ab} \epsilon^b. \end{aligned} \quad (1.40)$$

The second equation is just a general definition of the Faddeev-Popov operator. The integration measure times the Faddeev-Popov determinant is invariant with respect to (1.40), and hence

$$Z[j] = \int [\mathcal{D}\mathcal{A}] \det \mathcal{M}_{FP} e^{-\int d^4x \left(\mathcal{L}_{\text{QCD}} - \frac{(f^a[A])^2}{2\xi} + j_\mu^a A_\mu^a - \frac{1}{\xi} f^a \mathcal{M}_{FP}^{ab} \epsilon^b + j_\mu^a D_\mu^{ab} \epsilon^b \right)}. \quad (1.41)$$

Choosing a particular form for ϵ

$$\epsilon^b = \left(\mathcal{M}_{FP}^{-1} \right)^{bc} \omega^c \quad (1.42)$$

we obtain a functional relation for the generating functional Z

$$\left(\frac{1}{\xi} f^a \left[\frac{\delta}{\delta j} \right] - \int d^4 y j_\mu^b(y) D_\mu^{bc} \left[\frac{\delta}{\delta j} \right] \left(\mathcal{M}_{FP}^{-1} \right)^{ca} \left[x, y; \frac{\delta}{\delta j} \right] \right) Z[j] = 0. \quad (1.43)$$

In principle, one can use the relation (1.25) in order to obtain an equation for the functional $W[j]$. However, this derivation would lead to a very cumbersome expression. In fact it is much easier to use the Slavnov-Taylor relations obtained within the BRST formalism. The main idea of the derivation remains the same because the BRST transformation is just a specific form of the gauge transformation (1.40), $\mathcal{M}_{FP}^{-1}(x, y)$ being the propagator of the Faddeev-Popov ghost in the background field \mathcal{A} . One has using (1.17,1.18) and the BRST invariance of the generating functional $Z[j]$

$$\int d^4 x \int [\mathcal{D}\mathcal{A}\mathcal{D}c\mathcal{D}\bar{c}] e^{-\int d^4 x \mathcal{L}_{eff}} \left(j_\mu^a \cdot D_\mu^{ab} c^b - \frac{1}{\xi} \partial_\mu A_\mu^a \sigma^a - \bar{\sigma}^a \frac{g_0}{2} f^{abc} c^b c^c \right) = 0. \quad (1.44)$$

This equation (1.44) allows to obtain the Slavnov-Taylor identities for the Green functions by differentiating with respect to the sources $j, \sigma, \bar{\sigma}$. Writing (1.44) in terms of generating functionals W and Γ , one obtains (see [9], [7], [8] for details) the general form of Slavnov-Taylor identities between propagators and proper vertices. The relation that we shall use in the following relates the three-gluon vertex $\Gamma_{\lambda\mu\nu}(p, q, r)$ to the ghost-antighost-gluon vertex, and involves the complete ghost and gluon propagators. It reads ([7],[8])

$$\begin{aligned} p^\lambda \Gamma_{\lambda\mu\nu}(p, q, r) &= \frac{p^2 F^{(2)}(p^2)}{r^2 G^{(2)}(r^2)} \left(\delta_{\lambda\nu} r^2 - r_\lambda r_\nu \right) \tilde{\Gamma}_{\lambda\mu}(r, p; q) - \\ &- \frac{p^2 F^{(2)}(p^2)}{q^2 G^{(2)}(q^2)} \left(\delta_{\lambda\mu} q^2 - q_\lambda q_\mu \right) \tilde{\Gamma}_{\lambda\nu}(q, p; r). \end{aligned} \quad (1.45)$$

Some remarks regarding the non-perturbative validity of the Slavnov-Taylor identities are in order. The above derivation is invalid when \mathcal{M}_{FP}^{-1} is singular (see (1.40), (1.42) and (1.43)), i.e. for gauge fields lying on the Gribov horizon. However, this transformation is well defined inside the Gribov horizon. Note also that the general form of the Slavnov-Taylor identities does not depend on the choice of the integration domain inside the Gribov horizon (Λ or G). Another argument in favour of non-perturbative validity of the Slavnov-Taylor identities may be given within the stochastic quantisation formalism [5].

1.1.5 Renormalisation group equations

For the sake of completeness we present here another set of non-perturbative relations between the correlators, namely the exact renormalisation group equations (or ERGE, see [10] for a review). Those are flow equations describing the variation of the effective action with the infrared (or ultraviolet) cut-off. The infrared cut-off

is introduced by adding a special term to the action

$$\Delta S_k = \frac{1}{2} \sum_i \int \frac{d^4 p}{(2\pi)^4} \phi_i(p) R_i(k, p^2) \phi_i(-p), \quad (1.46)$$

where the momentum cut-off function R_i for the field ϕ_i satisfies

$$\begin{cases} R_i(k, p^2) \rightarrow 0 & p \gtrsim k \\ R_i(k, p^2) \rightarrow k^2 & p \lesssim k. \end{cases} \quad (1.47)$$

The role of ΔS_k is to suppress quantum fluctuations with momenta below k . Then one may show that the partition function satisfies the equation

$$\partial_k Z_k(j) = -\frac{1}{2} \int \frac{d^4 p}{(2\pi)^4} \partial_k R(k, p^2) \frac{\delta^2 Z_k(j)}{\delta j(p) \delta j(-p)}. \quad (1.48)$$

The problem that arises within the formalism of the RG equations is the loss of the gauge invariance caused by the cut-off term. However, this problem can be solved by considering a modified set of Slavnov-Taylor identities [11]. One may express the equation (1.48) in terms of the generating functional for proper vertices, that lead to an infinite system of partial differential equations relating different Green functions and the cut-off function (1.47). We shall review some of the results for solutions of the truncated system of such equations in the section 4.1.

1.2 Lattice QCD

1.2.1 Lattice QCD partition function

A fully non-perturbative study from the first principles of QCD phenomenon requires a direct calculation of the functional integral of the type (1.14). These integrals can be approximately evaluated by means of lattice simulations. Another interest in the lattice regularisation is that it preserves the gauge invariance. The inverse lattice spacing a^{-1} plays the role of the ultraviolet cut-off, and we recover the continuum limit theory by sending a to zero.

In what follows we discuss only pure Yang-Mills theories. In practice, when doing a lattice simulation, one considers a theory in a finite volume $V = L^4$ with (most often) periodical boundary conditions; and generates some (quite large) number M of gauge field configurations $\{C_i\}$ distributed according to the probability measure

$$d\mu[\mathcal{A}] = e^{-\int d^4 x \mathcal{L}_{\text{Yang-Mills}}(A)} [\mathcal{D}\mathcal{A}]. \quad (1.49)$$

Then one can calculate a Monte-Carlo approximation for any operator \mathcal{O}

$$O = \langle \mathcal{O}(\mathcal{A}_V) \rangle = \int d\mu \mathcal{O}(\mathcal{A}_V) \approx \frac{1}{M} \sum_{i=1}^M \mathcal{O}(C_i). \quad (1.50)$$

Let us now discuss the measure $d\mu[A]$ in the discrete case. Gauge fields are defi-

ned on the links of the Euclidean lattice (cf. Figure 1.5), and the fundamental lattice variable for the gauge field is the **link variable**

$$U(x, x + e_\mu) \equiv U_\mu(x) = e^{ig_0 a \mathcal{A}_\mu(x + \frac{a}{2} e_\mu)} \in SU(N_c), \quad (1.51)$$

where e_μ is a vector in direction μ , $\|e_\mu\| = a$. For small values of the lattice spacing a

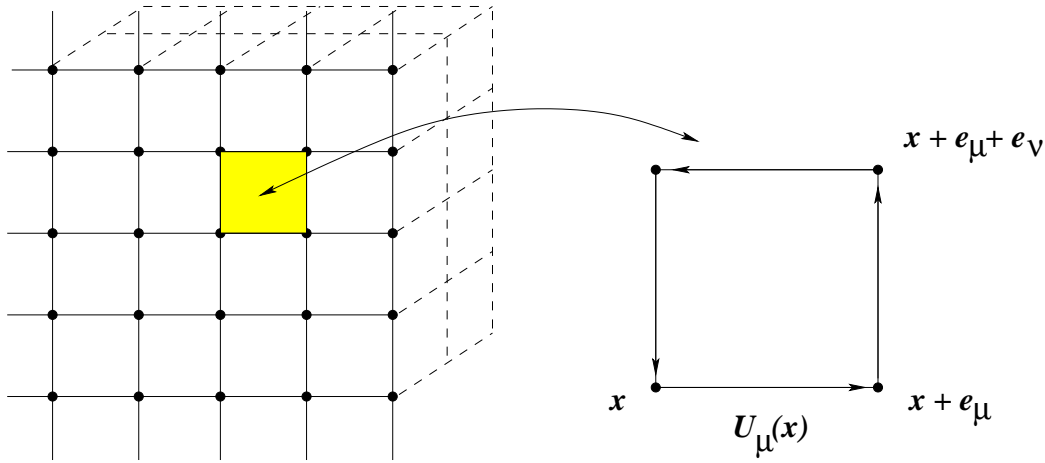


FIG. 1.5 – Gauge fields \mathcal{A}_μ are defined on the links of the lattice ($\|e_\mu\| = a$), and the fermion fields $\psi(x)$ are defined on its sites.

we can extract the field \mathcal{A}_μ using an approximate formula

$$\frac{U_\mu(x) - U_\mu^\dagger(x)}{2ia g_0} = \mathcal{A}_\nu \left(x + \frac{e_\mu}{2} \right) + O(a). \quad (1.52)$$

We use this definition of the gluon field in what follows. Then one can define an elementary gauge invariant variable - a **plaquette**

$$U(p) = U_\mu(x) U_\nu(x + a e_\mu) U_\mu^\dagger(x + a e_\nu) U_\nu^\dagger(x). \quad (1.53)$$

Using this variables we can write the simplest action that converges to the pure Yang-Mills' action in the continuum limit ([12], see [13],[14] for a review) :

$$S_g[U_\mu(x)] = \beta \sum_x \sum_{\mu, \nu} \left(\mathbb{I} - \frac{1}{N_c} \Re \epsilon \text{Tr} U(p) \right), \quad (1.54)$$

where the lattice bare coupling is defined by

$$\beta = \frac{2N_c}{g_0^2}. \quad (1.55)$$

Thus, the partition function in the lattice formulation reads

$$Z_{\text{lat}}[U] = \int [DU_\mu(x)] e^{-S_g[U]}. \quad (1.56)$$

Of course there exist an infinite number of lattice actions giving (1.14) in the continuum limit $a \rightarrow 0$. They should all give compatible results when the lattice spacing is small enough and the renormalisation group scaling laws are verified. In practice, one generates the gauge configurations $\{C_i\}, i = 1 \dots M$ according to the probability measure $[DU_\mu(x)]e^{-S_g[U]}$. In all our simulations we have used the Wilson action (1.54). Usually, the Metropolis or Heatbath algorithms are used for the Monte-Carlo generation. For a detailed review on this topic see [13],[14].

The important question that has not been discussed up to now is the removal of the ultraviolet divergences of the theory in the continuum limit. The regularised lattice partition function contains one parameter - the bare coupling constant g_0 (or, equivalently, the lattice spacing a). When calculating some physical quantity on the lattice, say, the string tension σ , we obtain it as a function of a . If the ultraviolet cut-off a^{-1} is large enough, the calculated quantity obeys the scaling law, and one can compare the result for $\sigma(a)$ of the lattice simulation to the known experimental data σ_{exp} , and thus determine the corresponding physical value of the lattice spacing a by solving the equation $\sigma(a) = \sigma_{\text{exp}}$. In the unquenched case one has to calculate several physical quantities because more non-fixed parameters are involved (the masses of quarks). When all free parameters of the lattice theory are fixed in the scaling region with some experimental inputs, all further calculations³ are automatically renormalised, and do not contain any divergences. Moreover, all the calculations are now the *predictions* of the theory. Thus, the only limitations of the numerical method *a priori* are discretisation errors and the errors on the experimental inputs. We discuss in details the systematic error of lattice simulations in the section 2.3. In practice one is also often limited by the computer power.

Let us say some words about the strong coupling limit of (1.56), corresponding to the perturbative expansion in the β parameter. The ordinary perturbation expansions in gauge theories (in powers of g_0) are at most asymptotic, but power series of (1.56) in β is proven to have a *finite* radius of convergence [15]. Many interesting results, like the existence of the mass gap and the area law for the Wilson loop, have been analytically proven within this approach. However, it has been argued that the region of the strong coupling is analytically disconnected from the weak-coupling domain, corresponding to the continuum limit of the theory [16]. Lattice gauge theories are believed to possess an essential singularity at some finite value β_{rough} , corresponding to an infinite order phase transition. This phenomenon is well known in statistical physics (roughening transition). Thus it is impossible to know whether the strong-coupling predictions are applicable in the physically interesting weak-coupling regime. In practice, one has to perform numerical simulations with $\beta > \beta_{\text{rough}}$.

1.2.2 Fixing the Minimal Landau gauge on the lattice

The continuum gauge fixing condition (1.6) is modified by the discretization, so one works with its lattice version $f_L(U_\mu) = 0$. A gauge configuration U_{C_0} generated during the simulation process does not satisfy the Landau gauge condition. One has to perform a gauge transformation $u(x)$ on it in order to move the field configura-

³of experimentally observable quantities

tion along its gauge orbit up to an intersection with the surface $f_L(U_\mu) = 0$. But there is no need to have an explicit form of $u(x)$. Instead we perform an iterative minimisation process that converges to the gauge fixed configuration $U_c^{(u)}$. Let us first illustrate it on the example of the Landau gauge in the continuum limit. For every gauge field \mathcal{A} we calculate the functional

$$F_{\mathcal{A}}[u(x)] = -\text{Tr} \int d^4x \left(\mathcal{A}_\mu^{(u)}(x) \mathcal{A}_\mu^{(u)}(x) \right), \quad u(x) \in SU(N_c). \quad (1.57)$$

Expanding it up to the second order around some element $u_0(x)$ we have ($u = e^X u_0$, $X \in \mathfrak{su}(N_c)$)

$$F_{\mathcal{A}}[u] = F_{\mathcal{A}}[u_0] - 2 \int d^4x \text{Tr} \left(X \partial_\mu \mathcal{A}_\mu^{(u_0)} \right) + \int d^4x \text{Tr} \left(X^\dagger \mathcal{M}_{\text{FP}} \left[\mathcal{A}^{(u_0)} \right] X \right) + \dots, \quad (1.58)$$

where the matrix \mathcal{M}_{FP} in the quadratic term defines the Faddeev-Popov operator. Obviously, if u_0 is a local minimum of (1.57) then we have a double condition

$$\begin{cases} \partial_\mu \mathcal{A}_\mu^{(u_0)} = 0 \\ \mathcal{M}_{\text{FP}} \left[\mathcal{A}^{(u_0)} \right] \text{ is positively defined.} \end{cases} \quad (1.59)$$

Hence, the minimisation of the functional (1.57) allows not only to fix the Landau gauge, but also to obtain a gauge configuration inside the Gribov horizon (because all the eigenvalues of \mathcal{M}_{FP} are positive). On the lattice, the discretized functional (1.57) reads

$$F_U[u(x)] = -\frac{1}{V} \Re \text{Tr} \sum_{x,\mu} u(x) U_\mu(x) u^\dagger(x + e_\mu). \quad (1.60)$$

Then at a local minimum u_0 we have a discretized Landau gauge fixing condition

$$\sum_\mu \left[\mathcal{A}_\mu^{(u_0)} \left(x + \frac{e_\mu}{2} \right) - \mathcal{A}_\mu^{(u_0)} \left(x - \frac{e_\mu}{2} \right) \right] = 0 \quad (1.61)$$

that we write in a compact form $\nabla_\mu \mathcal{A}_\mu^{(u_0)} = 0$. Indeed, if $u(x) = u_0(x) e^{s \omega(x)}$ where $\omega(x)$ is the element of the algebra $\mathfrak{su}(N_c)$ then

$$\frac{\delta}{\delta u} \Big|_{u_0} F(u) \equiv \frac{d}{ds} \Big|_{s=0} F(u(s, x)) = 0, \quad (1.62)$$

and hence

$$-\frac{1}{V} \Re \text{Tr} \sum_{x,\mu} \left([\omega(x + e_\mu) - \omega(x)] U_\mu(x) \right) = 0 \quad \forall \omega(x) \in \mathfrak{su}(N_c). \quad (1.63)$$

Thus

$$\sum_\mu \left[U_\mu(x) - U_\mu^\dagger(x) - U_\mu(x - e_\mu) + U_\mu^\dagger(x - e_\mu) \right] = 0 \quad (1.64)$$

and at leading order in the lattice spacing a (1.52) we obtain (1.61). The second derivative (the equivalent of the second-order term in (1.58)) can be written as

$$\frac{d^2}{ds^2}F(u(s, x)) = -\frac{1}{V} \left(\omega, \nabla_\mu \mathcal{A}'_\mu \right) \quad (1.65)$$

where

$$\mathcal{A}'_\mu = \frac{1}{2} \left(-\omega(x) U_\mu^{(u)}(x) + U_\mu^{(u)}(x) \omega(x + e_\mu) + \omega(x + e_\mu) U_\mu^{(u)\dagger}(x) - U_\mu^{(u)\dagger}(x) \omega(x) \right). \quad (1.66)$$

This defines a quadratic form

$$\begin{aligned} \left(\omega, \mathcal{M}_{FP}^{\text{lat}}[U] \omega \right) &= -\frac{1}{V} \Re \text{Tr} \sum_{x, \mu} \left([\omega^2(x + e_\mu) - 2\omega(x + e_\mu)\omega(x) + \omega^2(x)] U_\mu^{(u_0)}(x) \right) = \\ &= -\frac{1}{2V} \text{Tr} \sum_{x, \mu} \left((\omega(x + e_\mu) - \omega(x))^2 \left(U_\mu^{(u_0)}(x) + U_\mu^{(u_0)\dagger}(x) \right) - \right. \\ &\quad \left. - [\omega(x + e_\mu), \omega(x)] \left(U_\mu^{(u_0)}(x) - U_\mu^{(u_0)\dagger}(x) \right) \right). \end{aligned} \quad (1.67)$$

The operator $\mathcal{M}_{FP}^{\text{lat}}[U]$ is the lattice version of the Faddeev-Popov operator. It reads

$$\begin{aligned} \left(\mathcal{M}_{FP}^{\text{lat}}[U] \omega \right)^a(x) &= \frac{1}{V} \sum_\mu \left\{ G_\mu^{ab}(x) \left(\omega^b(x + e_\mu) - \omega^b(x) \right) - (x \leftrightarrow x - e_\mu) \right. \\ &\quad \left. + \frac{1}{2} f^{abc} \left[\omega^b(x + e_\mu) A_\mu^c \left(x + \frac{e_\mu}{2} \right) - \omega^b(x - e_\mu) A_\mu^c \left(x - \frac{e_\mu}{2} \right) \right] \right\}, \end{aligned} \quad (1.68)$$

where

$$G_\mu^{ab}(x) = -\frac{1}{2} \text{Tr} \left(\left\{ t^a, t^b \right\} \left(U_\mu(x) + U_\mu^\dagger(x) \right) \right) \quad (1.69)$$

$$A_\mu^c \left(x + \frac{e_\mu}{2} \right) = \text{Tr} \left(t^c \left(U_\mu(x) - U_\mu^\dagger(x) \right) \right). \quad (1.70)$$

For the Minimal Landau gauge fixing in our numerical simulation we have used the Overrelaxation algorithm [17] with $\omega = 1.72$. We stop the iteration process of the minimising algorithm when the following triple condition is fullfield :

$$\begin{aligned} \frac{1}{V(N_c^2 - 1)} \sum_{x, \mu} \text{Tr} \left[\left(\nabla_\mu \mathcal{A}_\mu^{(u^{(n)})} \right) \left(\nabla_\mu \mathcal{A}_\mu^{(u^{(n)})} \right)^\dagger \right] &\leq \Theta_{\max_x |\partial_\mu A_\mu^a|} = 10^{-18} \\ \frac{1}{V(N_c^2 - 1)} \left| \sum_x \text{Tr} \left[u^{(n)}(x) - \mathbb{I} \right] \right| &\leq \Theta_{\delta u} = 10^{-9} \\ \forall a, t_1, t_2 \quad \left| \frac{A_0^a(t_1) - A_0^a(t_2)}{A_0^a(t_1) + A_0^a(t_2)} \right| &\leq \Theta_{\delta A_0} = 10^{-7}. \end{aligned} \quad (1.71)$$

where $u^{(n)}(x)$ is the matrix of the gauge transformation $u(x)$ at the iteration step n ,

and the charge

$$A_0^a(t) = \int d^3\vec{x} A_0^a(\vec{x}, t) \quad (1.72)$$

must be independent of t in Landau gauge when periodical boundary conditions for the gauge field are used. The choice of numerical values for the stopping parameters is discussed in [18].

Chapitre 2

Lattice Green functions

In the functional integral formalism Green functions are defined as mean values of products of fields according to the functional measure, giving as a result the vacuum expectation values of these products. Often one is interested in the Green functions in Fourier space. Here we define the Fourier transformation on the lattice.

If a function $f(x)$ is defined on the *sites* of the four-dimensional lattice with periodical boundary conditions then

$$\begin{aligned}\tilde{f}(p) &= a^4 \sum_x f(x) e^{-ip \cdot x} & p_\mu &= \frac{2\pi}{aL} n_\mu, \quad n_\mu = 0, 1, \dots, L-1 \\ f(x) &= \frac{1}{V} \sum_p e^{ip \cdot x} \tilde{f}(p).\end{aligned}\tag{2.1}$$

In the case of the variables defined on the *links* of the lattice one should change the above formulae by $x_\mu \rightarrow x_\mu + \frac{e_\mu}{2}$. In the infinite-volume limit $V \rightarrow \infty$ we have

$$\frac{1}{V} \sum_p \longrightarrow \frac{1}{(2\pi)^4} \int_{[-\frac{\pi}{a}, \frac{\pi}{a}]^4} d^4 p.\tag{2.2}$$

We recall in the first part of this chapter the main definitions regarding the lattice two- and three-point Green functions in Landau gauge and the Momentum subtraction renormalisation scheme. Next we describe the details of the numerical calculation of the ghost propagator and discuss different sources of errors of the lattice approach. The last part is devoted to the Gribov ambiguity on the lattice and the influence of Gribov copies on the Green functions.

2.1 Green functions in Landau gauge

The gluon propagator in Landau gauge may be parametrised at all values of momenta as

$$G_{\mu\nu}^{(2)ab}(p, -p) \equiv \langle \tilde{A}_\mu^a(-p) \tilde{A}_\nu^b(p) \rangle = \delta^{ab} \left(\delta_{\mu\nu} - \frac{p_\mu p_\nu}{p^2} \right) G^{(2)}(p^2).\tag{2.3}$$

This implies that the scalar factor $G^{(2)}(p^2)$ may be extracted according to

$$G^{(2)}(p^2) = \frac{1}{3(N_C^2 - 1)} \sum_{\mu,a} G_{\mu\mu}^{(2)aa}(p, -p), \quad p^2 \neq 0 \quad (2.4)$$

completed with

$$G^{(2)}(0) = \frac{1}{4(N_C^2 - 1)} \sum_{\mu,a} G_{\mu\mu}^{(2)aa}(0, 0), \quad p^2 = 0. \quad (2.5)$$

The difference in normalisations at zero (2.5) and finite momenta (2.4) is due to an additional degree of freedom related to global gauge transformations on a periodic finite lattice ($p^2 = 0 \leftrightarrow x_\mu \sim x_\mu + L$).

The ghost propagator is parametrised in the common way :

$$F^{(2)ab}(p, -p) \equiv \langle \tilde{c}^a(-p) \tilde{c}^b(p) \rangle = \delta^{ab} F^{(2)}(p^2). \quad (2.6)$$

It is not defined at $p^2 = 0$ because in this case the Faddeev-Popov operator is strictly equal to zero and thus it is not invertible.

The renormalisation scheme that is widely used in order to renormalise the lattice Green functions is the so-called Momentum subtraction scheme (MOM). The virtue of this scheme is its non-perturbative definition. The renormalisation constants are defined by setting the corresponding Green functions to their tree values at some renormalisation point μ^2 . In the case of the two-point Green function the renormalisation constant $Z_3(\mu^2)$ of the gauge field or the one of the ghost field (denoted $\tilde{Z}_3(\mu^2)$) is unambiguously defined as :

$$Z_3(\mu^2) = \mu^2 G^{(2)}(\mu^2) \quad (2.7)$$

$$\tilde{Z}_3(\mu^2) = \mu^2 F^{(2)}(\mu^2). \quad (2.8)$$

The coupling constant has also to be renormalised to complete the renormalisation of a pure Yang-Mills theory. It can be defined non-perturbatively by an amputation of a three-point Green-functions from its external propagators. But this requires to fix the kinematic configuration of the three-point Green-function at the normalisation point. On the lattice one usually uses either a fully symmetric kinematic configuration (denoted MOM) or a zero point (ZP) kinematic configuration with one vanishing external momentum (denoted generically $\widetilde{\text{MOM}}$), see Figure 2.1.

Three-gluon vertex : symmetric case

There are only two independent tensors in Landau gauge in the case of the symmetric three-gluon Green function [19] :

$$\mathcal{T}_{\mu_1, \mu_2, \mu_3}^{[1]}(p_1, p_2, p_3) = \delta_{\mu_1 \mu_2} (p_1 - p_2)_{\mu_3} + \delta_{\mu_2 \mu_3} (p_2 - p_3)_{\mu_1} + \delta_{\mu_3 \mu_1} (p_3 - p_1)_{\mu_2} \quad (2.9)$$

$$\mathcal{T}_{\mu_1, \mu_2, \mu_3}^{[2]}(p_1, p_2, p_3) = \frac{(p_1 - p_2)_{\mu_3} (p_2 - p_3)_{\mu_1} (p_3 - p_1)_{\mu_2}}{p^2}. \quad (2.10)$$

Then the three-gluon Green function in MOM scheme ($p_1^2 = p_2^2 = p_3^2 = \mu^2$) can be parametrised as

$$\begin{aligned} \langle \tilde{A}_{\mu_1}^a(p_1) \tilde{A}_{\mu_2}^b(p_2) \tilde{A}_{\mu_3}^c(p_3) \rangle &= f^{abc} \left[G^{(3)\text{sym}}(\mu^2) \mathcal{T}_{\mu'_1, \mu'_2, \mu'_3}^{[1]}(p_1, p_2, p_3) \prod_{i=1,3} \left(\delta_{\mu'_i \mu_i} - \frac{p_{i\mu'_i} p_{i\mu_i}}{\mu^2} \right) + \right. \\ &\quad \left. + H^{(3)}(\mu^2) \mathcal{T}_{\mu_1, \mu_2, \mu_3}^{[2]}(p_1, p_2, p_3) \right] \end{aligned} \quad (2.11)$$

For a non-perturbative MOM definition of the renormalised coupling g_R one need to extract the scalar function $G^{(3)\text{sym}}(\mu^2)$, proportional to the coupling g_0 at the tree order. This is done by the following projection :

$$\begin{aligned} G^{(3)\text{sym}}(\mu^2) &= \left(\mathcal{T}_{\mu'_1, \mu'_2, \mu'_3}^{[1]}(p_1, p_2, p_3) \prod_{i=1,3} \left(\delta_{\mu'_i \mu_i} - \frac{p_{i\mu'_i} p_{i\mu_i}}{\mu^2} \right) + \frac{1}{2} \mathcal{T}_{\mu'_1, \mu'_2, \mu'_3}^{[2]}(p_1, p_2, p_3) \right) \times \\ &\quad \times \frac{1}{18\mu^2} \frac{f^{abc}}{N_c(N_c^2 - 1)} \langle \tilde{A}_{\mu_1}^a(p_1) \tilde{A}_{\mu_2}^b(p_2) \tilde{A}_{\mu_3}^c(p_3) \rangle \end{aligned} \quad (2.12)$$

Three-gluon vertex : asymmetric case

The three-gluon Green function with one vanishing external propagator ([20],[19]) can be parametrised as

$$G_{\mu\nu\rho}^{(3)abc}(p, 0, -p) \equiv \langle \tilde{A}_\mu^a(-p) \tilde{A}_\nu^b(p) \tilde{A}_\rho^c(0) \rangle = 2f^{abc} p_\rho \left(\delta_{\mu\nu} - \frac{p_\mu p_\nu}{p^2} \right) G^{(3)\text{asym}}(p^2), \quad (2.13)$$

and thus

$$G^{(3)\text{asym}}(p^2) = \frac{1}{6p^2} \frac{f^{abc}}{N_c(N_c^2 - 1)} \delta_{\mu\nu} p_\rho G_{\mu\nu\rho}^{(3)abc}(p, 0, -p). \quad (2.14)$$

Ghost-gluon vertex

Similar parametrisation may be written in the case of the ghost-ghost-gluon Green function (cf. Figure 2.2). But in this case one obtains two different renor-

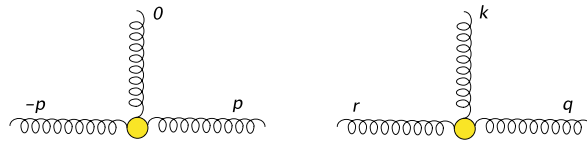


FIG. 2.1 – Definitions of the $\widetilde{\text{MOM}}$ scheme, $p^2 = \mu^2$ (left) and MOM, $q^2 = r^2 = k^2 = \mu^2$ (right)

malisation schemes $\widetilde{\text{MOM}}_c$ and $\widetilde{\text{MOM}}_{c0}$ corresponding to the zero-point kinematic configuration with vanishing momentum of, respectively, the gluon and the entering ghost. We denote by $\widetilde{G}_K^{(3)}$ a generic scalar function extracted from a three-point

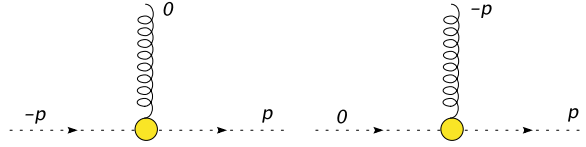


FIG. 2.2 – Kinematic configurations of the $\widetilde{\text{MOM}}_c$, $\widetilde{\text{MOM}}_{c0}$ schemes, $p^2 = \mu^2$.

function in a particular kinematic configuration K . Then the gauge coupling at the renormalisation scale μ^2 is defined by

$$g_R^{(K)}(\mu^2) = \frac{G_K^{(3)}(p_1^2, p_2^2, p_3^2)}{G^{(2)}(p_1^2)G^{(2)}(p_2^2)G^{(2)}(p_3^2)} Z_3^{3/2}(\mu^2) \quad (2.15)$$

in the case of three-gluon vertices, where the choice of p_i determines the renormalisation scheme. For of ghost-ghost-gluon vertices the coupling is defined by

$$\tilde{g}_R^{(K)}(\mu^2) = \frac{\tilde{G}_K^{(3)}(p_1^2, p_2^2, p_3^2)}{F^{(2)}(p_1^2)F^{(2)}(p_2^2)G^{(2)}(p_3^2)} Z_3^{1/2}(\mu^2) \tilde{Z}_3(\mu^2). \quad (2.16)$$

where $\tilde{G}_K^{(3)}(p_1^2, p_2^2, p_3^2)$ is the scalar factor of the ghost-gluon three point function $\langle \tilde{\mathcal{A}}_\mu(p_1) \tilde{c}(p_2) \tilde{c}(p_3) \rangle$. In fact, only the coupling in the $\widetilde{\text{MOM}}_c$ scheme can be defined non-perturbatively for the reasons explained in the following section.

2.2 Numerical calculation of the ghost Green functions in Landau gauge

2.2.1 Lattice implementation of the Faddeev-Popov operator

In order to calculate numerically [21] the ghost propagator

$$F^{(2)}(x-y)\delta^{ab} \equiv \left\langle \left(\mathcal{M}_{FP}^{\text{lat}} \right)^{-1}_{xy}{}^{ab} \right\rangle \quad (2.17)$$

one uses the lattice definition (1.68) of the Faddeev-Popov operator. Most lattice implementations of the Faddeev-Popov operator use its explicit component form. But as we have seen the action of the Faddeev-Popov operator on a vector ω can also be written as a lattice divergence

$$\mathcal{M}_{FP}^{\text{lat}}[U]\omega = -\frac{1}{V} \nabla_\mu \mathcal{A}'_\mu \quad (2.18)$$

where \mathcal{A}' is defined by (1.66). This form allows a very efficient lattice implementation which is based on the fast routines coding the group multiplication law :

```

#  $\omega_{in}, \omega_{out}$  are the ghost fields.
#  $U_\mu(x)$  is the gauge configuration.
type  $SU(N_c)$    $U_\mu(x), dU, W, W_+, W_-$ 
type  $su(N_c)$    $\omega_{in}(x), \omega_{out}(x)$ 
for all  $x$  do
   $dU = 0.$ 
   $W = \omega_{in}(x)$ 
  do  $\mu = 1 \dots 4$ 
     $W_+ = \omega_{in}(x + e_\mu)$ 
     $W_- = \omega_{in}(x - e_\mu)$ 
     $dU = dU + U_\mu(x - e_\mu) * W + W * U_\mu(x)$ 
       $- U_\mu(x) * W_+ - W_- * U_\mu(x - e_\mu)$ 
  end do
   $\omega_{out}(x) = dU - dU^\dagger - \frac{1}{N_c} \text{Tr}(dU - dU^\dagger)$ 
end do

```

2.2.2 Numerical inversion of the Faddeev-Popov operator

We invert the Faddeev-Popov operator by solving the equation

$$\sum_{y,b} \mathcal{M}_{FP}^{\text{lat}}[U]^{ab}(x,y) \eta^b(y) = S^a(x), \quad (2.19)$$

for some source $S^a(x)$ using an appropriate algorithm (for a review of algorithms see [22]). The operator $\mathcal{M}_{FP}^{\text{lat}}[U]$ has zero-modes, that is why the inversion can only be done in the vector subspace K^\perp orthogonal to the kernel of the operator. The trivial zero-modes are constant fields. If we neglect Gribov copies then the Faddeev-Popov operator has no other zero-modes, and thus the non-zero Fourier modes form a basis of K^\perp :

$$\eta(y) = \sum_{p \neq 0} c_p e^{ip \cdot y}, \quad \forall \eta \in K^\perp. \quad (2.20)$$

The inversion in one Fourier mode

Choosing the source for inversion in the form

$$S_p^a(x) = \delta^{ab} e^{ip \cdot x} \quad (2.21)$$

and taking the scalar product of the inverse $\mathcal{M}_{FP}^{\text{lat}}[U]^{-1}S_p^a$ with the source one obtains

$$\left\langle \left(S_p^a \mid \mathcal{M}_{FP}^{\text{lat}}{}^{-1} S_p^a \right) \right\rangle = \sum_{x,y} \left\langle \left(\mathcal{M}_{FP}^{\text{lat}}{}^{-1} \right)_{xy}^{aa} \right\rangle e^{-ip \cdot (x-y)} \quad (2.22)$$

$$= V \tilde{F}^{(2)}(p) \quad (2.23)$$

after averaging over the gauge field configurations. This method requires one matrix inversion for each momentum p . It is suitable only when one is interested in a few values of the ghost propagator.

The inversion in all Fourier modes

One can calculate the ghost propagator for all momenta p doing only one matrix inversion noticing that

$$\delta_{x,y} = \frac{1}{V} + \frac{1}{V} \sum_{p \neq 0} e^{-ip \cdot (x-y)} \quad (2.24)$$

and choosing for the source :

$$S_0^a(x) = \delta^{ab} \left(\delta_{x,0} - \frac{1}{V} \right). \quad (2.25)$$

The Fourier transform of $M^{-1}S_0^a$, averaged over the gauge configurations, yields :

$$\begin{aligned} \sum_x e^{-ip \cdot x} \left\langle \mathcal{M}_{FP}^{\text{lat}}{}^{-1} S_0^a \right\rangle &= \sum_x e^{-ip \cdot x} \left\langle \left(\mathcal{M}_{FP}^{\text{lat}}{}^{-1} \right)_{x0}^{aa} \right\rangle - \frac{1}{V} \sum_{x,y} e^{-ip \cdot x} \left\langle \left(\mathcal{M}_{FP}^{\text{lat}}{}^{-1} \right)_{xy}^{aa} \right\rangle \\ &= \sum_x e^{-ip \cdot x} F^{(2)}(x) - \frac{1}{V} \sum_{x,y} e^{-ip \cdot x} F^{(2)}(x-y) \\ &= \tilde{F}^{(2)}(p) - \delta(p) \sum_x F^{(2)}(x), \end{aligned} \quad (2.26)$$

where we have used the translational invariance of the ghost propagator. Therefore, with this choice of the source, only one matrix inversion followed by one Fourier transformation of the solution is required to get the ghost propagator for all values of the lattice momenta.

Because in the case of the source (2.25) one inverts in all modes at the same time, some statistical accuracy is lost. However, it turns out to be sufficient for our purposes.

There is one important technical point that should be mentioned. During the inversion process it is mandatory to check, whatever the choice of sources, that rounding errors during the inversion do not destroy the condition that the solution is still orthogonal to the kernel of the Faddeev - Popov operator :

$$\sum_x \left(\mathcal{M}_{FP}^{\text{lat}}{}^{-1} S \right) (x) = 0 \quad (2.27)$$

Indeed, if the zero-mode component of the solution grows beyond some threshold during the inversion of the Faddeev-Popov operator on a gauge configuration, then this component starts to increase exponentially, and a sizeable bias is produced in other components as well. We have observed this phenomenon occasionally, about one gauge configuration every few hundreds, when using the componentwise implementation of the lattice Faddeev-Popov operator based on (1.68). However, we have never observed sizeable deviations from (2.27) using the efficient implementation of the Faddeev-Popov operator exposed in the subsection 2.2.1.

2.2.3 Calculation of the ghost-gluon vertex

In order to calculate the ghost-gluon three-point function in $\widetilde{\text{MOM}}_c$ and $\widetilde{\text{MOM}}_{c0}$ renormalisation schemes one has to calculate the corresponding ghost two-point function :

$$\left\langle \widetilde{\mathcal{A}}_\mu(p_1) \underbrace{\widetilde{c}(p_2)\widetilde{c}(p_3)} \right\rangle \xrightarrow{\text{lattice}} \sum_{\text{conf. } i} \widetilde{\mathcal{A}}_\mu(p_1) (\mathcal{M}_{FP}^{\text{lat}}[U_i]^{-1})(p_2, p_3) \quad (2.28)$$

It is quite easy to calculate this Green function in the $\widetilde{\text{MOM}}_c$ kinematic configuration, because in this case $p_2 = -p, p_3 = p$ and $(\mathcal{M}_{FP}^{\text{lat}}[U_i]^{-1})(-p, p)$ is just a ghost propagator in the background gluon field defined by U_i .

The situation changes when considering the kinematic configurations like $\widetilde{\text{MOM}}_{c0}$, when the momentum of the entering (or of the outgoing) ghost is set to zero. In this case the inversion of the Faddeev-Popov operator has to be performed with the source (2.21). In other words we try to solve the equation

$$\mathcal{M}_{FP}^{\text{lat}}[U]_{xy} \eta_{yz} = e^{ip \cdot (x-z)}. \quad (2.29)$$

The vector $\bar{\eta}_y = \frac{1}{V} \sum_z \eta_{yz} e^{ip \cdot z}$ is the solution of

$$\mathcal{M}_{FP}^{\text{lat}}[U]_{xy} \bar{\eta}_y = e^{ip \cdot x}, \quad (2.30)$$

and

$$\bar{\eta}_y = \frac{1}{V} \sum_z \eta_{yz} e^{ip \cdot z} = \frac{1}{V} \sum_z c(y) \bar{c}(z) e^{ip \cdot z} \equiv c(y) \widetilde{c}(p). \quad (2.31)$$

Doing a summation on y we obtain a Fourier transform of the field $c(y)$:

$$\frac{1}{V} \sum_y \bar{\eta}_y = \widetilde{c}(0) \widetilde{c}(p). \quad (2.32)$$

But the last equation expresses the orthogonality condition (2.27). Thus we find $\widetilde{c}(0) \widetilde{c}(p) = 0$ in this case. That means that (2.28) is also zero, and the vertex function cannot be directly extracted (on the lattice) in the kinematic configuration with vanishing ghost momentum $\widetilde{\text{MOM}}_{c0}$, but only in the $\widetilde{\text{MOM}}_c$ scheme.

2.3 Errors of the calculation

There are three main sources of errors when calculating Green functions on the lattice : the statistical errors of the Monte-Carlo method, the systematic bias coming from the space-time discretisation and finally the error due to the gauge fixing (influence of lattice Gribov copies). The last is discussed in the following section.

2.3.1 Estimating the statistical error

The gauge-field configurations produced via the Monte-Carlo generation process (see [13] for a review) are not completely decorrelated. However, the residual correlations may be neglected. Nevertheless, all data points (as function of momentum p) of a Green function are calculated on the same set of gauge configurations $\{C_i\}$, and in this sense they are not independent. This problem arises when calculating quantities involving functions of mean values, like the coupling constant in a MOM scheme. In order to take in account the bias induced by this correlation one uses a special method (called **Jackknife** [23], [24]) of computation of the error. Generally speaking this method is a standard bootstrap method (of the estimation of the variance in the case of a non-Gaussian distribution) based on a resampling with replacement from the original sample. We start with a Monte-Carlo sample of size M . Our purpose is to calculate the error on the estimation of the mean of this sample. We divide it into $[M/m]$ groups of m elements :

$$\left[\mathcal{O}(C_1), \dots, \mathcal{O}(C_m) \right] \quad \left[\mathcal{O}(C_{m+1}), \dots, \mathcal{O}(C_{2m}) \right] \quad \dots \quad \left[\dots, \mathcal{O}(C_M) \right]. \quad (2.33)$$

Next one defines the partial averages

$$a_k = \frac{\sum_{i=1}^M \mathcal{O}(C_i) - \sum_{i=km}^{(k+1)m} \mathcal{O}(C_i)}{M - m}, \quad k = 1 \dots \tilde{M} = \left\lfloor \frac{M}{m} \right\rfloor, \quad (2.34)$$

and finally obtains the following expression for the error :

$$\Delta_{\text{jackknife}} \langle \mathcal{O} \rangle = \sqrt{\frac{\tilde{M} - 1}{\tilde{M}} \left(\sum_{k=1}^{\tilde{M}} a_k^2 - \frac{\left(\sum_{k=1}^{\tilde{M}} a_k \right)^2}{\tilde{M}} \right)}. \quad (2.35)$$

This analytical expression differs from the standard formula for the dispersion of the mean value by an additional factor $\sim \tilde{M}$.

2.3.2 Handling the discretisation errors

Because of discretisation of the space-time, lattice theory ¹ loses the rotational symmetry $SO(4)$ inherited from the Lorentz invariance in Minkowski space. This symmetry is replaced by a discret isometry group $H_4 = S_4 \times P_4$ (semiproduct of the

¹we suppose that the lattice is hypercubic.

permutation and reflection groups) having $4! \cdot 2^4 = 384$ elements. A generic scalar function $\widehat{G}(p)$ extracted from Green functions is thus invariant along the orbit $O(p)$ generated by the action of the group H_4 on the components of the lattice momentum $p \equiv \frac{2\pi}{La} \times (n_1, n_2, n_3, n_4)$. It may be proven in the theory of group invariants that each orbit is characterised by four group invariants

$$p^{[n]} = a^n \sum_{\mu} p_{\mu}^n, \quad n = 2, 4, 6, 8 \quad (2.36)$$

One may average on the gauge orbit of the H_4 group in order to increase the statistics :

$$a^2 G_L(p^{[2]}, p^{[4]}, p^{[6]}, p^{[8]}) = \frac{1}{\text{card } O(p)} \sum_{p \in O(p)} \widehat{G}(p), \quad (2.37)$$

where $\text{card } O(p)$ is the number of elements in the orbit $O(p)$. The resulting average is a function of the four invariants $p^{[n]}$. But in the continuum limit any scalar function is a function of the rotational invariant $p^{[2]}$. We will explain how it is possible to remove the dependence on the three other invariants with the example of the free lattice gluon propagator :

$$G_0(p) = \frac{1}{\sum_{\mu} \widehat{p}_{\mu}^2}, \quad \text{where} \quad \widehat{p}_{\mu} = \frac{2}{a} \sin\left(\frac{ap_{\mu}}{2}\right). \quad (2.38)$$

If all the components of the lattice momentum verify the condition $ap_{\mu} \ll 1$, then $\sum_{\mu} \widehat{p}_{\mu}^2 \simeq p^2 - \frac{1}{12} a^2 p^{[4]}$, and thus one has up to terms of order $\sim a^4$

$$G_0(p) = \frac{1}{p^2} \left(1 + \frac{1}{12} \frac{a^2 p^{[4]}}{p^2} + O(a^4) \right). \quad (2.39)$$

So, taking the continuum limit $a \rightarrow 0$ is equivalent to taking the limit $p^{[4]} \rightarrow 0$. We apply this idea to (2.37). Making the reasonable hypothesis of regularity near the continuum limit, we expand :

$$G_L(p^{[2]}, p^{[4]}, p^{[6]}, p^{[8]}) \approx G_L(p^{[2]}, 0, 0, 0) + p^{[4]} \frac{\partial G_L}{\partial p^{[4]}}(p^{[2]}, 0, 0, 0) + \dots \quad (2.40)$$

and $G_L(p^{[2]}, 0, 0, 0)$ is nothing but the scalar factor in the continuum in a finite volume, up to lattice artifacts which do not break $O(4)$ invariance. When several orbits exist with the same p^2 , we can remove an important part of the hypercubic artifacts by extrapolating the lattice data towards $G_L(p^{[2]}, 0, 0, 0)$ using a linear regression with respect to $p^{[4]}$ (the other invariants are of higher order in a).

There are vectors p that have only one orbit. In order to include them in the data analysis one should interpolate the slopes obtained in the extrapolation of (2.40). This can be done either numerically or by assuming a functional dependence of the slope with respect to p^2 . In principle the p^2 dependence of the slope may be calculated using lattice perturbation theory. A dimensional analysis suggests the

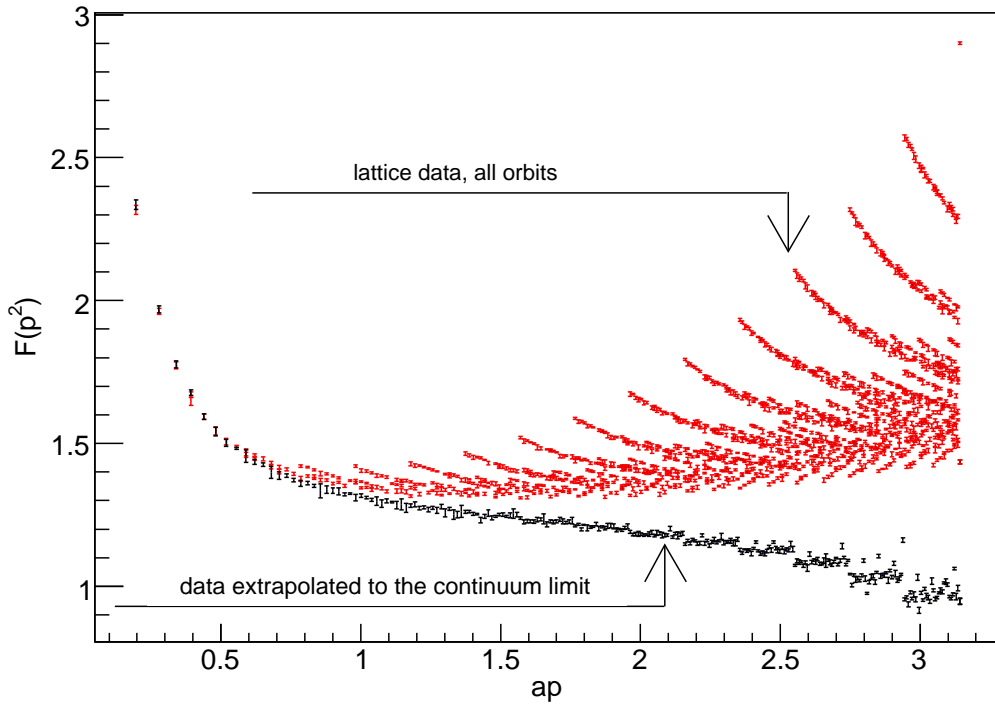


FIG. 2.3 – Example of the extrapolation in $p^{[4]}$ for the ghost scalar factor $F(p)$ in the case of the $SU(3)$ gauge group for the lattice volume 32^4 and at $\beta = 6.4$. Red round dots correspond to the bare data, and blue squares to the extrapolated one. In practice we do not consider the moments above $ap = \frac{\pi}{2}$.

form $\sim \frac{c_1}{(p^2)^2}$. We have used the function

$$\frac{\partial G_L}{\partial p^{[4]}}(p^{[2]}, 0, 0, 0) = \frac{1}{(p^{[2]})^2} (c_1 + c_2 p^{[2]}) \quad (2.41)$$

with two fit parameters in order to fit the slopes. The validity of the exposed method is qualitatively checked by the smoothness of the resulting curve. At Figure 2.3 we present an example of removing the hypercubic artifacts. We see that the method works very well, even at large values of ap . In practice we do not consider the momenta above $ap = \frac{\pi}{2}$.

2.4 Gribov ambiguity and lattice Green functions

We have discussed in the previous sections different uncertainties introduced by the discretisation of space-time. Another bias comes from the gauge fixing (see section 1.1.2). As we have already mentioned, the Minimal Landau gauge fixing quantisation is equivalent to realising the Gribov quantisation prescription. Thus lattice Green functions are calculated within this prescription. However, the gauge is not fixed in a unique way. The Gribov ambiguity on the lattice shows up by the non-uniqueness of the minimum (1.59) of the functional (1.60). Indeed, the functional (1.60) has a form similar to the energy of a spin glass which is known to have

exponentially-many metastable states (cf. Figure 2.4). All these lattice Gribov copies are situated inside the Gribov horizon. On a finite lattice one can (in principle) fix the gauge in a unique way. However this is very expensive in terms of computer time.

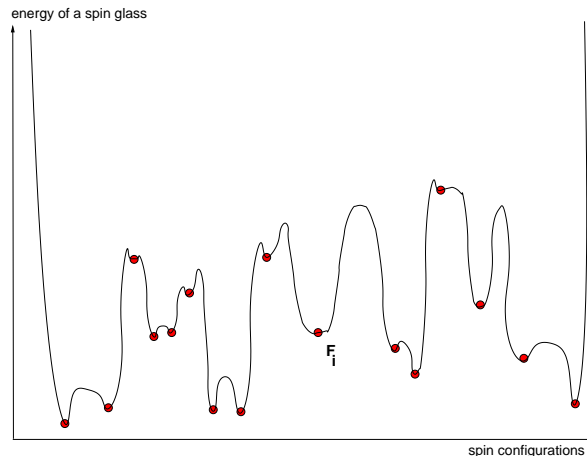


FIG. 2.4 – Landscape of minima for a generic spin glass. Circles mark the configurations corresponding to metastable states. Their number grow like $\exp(\text{const} \cdot N)$ as function of the number of spins N .

Nevertheless one has to understand the influence of the choice of the minimum of the functional (1.60) on the mean values yielding Green functions. For this purpose we studied the landscape of minima of the gauge-fixing functional [18]. In the following subsection we define a specific probability to find a Gribov copy, as function of the physical momentum. In the next-to-the-following subsection we discuss the influence of these copies on the Green functions, and the Zwanziger's conjecture on the equivalence of the integration over the Gribov region and the fundamental modular region in the infinite volume limit.

2.4.1 The landscape of minima of the gauge-fixing functional

Let us consider the landscape of the functional F_U . One of its characteristics is the distribution of values at minima F_{\min} of F_U . We know that for small magnitudes of the gauge field all the link matrices $U_\mu(x)$ (they play the role of couplings between the "spin" variables) are close to the identity matrix, and thus the minimum is unique. Their number increases when the bare lattice coupling β decreases, because the typical magnitude of the phase of $U_\mu(x)$ grows in this case and thus link matrices move farther from the identity matrix. The number of minima also increases with the number of links (at fixed β) because in this case there are more degrees of freedom in the system.

We can define a probability to find a secondary minimum, as a function of the β parameter. For each orbit we fix the gauge N_{GF} times, each gauge fixing starts after a (periodic) random gauge transformation of the initial field configuration. We thus obtain a distribution of minima F_{\min} . This distribution gives us the number of minima $N(F^i)$ as a function of the value of $F^i \equiv F_{\min}^i$. The relative frequency of a minimum F^i is defined by

$$\omega_i = \frac{N(F^i)}{\sum_i N(F^i)}, \quad (2.42)$$

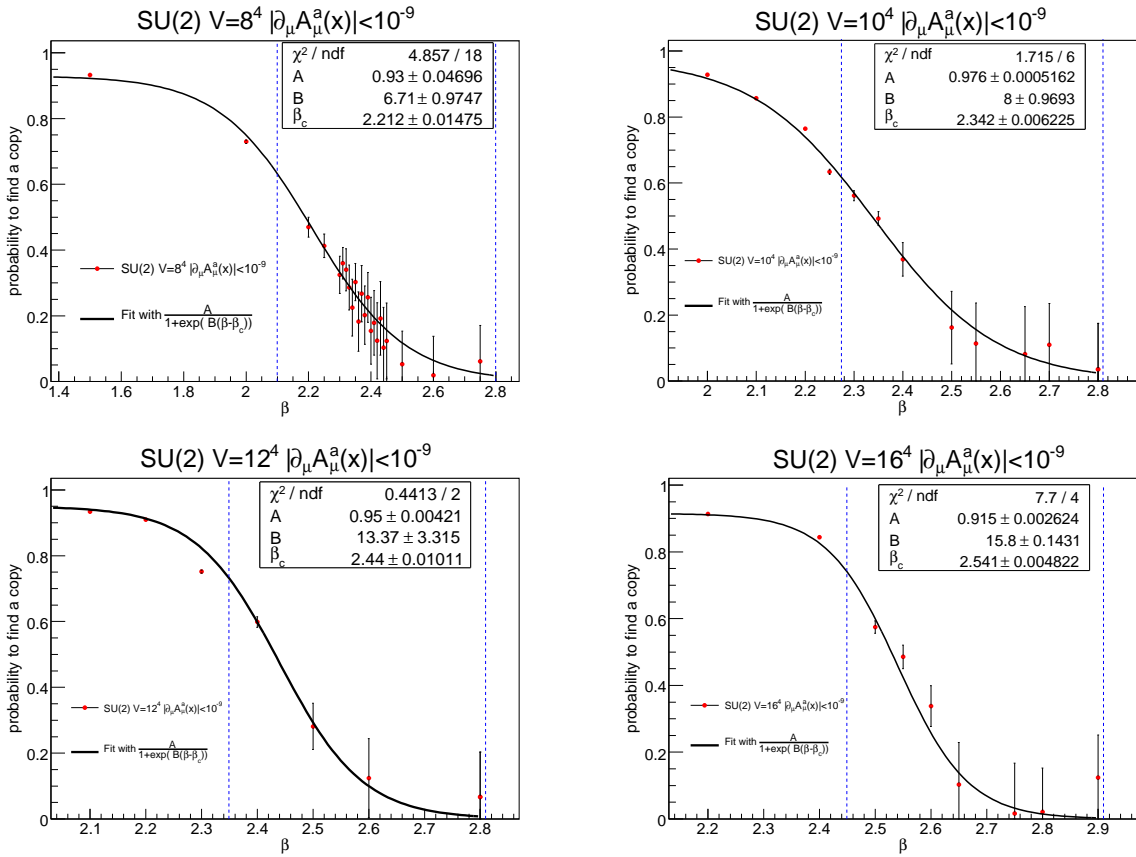


FIG. 2.5 – Probability (averaged over gauge orbits) to find a secondary minimum as a function of β at volumes $V = 8^4, 10^4, 12^4, 16^4$. Solid line represents a fit with an empirical formula (2.46). The vertical dashed lines delimit the window of each fit.

where $\sum_i N(F^i) = N_{\text{GF}}$. Then the weighted mean number of copies per value of F_{min} is given by

$$\bar{N} = \sum_i \omega_i N(F^i). \quad (2.43)$$

This allows us to define a probability to find a secondary minimum when fixing the Minimal Landau gauge for a given gauge field configuration :

$$p_{1\text{conf}} = 1 - \frac{\bar{N}}{\sum_i N(F^i)}. \quad (2.44)$$

If one finds the same value of F_{min} for all N_{GF} tries then this probability is zero. On the contrary, if all F_i are different then $p_{1\text{conf}}$ is close to one.

Having the probability to find a secondary minimum when fixing the gauge for *one particular* configuration we can calculate the Monte-Carlo *average* $\langle \bullet \rangle$ on gauge orbits, i.e. on “spin couplings” $U_\mu(x)$. We obtain finally the overall probability to find a secondary minimum during a numerical simulation at given β :

$$P(\beta) \equiv \langle p_{1\text{conf}} \rangle_{\{U_\mu(x)\}} = 1 - \left\langle \frac{\bar{N}}{\sum_i N(F^i)} \right\rangle_{\{U_\mu(x)\}}. \quad (2.45)$$

We have performed simulations in the case of $SU(2)$ lattice gauge theory at volumes $V = \{8^4, 10^4, 12^4, 16^4\}$ for β varying from 1.4 to 2.9. For each value of β we generated 100 independent Monte-Carlo gauge configurations, and we fixed the gauge $N_{\text{GF}} = 100$ times for every configuration. Between each gauge fixing a random gauge transformation of the initial gauge configuration was performed, and the minimising algorithm stops when the triple condition (1.71) is satisfied. Examples of the resulting probability to find a secondary minimum are presented at Figure 2.5.

As expected, the probability is small when β is large, and it is close to one when β is small. The dispersion was calculated using the Jackknife method (discussed in the subsection 2.3.1). The physical meaning of this dispersion is the following : when the error is small, all gauge configurations have a similar number of secondary minima. On the contrary, this dispersion is large if there are some exceptional gauge configurations having a different number of copies. At small β almost all gauge configurations have many secondary minima, that is why the dispersion of the probability is small. At large β almost all gauge configurations have a unique minimum, but some of them can have copies. This may considerably increase the dispersion of the probability. The appearance of exceptional gauge configuration possessing a large density of close-to-zero eigenvalues of the Faddeev-Popov operator has been recently reported [25]. Probably these fields are related with those having a lot of secondary minima at large β 's, and this correlation deserves a separate study.

We can fit our data (Figure 2.5) for the probability (2.45) with an empirical formula

$$P(\beta) = \frac{A}{1 + e^{B(\beta - \beta_c)}} \quad (2.46)$$

in order to define a characteristic coupling β_c when the probability to find a copy decreases considerably. One can define β_c as corresponding to the semi-heights of the probability function $P(\beta)$. At this value of β an equally probable secondary attractor of the functional F_U appears. The fit has been performed for the points between dashed lines at Figure 2.5, and the results for the fit parameters are given ibidem and in Table 2.1. We see that β_c depends on the volume of the lattice. Let us check whether these values correspond to some physical scale. According to works [26],[27] one has the following expression for the string tension σ for $\beta \geq 2.3$:

$$[\sigma a^2](\beta) \simeq e^{-\frac{4\pi^2}{\beta_0} \beta + \frac{2\beta_1}{\beta_0^2} \log\left(\frac{4\pi^2}{\beta_0} \beta\right) + \frac{4\pi^2}{\beta_0} \frac{d}{\beta} + c} \quad (2.47)$$

with $c = 4.38(9)$ and $d = 1.66(4)$ ². Using this formula, we define a characteristic scale corresponding to the critical values β_c from Figure 2.5 :

$$\lambda_c = a(\beta_c) \cdot L$$

in the string tension units, L is the length of the lattice. In the last column of the Table 2.1 we summarise the results. We see that for the values of β_c in the scaling regime, when the formula (2.47) is applicable ($\beta \geq 2.3$), we obtain compatible values for the physical length λ_c .

²in this cited formula we kept the original convention for the RG β -function, namely $\beta_0 = 11/3N_C$, $\beta_1 = 17/3N_C^2$. They are different from the one we use in the following.

L	β_c	χ^2/ndf	λ_c , in units of $1/\sqrt{\sigma}$
8	2.221(14)	0.27	3.85(31)
10	2.342(6)	0.28	3.20(21)
12	2.44(1)	0.22	2.78(20)
16	2.541(5)	1.92	2.68(17)

TAB. 2.1 – The characteristic length defining the appearance of secondary minima. The errors for λ_c include errors for d and c parameters, and the fitted error for β_c

This suggests that in the case of $SU(2)$ gauge theory lattice Gribov copies appear when the physical size of the lattice exceeds a critical value around $2.75/\sqrt{\sigma}$. At first approximation λ_c is scale invariant, but a slight dependence in the lattice spacing remains.

In principle, the parameter β_c can be calculated with good precision. One should do it in the case of $SU(3)$ gauge group, because the dependence of the lattice spacing on the bare coupling is softer, and the scaling of the theory has been better studied than in the case of the $SU(2)$ theory.

A natural question that arises after the study of the distribution of F_{\min} is whether the gauge configurations having the same value of F_{\min} are equivalent, i.e. they differ only by a global gauge transformation. This can be checked by calculating the two-point gluonic correlation function on the gauge configuration. Indeed, according to the lattice definition of the gauge field that we used (1.52),

$$G_{1\text{conf}}^{(2)}(x-y) \propto \text{Tr} \left[\left(U_\mu(x) - U_\mu^\dagger(x) \right) \cdot \left(U_\nu(y) - U_\nu^\dagger(y) \right) \right]. \quad (2.48)$$

Applying a global gauge transformation $U_\mu(x) \rightarrow V U_\mu(x) V^\dagger$ we see that the gluon propagator remains unchanged. This is also the case of the ghost propagator scalar function. We have checked numerically that the values of the gluon and the ghost propagators in Fourier space are the same for gauge configurations having the same F_{\min} . Thus we conclude that gauge configurations having the same F_{\min} are in fact equivalent [18].

2.4.2 Lattice Green functions and the Gribov ambiguity

As we have mentioned in the subsection 1.1.2, there is a conjecture [5] saying that in the infinite volume limit the expectation values calculated by integration over the Gribov region or the fundamental modular region become equal. Let us briefly recall the argument given in [5]. Let B_μ denote a field lying on the Gribov horizon :

$$\begin{cases} \partial_\mu B_\mu = 0 \\ \mathcal{M}_{FP}(B)\omega_0 = 0, & \omega_0(x) \neq \text{const}, \quad \omega_0(x) \in \mathfrak{su}(N_c). \end{cases} \quad (2.49)$$

We write $F_B(t, \omega)$ for the functional (1.57), with $u(x) = \exp t\omega(x)$. On the boundary one has

$$\begin{cases} F'_B(0, \omega_0) = 0 \\ F''_B(0, \omega_0) = 0 \\ F'''_B(0, \omega_0) \neq 0 \propto \sqrt{V} \\ F''''_B(0, \omega_0) = \frac{3}{2} \int d^4x [d_\mu(\omega_0^2)]^2 \propto V \end{cases} \quad (2.50)$$

So for small variations of t one has for the functional (1.57)

$$F_B(t) = F_B(0) + \frac{1}{3!} F'''_B(0) t^3 + \frac{1}{4!} F''''_B(0) t^4, \quad (2.51)$$

and the last expression is minimised for $t = \bar{t} \equiv -3F'''_B(0)/F''''_B(0)$. The value that is achieved at this secondary minimum inside the Gribov horizon is

$$F_B(\bar{t}) = F_B(0) - \frac{9}{8} \frac{[F'''_B(0)]^4}{[F''''_B(0)]^3}. \quad (2.52)$$

Using the estimations (2.50) and the fact that the third order derivative appears in an even power, one sees that the secondary minimum is *lower* than the one on the boundary, and the difference between them *decreases* with the volume V . The corresponding gauge configuration can be written as

$$B_\mu(x, \bar{t}) = B_\mu(x, 0) + \bar{t} [D_\mu(B)\omega_0](x) = B_\mu(x, 0) - 3 \frac{F'''_B(0)}{F''''_B(0)} [D_\mu(B)\omega_0](x). \quad (2.53)$$

When the lattice volume V is large, the integration (over G or Λ) on the gauge configurations is dominated by a small shell near the boundary, because the dimension of the configuration space is large ($2dV(N_C^2 - 1)$). According to the above argument the configurations near the boundaries ∂G and $\partial \Lambda$ draw together. So, having (2.53) for a typical gauge field configuration, it is natural to suppose that in the infinite volume limit the average calculated by integration over the domains G or Λ become equal. However at a finite lattice this is clearly not the case, that is why it is very important to know what is the influence of lattice Gribov copies on the Green functions. This question that has already been considered by different authors ([28],[29],[30],[31],[32],[33],[25]). To check the dependence of Green functions on the procedure of the choice of the minimum we adopted the same strategy as in above citations : for every of the 100 gauge configurations used to compute Green functions the gauge was fixed 100 times (a periodic random gauge transformation is done after each gauge fixing). The Monte-Carlo average was computed with respect to the “first copy” (fc) found by the minimisation algorithm and the “best copy” (bc), having the smallest value of F_{\min} . We have calculated the gluon and the ghost propagators, and also the three-gluon Green functions in symmetric and asymmetric kinematic configurations. The simulations have been performed in the case of the $SU(2)$ group on lattices of volumes 8^4 and 16^4 for $\beta = 2.1, 2.2, 2.3$. According to the results of the subsection 2.4.1, at these values of β we are sure to have lattice Gribov copies. We conclude [18] that no systematic effect could be found for gluonic two- and three-point Green functions, the Monte-Carlo average values in the cases of (fc)

β	L	n^2	$F_{\text{fc}}^{(2)}(p^2) - F_{\text{bc}}^{(2)}(p^2)$	$\frac{F_{\text{fc}}^{(2)}(p^2) - F_{\text{bc}}^{(2)}(p^2)}{F_{\text{bc}}^{(2)}}$
2.1	8	1	0.211	0.045
			∨	
2.1	16	4 $n^{[4]}=16$	0.145	0.033
2.2	8	1	0.078	0.019
			∨	
2.2	16	4 $n^{[4]}=16$	0.023	0.006
2.3	8	1	0.086	0.024
			∧	
2.3	16	4 $n^{[4]}=16$	0.114	0.034

TAB. 2.2 – Volume dependence of the ghost propagators [18], $p_\mu = \frac{2\pi}{aL} n_\mu$

β	L	$\langle F_{\text{min}} \rangle_{\{U\}}$	$\delta \langle F_{\text{min}} \rangle_{\{U\}}$
2.2	8	-0.8236	0.003744
	10	-0.8262	0.002367
	12	-0.8272	0.001377
	16	-0.8279	0.000802
2.4	8	-0.8642	0.005270
	12	-0.8669	0.002739
	12	-0.8686	0.001849
	16	-0.8702	0.001003

TAB. 2.3 – Volume dependence of the Monte-Carlo+gauge orbit mean value at minima F_{min} and the dispersion of this mean.

and (bc) being compatible within the statistical errors. However the ghost propagator is quite sensitive to the choice of the minimum - in the case of (bc) the infrared divergence is lessened. This dependence has been found to decrease slowly with the volume [33]. The results of the subsection 2.4.1 indicate that the convergence can happen only beyond the critical volume λ_c^4 . To check this we compare the fc/bc values of the ghost propagator, at one physical value of the momentum, for the orbit $n^2 = 1$ on a 8^4 lattice and the orbit $n^2 = 4, n^{[4]} = 16$ on the 16^4 lattice³ at the same β (see Table 2.2). It happens indeed that the decrease is observed only at $\beta = 2.1$ and 2.2, in accordance with Table 2.1. However, these values of β are not in the scaling regime, and thus a study on larger lattices would be welcome. It is not surprising that the ghost propagator depends on the bc/fc choice : the (bc) corresponds to the fields further from the Gribov horizon where the Faddeev-Popov operator has a zero mode, whence the inverse Faddeev-Popov operator (ghost propagator) is expected to be smaller as observed. The correlation between the bc/fc choice and the gluon propagator is not so direct. Another quantity is obviously strongly correlated to the bc/fc choice : the value of F_{min} . We tested the volume dependence of the Monte-Carlo+gauge orbit mean value of the quantity F_{min} (see Tab.2.3). According to the argument given in [5], all minima become degenerate in the infinite volume limit, and closer to the absolute minimum (in the fundamental modular region). We see from the Table 2.3 that their average value and dispersion decrease with the volume

³Remember that the momentum in physical units is equal to $2\pi n / (La)$ in our notations.

at fixed β , in agreement with [5].

We finish this section with a brief summary of our results [18] regarding the Gribov ambiguity on the lattice :

1. Lattice Gribov copies appear and their number grows very fast when the physical size of the lattice exceeds some critical value ($\approx 2.75/\sqrt{\sigma}$ in the case of the $SU(2)$ theory). This result is fairly independent of the lattice spacing.
2. The configurations lying on the same gauge orbit and having the same F_{\min} are equivalent, up to a global gauge transformation, and yield the same Green functions. Those corresponding to minima of F_U with different values of F_{\min} differ by a non-trivial gauge transformation, and thus they are not equivalent.
3. We confirm the result ([28],[29],[30],[31],[32],[33],[25]) that the divergence of the ghost propagator is lessened when choosing the “best copy” (corresponding to the choice of the gauge configuration having the smallest value of F_U). We also showed that gluonic Green functions calculated in the “first copy” and “best copy” schemes are compatible within the statistical error, no systematic effect was found (with periodic gauge transformations).
4. We found that the influence of Gribov copies on the ghost propagator decreases with the volume when the physical lattice size is larger than the critical length discussed above. We also show that the quantity F_{\min} decreases when the volume increases. These two points are in agreement with the Zwanziger’s argument [5] on the equality of the averages over the Gribov region and the fundamental modular region.

Chapitre 3

The ultraviolet behaviour of Green functions

The Lagrangian of the Pure Yang-Mills theory in a four-dimensional space-time does not contain any dimensional parameters susceptible to fix an energy scale for dimensionless quantities. However, the spectrum of the corresponding quantum theory contains massive states (glueballs). As a matter of fact, the quantum theory possesses a finite energy scale called Λ_{QCD} , which is generated by the quantisation process followed by the renormalisation. All dimensionful physical quantities are expressed as multiples of powers of this scale, and thus it should be a renormalisation group invariant :

$$\mu \frac{d}{d\mu} \Lambda_{\text{QCD}}(\mu, g(\mu^2)) = 0 \quad \rightarrow \quad \left[\mu \frac{\partial}{\partial \mu} + \beta(g(\mu^2)) \frac{\partial}{\partial g} \right] \Lambda_{\text{QCD}}(\mu, g(\mu^2)) = 0, \quad (3.1)$$

where $\beta(g(\mu^2))$ is the renormalisation group beta function and μ is the renormalisation scale. The solution of the above equation reads

$$\Lambda_{\text{QCD}}(\mu, g(\mu^2)) = \mu \exp \left(- \int_{g_1}^{g(\mu^2)} \frac{dg'}{\beta(g')} \right), \quad (3.2)$$

where g_1 is an arbitrary integration constant. Λ_{QCD} is a renormalisation scheme-dependent quantity, although it is a renormalisation group invariant within one particular scheme. So it is not a real physical quantity. Still, its value is important for estimating the lowest bound of the domain of validity of perturbation theory. Knowing several first coefficients of the β -function we find from the equation (3.2) :

$$\Lambda_{\text{QCD}}(\mu, g(\mu^2)) = \mu \exp \left[\frac{1}{2\beta_0} \left(\frac{1}{g_1^2} - \frac{1}{g^2(\mu^2)} \right) + \frac{\beta_1}{2\beta_0^2} \log \frac{g_1^2}{g^2(\mu^2)} \right] + O(g^2). \quad (3.3)$$

We see that there is an essential singularity when $g^2(\mu^2) \rightarrow 0$, and thus a perturbative calculation of related quantities (for example, the string tension $\sqrt{\sigma} = c_\sigma \Lambda_{\text{QCD}}$) is impossible. In the following sections we describe the method of calculation of Λ_{QCD} from lattice Green functions in Landau gauge. We start with a review of the

purely perturbative results for Green functions. The momentum range available on the lattice is situated at rather low energies where the non-perturbative power corrections are not negligible. The section 3.2 is devoted to the estimation of the dominant power corrections. At the end of this chapter we present the results of analysis of our lattice data.

3.1 Λ_{QCD} and perturbative expressions for Green functions

Different scalar factors of Green functions depend on the Λ_{QCD} parameter discussed in the previous subsection. These scalar factors can be calculated non-perturbatively in lattice simulations, and one can extract Λ_{QCD} by fitting the lattice data in the ultraviolet domain to the corresponding perturbative formulae. Here we make a review of available perturbative Landau gauge calculations for the ghost and gluon propagators in the MOM schemes.

If $\Gamma_R^{(N)}(p_i, g_R^2, \mu^2)$ is a renormalised proper vertex in Landau gauge, then the corresponding proper bare vertex function is independent of the renormalisation point μ . This fact is reflected by the Callan-Symanzik equation for the renormalised function :

$$\left(\frac{\partial}{\partial \ln \mu^2} + \beta(g_R(\mu^2)) \frac{\partial}{\partial g} - \frac{N}{2} \gamma(g_R(\mu^2)) \right) \Gamma_R^{(N)}(p_i, g_R^2, \mu^2) = 0 \quad (3.4)$$

where $\gamma(g_R(\mu^2))$ is the anomalous dimension. In the Momentum subtraction schemes, the renormalisation conditions are defined by setting some of the two- and three-point functions to their tree-level values at the renormalisation point. Then (3.4) simplifies to

$$\lim_{a^{-1} \rightarrow \infty} \frac{d \ln(Z_{3,\text{MOM}}(p^2 = \mu^2, a^{-1}))}{d \ln \mu^2} = \gamma_{3,\text{MOM}}(g_{\text{MOM}}) \quad (3.5)$$

in the case of two-point Green functions, where $Z_3(\mu^2)$ is defined in (2.7), a^{-1} stands for the ultraviolet regularisation and $\gamma_{3,\text{MOM}}(g_{\text{MOM}})$ is the anomalous dimension. A similar expression can be written for the ghost propagator renormalisation factor \widetilde{Z}_3 . As we have already seen in the section 2.1, there is an infinite number of MOM schemes differing by kinematic configurations at the subtraction point. We limit ourselves to the configurations defined by the subtraction of the transverse part of the three-gluon vertex ($\widetilde{\text{MOM}}$) and that of the ghost-gluon vertex with vanishing gluon momentum ($\widetilde{\text{MOM}}_c$) and vanishing incoming ghost momentum ($\widetilde{\text{MOM}}_{c0}$), discussed in the section 2.1.

Both anomalous dimensions for ghost and gluon propagators have been recently

computed ([34], [35]) in the $\overline{\text{MS}}$ scheme. The result at four-loop order reads

$$\begin{aligned}
\frac{d \ln(Z_{3,\text{MOM}})}{d \ln \mu^2} &= \frac{13}{2} h_{\overline{\text{MS}}} + \frac{3727}{24} h_{\overline{\text{MS}}}^2 + \left(\frac{2127823}{288} - \frac{9747}{16} \zeta_3 \right) h_{\overline{\text{MS}}}^3 \\
&+ \left(\frac{3011547563}{6912} - \frac{18987543}{256} \zeta_3 - \frac{1431945}{64} \zeta_5 \right) h_{\overline{\text{MS}}}^4 \\
\frac{d \ln(\tilde{Z}_{3,\text{MOM}})}{d \ln \mu^2} &= \frac{9}{4} h_{\overline{\text{MS}}} + \frac{813}{16} h_{\overline{\text{MS}}}^2 + \left(\frac{157303}{64} - \frac{5697}{32} \zeta_3 \right) h_{\overline{\text{MS}}}^3 \\
&+ \left(\frac{219384137}{1536} - \frac{9207729}{512} \zeta_3 - \frac{221535}{32} \zeta_5 \right) h_{\overline{\text{MS}}}^4
\end{aligned} \tag{3.6}$$

where $h = g^2 / (4\pi)^2$. In order to obtain the coefficients of the anomalous dimensions (3.5) in a MOM scheme one has to express the above expressions in terms of the corresponding coupling. We use the results of the article [34] where the three-loop perturbative subtraction of all the three-vertices appearing in the QCD Lagrangian for kinematic configurations with one vanishing momentum are given. In Landau gauge and in the pure Yang-Mills case one has the following relations between the couplings in different MOM schemes and $h_{\overline{\text{MS}}}$:

$$\begin{aligned}
h_{\widetilde{\text{MOM}}_g} &= h_{\overline{\text{MS}}} + \frac{70}{3} h_{\overline{\text{MS}}}^2 + \left(\frac{51627}{576} - \frac{153}{4} \zeta(3) \right) h_{\overline{\text{MS}}}^3 + \\
&+ \left(\frac{304676635}{6912} - \frac{299961}{64} \zeta_3 - \frac{81825}{64} \zeta_5 \right) h_{\overline{\text{MS}}}^4 \\
h_{\widetilde{\text{MOM}}_c} &= h_{\overline{\text{MS}}} + \frac{223}{12} h_{\overline{\text{MS}}}^2 + \left(\frac{918819}{1296} - \frac{351}{8} \zeta(3) \right) h_{\overline{\text{MS}}}^3 + \\
&+ \left(\frac{29551181}{864} - \frac{137199}{32} \zeta_3 - \frac{74295}{64} \zeta_5 \right) h_{\overline{\text{MS}}}^4 \\
h_{\widetilde{\text{MOM}}_{c0}} &= h_{\overline{\text{MS}}} + \frac{169}{12} h_{\overline{\text{MS}}}^2 + \left(\frac{76063}{144} - \frac{153}{4} \zeta(3) \right) h_{\overline{\text{MS}}}^3 + \\
&+ \left(\frac{42074947}{1728} - \frac{35385}{8} \zeta(3) - \frac{66765}{65} \zeta(5) \right) h_{\overline{\text{MS}}}^4.
\end{aligned} \tag{3.7}$$

Thus, inverting (3.7) and substituting in (3.6), we obtain the anomalous dimensions of the gluon and ghost propagator in the three above-mentioned renormalisation schemes. In a MOM scheme, the equations (3.6) may be integrated as functions of h (cf. 3.5)¹ :

$$\begin{aligned}
\ln \left(\frac{Z_{\Gamma,\text{MOM}}}{Z_0} \right) &= \log(h) \frac{\bar{\gamma}_0}{\beta_0} + h \frac{(\beta_0 \bar{\gamma}_1 - \beta_1 \bar{\gamma}_0)}{\beta_0^2} \\
&+ h^2 \frac{(\beta_0^2 \bar{\gamma}_2 - \beta_0 \beta_1 \bar{\gamma}_1 - (\beta_0 \beta_2 - \beta_1^2) \bar{\gamma}_0)}{2\beta_0^3} +
\end{aligned}$$

¹We omit the index specifying the renormalisation scheme both for h and Λ_{QCD} in the following formulae

$$\begin{aligned}
& + h^3 (\beta_0^3 \bar{\gamma}_3 - \beta_0^2 \beta_1 \bar{\gamma}_2 + (\beta_0 \beta_1^2 - \beta_0^2 \beta_2) \bar{\gamma}_1 \\
& + (-\beta_0^2 \beta_3 + 2 \beta_0 \beta_1 \beta_2 - \beta_1^3) \bar{\gamma}_0) \frac{1}{3\beta_0^4} + \dots
\end{aligned} \tag{3.8}$$

where $\bar{\gamma}_i$ are the expansion coefficients of the anomalous dimension in a generic MOM type scheme and Z_0 is an integration constant. The knowledge of the β -function

$$\beta(h) = \frac{dh}{d \ln \mu^2} = - \sum_{i=0}^n \beta_i h^{i+2} + \mathcal{O}(h^{n+3}) \tag{3.9}$$

at some order n allows to calculate the momentum dependence of h . At four-loop order one has

$$\begin{aligned}
h(t) = & \frac{1}{\beta_0 t} \left(1 - \frac{\beta_1 \log(t)}{\beta_0^2 t} + \frac{\beta_1^2}{\beta_0^4} \frac{1}{t^2} \left(\left(\log(t) - \frac{1}{2} \right)^2 + \frac{\beta_2 \beta_0}{\beta_1^2} - \frac{5}{4} \right) \right) + \\
& + \frac{1}{(\beta_0 t)^4} \left(\frac{\beta_3}{2\beta_0} + \frac{1}{2} \left(\frac{\beta_1}{\beta_0} \right)^3 \left(-2 \log^3(t) + 5 \log^2(t) + \left(4 - 6 \frac{\beta_2 \beta_0}{\beta_1^2} \right) \log(t) - 1 \right) \right),
\end{aligned} \tag{3.10}$$

where $t = \ln \frac{\mu^2}{\Lambda_{\text{QCD}}^2}$. The last equation together with (3.8) allows us to write the ghost and gluon propagators as functions of the momentum and Λ_{QCD} . The numerical coefficients for the β -function in (3.9) are summarised in the Table 3.1 :

	\widetilde{MOM}	\widetilde{MOM}_c	\widetilde{MOM}_{c0}
β_0	11		
β_1	102		
β_2	2412.16	2952.73	3040.48
β_3	84353.8	101484	100541

TAB. 3.1 – The numerical coefficients for the β -function for different MOM schemes [36]

3.2 OPE for the Green functions and dominant power corrections

The momentum dependence of the QCD Green functions at low energies is modified by non-perturbative effects. These effects show up by presence of power-corrections to logarithmic series or, in other words, by non-zero values of corresponding condensates. For example, such a non-perturbative object as instanton has a weight $\propto \exp -\frac{8\pi^2}{g^2(p^2)}$, giving at leading order a power correction $\propto \frac{1}{p^2}$. It is argued in ([37],[38]) that non-perturbative lattice gluonic two- and three-point functions include such contributions up to quite large energies of around 10 GeV. For a systematic study of Λ_{QCD} one has to know the influence of power corrections on the

Green functions.

A powerful tool to study the dependence of Green functions on the non-perturbative condensates is the Operator Product Expansion (OPE) [39]. This method is applicable to the problems having a specific energy hierarchy, or two very different characteristic energy scales. For example, in QCD it may be applied to the study of the influence of some background semi-classical field configurations. We recall here the idea of this method on the example of a two-point correlation function of a generic field ϕ

$$G(x) = \left\langle \phi \left(\frac{x}{2} \right) \phi \left(-\frac{x}{2} \right) \right\rangle. \quad (3.11)$$

It is postulated that when $x \rightarrow 0$ the product of the fields may be expanded as

$$\phi \left(\frac{x}{2} \right) \phi \left(-\frac{x}{2} \right) = \sum_{n=0}^{\infty} \sum_i w_i^n(x) \mathcal{O}_i^{[2n]}(0), \quad (3.12)$$

where the second sum is performed on all local operators $\mathcal{O}_i^{[2n]}$ of mass dimension $2n$ having the same quantum number than the l.h.s. The OPE suggests that all the features of the short-distance behaviour are stored in the Wilson coefficients

$$w_i^n(x) \sim \left(x^2 \right)^{(n-1)} \times \left[\text{series in } \alpha_s \right], \quad (3.13)$$

that can be calculated in perturbation theory. In Fourier space they behave as

$$\tilde{w}_i^n(p) \sim \left(\frac{1}{p^2} \right)^{(n+1)} \times \left[\text{series in } \alpha_s \right], \quad (3.14)$$

and thus

$$\tilde{G}(p) = \sum_{n=0}^{\infty} \sum_i \tilde{v}_i^n \left(\alpha_s, \log \left(p^2 / \mu^2 \right), a^{-1} \right) \frac{\langle \mathcal{O}_i^{[2n]} \rangle}{(p^2)^{n+1}}, \quad (3.15)$$

where the coefficients \tilde{v}_i^n are computed in perturbation theory, and $\langle \mathcal{O}_i^{[2n]} \rangle$ are **vacuum condensates**. At $n = 0$, corresponding to the trivial basic operator \mathbb{I} , we find an ordinary perturbative series for \tilde{G} . But other condensates may lead to the appearance of non-perturbative power corrections. Usually this method is applied to gauge-invariant product of currents, and involves only gauge invariant quantities (for a recent review see [40]). However it can be extended to gauge-dependent operators (like QCD propagators) and involve gauge-variant condensates ([41],[42]). We do not discuss here the subtle question of the renormalisation of condensates and of calculation of their anomalous dimensions. On the lattice the MOM-type renormalisation process is non-ambiguous ([43],[44]), because the non-perturbative value for the l.h.s in (3.15) is available. This allows to define the condensates at fixed ultra-violet cut-off. Then one can apply a MOM renormalisation prescription on the both sides of (3.15) and thus renormalise the condensates $\langle \mathcal{O}_i^{[2n]} \rangle$.

In the following paragraph we will discuss the dominant power corrections, and corresponding condensates, in the case of the gluon and ghost correlators.

3.2.1 The dominant OPE power correction for the gluon propagator

The basis of operators in the pure Yang-Mills case is

$$\underline{\mathbb{I}} \quad A_\mu^a \quad c^a \quad \partial_\mu A_\nu^a \quad \bar{c}^a c^b \quad A_\mu^a c^b \quad \underline{A_\mu^a A_\nu^b} \quad \partial_\mu c^a \quad \bar{c}^a \bar{c}^b \quad c^a c^b \quad \dots \quad (3.16)$$

At the leading order ($\alpha \propto 1/p^2$ power correction compared to perturbation theory) only underlined operators contribute [43] to the gluon propagator, because operators with an odd number of fields cannot satisfy colour and Lorentz invariance and $\bar{c}c$ does not contribute because of the particular structure of the ghost-gluon vertex (cf. Figure 3.1(b)). We write then for the gluon propagator :

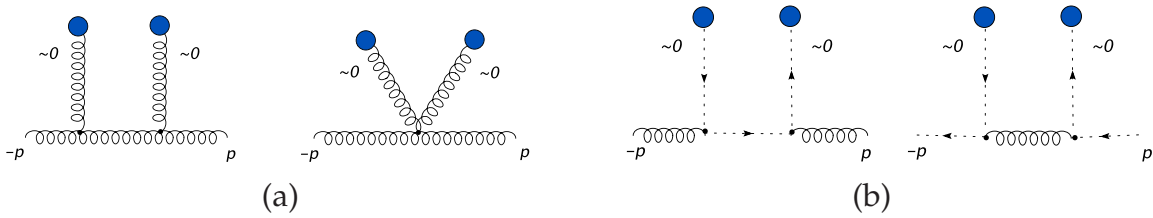


FIG. 3.1 – (a) Contribution of the gluon A^2 -condensate (represented as soft external gluons) to the gluon two-point function (b) Contribution of the ghost $\bar{c}c$ condensate (represented as soft external ghosts) to the gluon and ghost two-point functions. These contributions vanish because they are proportional to (\sim zero) momentum of the outgoing ghost is the ghost-gluon vertex.

$$\begin{aligned} \left(\tilde{G}^{(2)}\right)_{\mu\nu}^{ab}(p^2) &\equiv \left\langle T \left(\tilde{A}_\mu^a(-p) \tilde{A}_\nu^b(p) \right) \right\rangle = \\ &= (V_0)_{\mu\nu}^{ab}(p^2) + (V_2)_{\mu\nu\mu'\nu'}^{aba'b'}(p^2) \delta^{a'b'} \delta_{\mu'\nu'} \frac{\left\langle : A_\rho^c(0) A_\rho^c(0) : \right\rangle}{4(N_c^2 - 1)} + \dots, \end{aligned} \quad (3.17)$$

where $\langle \bullet \rangle$ is a v.e.v with respect to the non-perturbative vacuum and $: A_\rho^c(0) A_\rho^c(0) :$ is a free-field normal product. In the perturbative vacuum the v.e.v. of all the normal products give zero, and thus only V_0 is non-vanishing. Hence

$$(V_0)_{\mu\nu}^{ab}(p^2) = \left(\tilde{G}_{\text{pert}}^{(2)}\right)_{\mu\nu}^{ab}(p^2). \quad (3.18)$$

The coefficient V_2 is obtained at the tree-level order from

$$\langle g | : A_\rho^c(0) A_\rho^c(0) : | g \rangle = 2 + O(\alpha_s) \quad (3.19)$$

and

$$\langle g | T \left(\tilde{A}_\mu^a(-p) \tilde{A}_\nu^b(p) \right) | g \rangle_{\text{connected}} = (V_2)_{\mu\nu\mu'\nu'}^{aba'b'}(p^2) \langle g | : \tilde{A}_{\mu'}^{a'}(0) \tilde{A}_{\nu'}^{b'}(0) : | g \rangle, \quad (3.20)$$

where $|g\rangle$ is a soft gluon state. So, using the LSZ rule to cut the soft external gluons, we obtain

$$(V_2)_{\mu\nu\mu'\nu'}^{aba'b'}(p^2) = \frac{1}{2} \frac{\langle \tilde{A}_\tau^t(0) \tilde{A}_\mu^a(-p) \tilde{A}_\nu^b(p) \tilde{A}_\sigma^s(0) \rangle}{\left(G_{\text{pert}}^{(2)}(0)\right)_{\tau\mu'}^{ta'} \left(G_{\text{pert}}^{(2)}(0)\right)_{\sigma\nu'}^{sb'}}, \quad (3.21)$$

which can be computed in perturbation theory (cf. Figure 3.1(a)). Finally,

$$\left(\tilde{G}^{(2)}\right)_{\mu\nu}^{ab}(p^2) = \frac{1}{p^2} \left(\delta_{\mu\nu} - \frac{p_\mu p_\nu}{p^2} \right) \left(p^2 \tilde{G}_{\text{pert}}^{(2)}(p^2) + N_C \frac{g_0^2 \langle A^2 \rangle}{4(N_C^2 - 1)} \frac{1}{p^2} + O(g^4, p^{-4}) \right). \quad (3.22)$$

A MOM-type renormalisation prescription may be defined non-perturbatively. This allows an easy renormalisation procedure for the A^2 -condensate [43]. Here we do not include the effects of the anomalous dimension of the A^2 operator [45] and hence we apply the MOM prescription by imposing the tree-level value to the Wilson coefficient at the renormalisation point $p^2 = \mu^2$ for the last equation. This allows to factorise the perturbative gluon propagator giving finally

$$Z_3(\mu^2) = Z_{3,\text{pert}}(\mu^2) \left(1 + \frac{N_C}{\mu^2} \frac{g_R^2 \langle A^2 \rangle_R}{4(N_C^2 - 1)} + O(g_R^4, \mu^{-4}) \right). \quad (3.23)$$

3.2.2 The dominant OPE power correction for the ghost propagator

In the case of the ghost propagator the set of basic operators is the same, the ghost condensate $\bar{c}c$ does not contribute for the same reasons as for the gluon propagator (cf. Figure 3.1(b)). Thus, applying the OPE to the ghost two-point function, we obtain :

$$\begin{aligned} \tilde{F}^{(2)ab}(p^2) &= (\tilde{V}_0)^{ab}(p^2) + \left(\tilde{V}_2\right)_{st}^{ab\sigma\tau}(p^2) \langle : A_\sigma^s(0) A_\tau^t(0) : \rangle + \dots \\ &= F_{\text{pert}}^{(2)ab}(p^2) + w^{ab} \frac{\langle A^2 \rangle}{4(N_C^2 - 1)} + \dots \end{aligned} \quad (3.24)$$

where, in analogy with (3.21), the Wilson coefficient reads

$$w^{ab} = \left(\tilde{V}_2\right)_{st}^{ab\sigma\tau} \delta^{st} \delta_{\sigma\tau} = \frac{1}{2} \delta^{st} \delta_{\sigma\tau} \frac{\int d^4x e^{ip \cdot x} \langle \tilde{A}_{\tau'}^{t'}(0) T \left(\bar{c}^a c^b \right) \tilde{A}_{\sigma'}^{s'}(0) \rangle_{\text{connected}}}{G_{\sigma\sigma'}^{(2)ss'}(0) G_{\tau\tau'}^{(2)tt'}(0)} \quad (3.25)$$

which is equal to twice the diagram represented on the Figure 3.2 that describes the coupling of the ghost propagator to the gluon A^2 -condensate. Hence

$$w^{ab} = \frac{1}{2} \delta^{st} \delta_{\sigma\tau} \cdot 2 \frac{\delta^{aa_1}}{p^2} (ig_0 f^{a_2 t a_1}) \frac{\delta^{a_2 a_3}}{p^2} (ig_0 f^{a_4 s a_3}) \frac{\delta^{a_4 b}}{p^2} = N_C \frac{g_0^2}{p^2} \tilde{F}_{\text{tree}}^{(2)ab}(p^2). \quad (3.26)$$

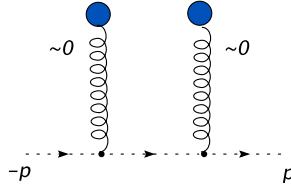


FIG. 3.2 – Contribution of the gluon A^2 -condensate (external soft gluons) to the ghost propagator

This gives the leading non-perturbative contribution, because the first Wilson coefficient trivially gives the perturbative ghost propagator. Finally,

$$\tilde{F}^{(2)ab}(p^2) = \tilde{F}_{\text{pert}}^{(2)ab}(p^2) \left(1 + \frac{N_C}{q^2} \frac{g_0^2 \langle A^2 \rangle}{4(N_C^2 - 1)} + \mathcal{O}(g_0^4, q^{-4}) \right) \quad (3.27)$$

where all quantities are bare. Performing the MOM renormalisation we obtain for the renormalisation factor :

$$\widetilde{Z}_3(\mu^2) = \widetilde{Z}_{3,\text{pert}}(\mu^2) \left(1 + \frac{N_C}{\mu^2} \frac{g_R^2 \langle A^2 \rangle_R}{4(N_C^2 - 1)} + \mathcal{O}(g_R^4, \mu^{-4}) \right), \quad (3.28)$$

where the A^2 -condensate is renormalised as in the case of the gluon propagator. We see that the dominant multiplicative correction to the perturbative $\widetilde{Z}_{3,\text{pert}}$ is identical to the one obtained in the previous section for the gluon propagator (3.23).

3.2.3 Constraints on the Wilson coefficients from the Slavnov-Taylor identity

The gauge-dependent power corrections due to the $\langle A^2 \rangle$ -condensate are obviously absent in gauge-invariant quantities. Because of this the Wilson coefficients for the $\langle A^2 \rangle$ -condensate in different Green functions are not independent. Some relations may be obtained from the Slavnov-Taylor identity (1.45) but their role in the MOM renormalisation constants is not obvious.

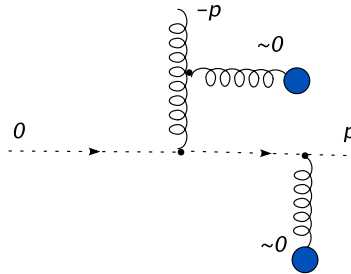


FIG. 3.3 – The $\langle A^2 \rangle$ contribution to the ghost-gluon vertex with vanishing entering momentum. The above diagram is zero in Landau gauge because of the projector in the gluon propagator.

It is interesting to know if there are any power corrections to this vertex, because perturbation theory predicts the non-renormalisation of this vertex, i.e. it is

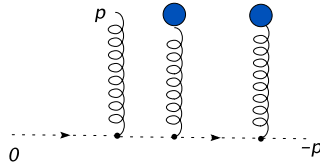


FIG. 3.4 – Non-zero dominant $\langle A^2 \rangle$ contribution to the ghost-gluon vertex with vanishing entering momentum. This term contribute to the external ghost propagator.

equal to 1 to all orders ([8],[34]). If the $\langle A^2 \rangle$ power corrections are present they will constitute the main contribution at low energies. One can directly evaluate the Wilson coefficient to the ghost-gluon vertex $\tilde{\Gamma}_\mu^{abc}(-p, 0; p)$ with vanishing entering ghost momentum.

The only non-zero correction to the ghost-gluon vertex with one vanishing ghost momentum is the one that contributes to the external ghost propagator (see Figure 3.4). But all the diagrams with the condensate interaction attached to different external legs are zero in Landau gauge (see Figure 3.3). Thus the ghost-gluon vertex in this particular kinematic configuration does not contain the $\frac{1}{p^2}$ power-corrections, and thus the non-renormalisation theorem holds at this order. However, this it is not true if the external ghost momentum is not *exactly* zero.

3.3 Data analysis

We calculated, using the techniques described in the chapter 2, the ghost and the gluon propagators of the Landau gauge $SU(3)$ gauge theory at different lattice volumes and different values of the β parameter (cf. Table 3.2) [21]. The lattices mar-

β	V	a^{-1} (GeV)	V_{phys} (fm ⁴)	# Configurations
→ 6.0	16 ⁴	1.96	6.73	1000
6.0	24 ⁴	1.96	33.17	500
→ 6.2	24 ⁴	2.75	8.43	500
→ 6.4	32 ⁴	3.66	8.85	250

TAB. 3.2 – Lattice setup parameters. The lattice spacings are taken from Table 3 in [46] with a physical unit normalised by $\sqrt{\sigma} = 445$ MeV. The lattices marked by the “→” symbol have similar physical volume.

ked by the “→” symbol correspond to similar physical volume. The produced data allow us to study the propagators in the momentum range [$\approx 2\text{GeV}$, $\approx 6.5\text{GeV}$].

This section is organised in the following way. In the first subsection we present the fits of the ghost and the gluon propagators separately, and compare the fitted values for Λ_{QCD} . Thus we test the self-consistency of the method. Non-perturbative effects are quite important in the energy interval accessible to us. This is why another motivation is to study the asymptoticity of the perturbative series. The latter is done by comparing the results in different renormalisation schemes ($R = \overline{\text{MS}}, \widetilde{\text{MOM}}, \widetilde{\text{MOM}}_c, \widetilde{\text{MOM}}_{c0}$) and at different orders (from two to four loops). In the second subsection we use the analytical result of the previous section namely that

the dominant non-perturbative effects are the same for the ghost and for the gluon propagators, and hence the ratio of the gluon and the ghost dressing functions is better described by perturbation theory at low energies. We shall see that lattice data support this claim.

3.3.1 Fitting the gluon and the ghost propagators

We extracted Λ_{QCD} from the dressing functions of our lattice propagators by fitting them to the formula (3.8) (with h given by (3.10)) in different MOM renormalisation schemes. There are two parameters of the fit - the wanted Λ_{QCD} and the integration constant Z_0 . An example of such a fit is presented at Figure 3.5. The ob-

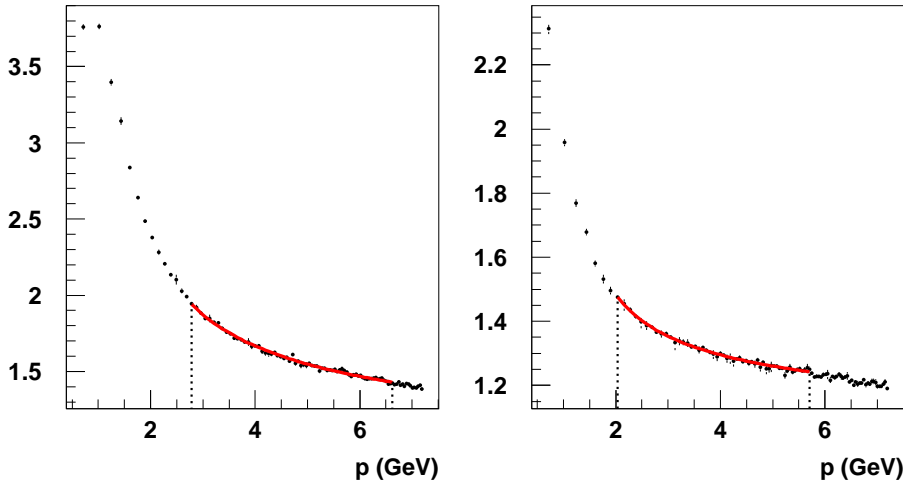


FIG. 3.5 – Extrapolated lattice data at $\beta = 6.4$ for $G(p)$ (left) and $F(p)$ (right). The solid line is the fit at four-loop order in the $\overline{\text{MS}}$ scheme. The vertical dotted lines delimit the window of each fit.

tained value of Λ_R in a scheme R is converted to the $\overline{\text{MS}}$ scheme using the exact² asymptotic formulae

$$\begin{aligned}\Lambda_{\overline{\text{MS}}} &= 0.346 \Lambda_{\widetilde{\text{MOM}}} \\ \Lambda_{\overline{\text{MS}}} &= 0.429 \Lambda_{\widetilde{\text{MOM}}_c} \\ \Lambda_{\overline{\text{MS}}} &= 0.428 \Lambda_{\widetilde{\text{MOM}}_{c0}}\end{aligned}\quad (3.30)$$

The results in $\overline{\text{MS}}$ are given in Tables 3.3,3.4,3.5. The errors include the statistical error, extrapolation errors and the bias due to the choice of the fit window. We see from these tables that at a given order and in a given renormalisation scheme

²A relation between the values of Λ_{QCD} in different schemes A and B reads

$$\frac{\Lambda^B}{\Lambda^A} = \exp \left[\frac{1}{2\beta_0} \left(\frac{1}{g_A^2(\mu^2)} - \frac{1}{g_B^2(\mu^2)} \right) + O(g^2(\mu^2)) \right]. \quad (3.29)$$

If $g_B^2 = g_A^2 \left(1 + \zeta \frac{g_A^2}{4\pi} + \dots \right)$ then the asymptotic freedom gives $\Lambda^B = \Lambda^A e^{\frac{\zeta}{2\beta_0}}$. Thus the exact conversion coefficient is given by an one-loop calculation [47].

β	$\Lambda_{\overline{\text{MS}},\text{gluon}}^{(3)}$	$\Lambda_{\overline{\text{MS}},\text{ghost}}^{(3)}$	$\Lambda_{\overline{\text{MS}},\text{gluon}}^{(4)}$	$\Lambda_{\overline{\text{MS}},\text{ghost}}^{(4)}$
6.0	$519(6)_{-4}^{+12}$	$551(12)_{-16}^{+33}$	$441(4)_{-4}^{+8}$	$461(10)_{-14}^{+29}$
6.2	$509(6)_{-27}^{+17}$	$550(8)_{-63}^{+27}$	$435(6)_{-19}^{+11}$	$465(8)_{-36}^{+33}$
6.4	$476(7)_{-40}^{+44}$	$549(7)_{-51}^{+55}$	$410(4)_{-29}^{+33}$	$468(7)_{-40}^{+48}$

TAB. 3.3 – Three-loop and four-loop physical values of $\Lambda_{\overline{\text{MS}}}$ in MeV extracted from fits in the $\overline{\text{MS}}$ scheme.

β	$\Lambda_{\overline{\text{MS}},\text{gluon}}^{(3)}$	$\Lambda_{\overline{\text{MS}},\text{ghost}}^{(3)}$	$\Lambda_{\overline{\text{MS}},\text{gluon}}^{(4)}$	$\Lambda_{\overline{\text{MS}},\text{ghost}}^{(4)}$
6.0	$324(2)_{-5}^{+2}$	$322(8)_{-16}^{+20}$	—	—
6.2	$320(2)_{-14}^{+8}$	$326(5)_{-33}^{+26}$	—	$331(8)_{-16}^{+21}$
6.4	$312(1)_{-25}^{+9}$	$331(4)_{-35}^{+42}$	$320(4)_{-4}^{+6}$	$353(9)_{-38}^{+17}$

TAB. 3.4 – Three-loop physical values of $\Lambda_{\overline{\text{MS}}}$ in MeV converted from fits in the $\widetilde{\text{MOM}}$ scheme.

β	$\Lambda_{\overline{\text{MS}},\text{gluon}}^{(3)}$	$\Lambda_{\overline{\text{MS}},\text{ghost}}^{(3)}$	$\Lambda_{\overline{\text{MS}},\text{gluon}}^{(4)}$	$\Lambda_{\overline{\text{MS}},\text{ghost}}^{(4)}$
6.0	$345(3)_{-4}^{+4}$	$369(9)_{-2}^{+3}$	—	—
6.2	$341(2)_{-7}^{+6}$	$364(8)_{-19}^{+11}$	$344(4)_{-6}^{+9}$	$357(10)_{-16}^{+8}$
6.4	$323(2)_{-11}^{+17}$	$354(8)_{-20}^{+28}$	$332(2)_{-30}^{+14}$	$351(8)_{-25}^{+23}$

TAB. 3.5 – Three-loop physical values of $\Lambda_{\overline{\text{MS}}}$ in MeV converted from fits in the $\widetilde{\text{MOM}}_c$ scheme.

the values obtained from the gluon and ghost propagators are consistent within the error bars, and are quite independent of the ultraviolet cut-off. The results from a direct fit in the $\overline{\text{MS}}$ scheme (Table 3.3) confirm the old claim that we are still far from asymptoticity in the considered momentum interval in this scheme [48]. Our analysis suggests that the perturbative series become asymptotic at the NNLO in the case of $\widetilde{\text{MOM}}$ and $\widetilde{\text{MOM}}_c$ renormalisation schemes. However, the property of asymptoticity is only approximate at considered momenta. To see this one can use the perturbative expression (analogue to (3.3)) for Λ_R in terms of the coupling h_R to the order four

$$2 \ln \Lambda_R^{(4)} = \ln \mu^2 - \frac{1}{\beta_0 h_R} - \frac{\beta_1}{\beta_0^2} \ln(\beta_0 h_R) - \frac{\beta_0 \beta_2 - \beta_1^2}{\beta_0^3} h_R - \frac{\beta_0^2 \beta_3 - 2\beta_0 \beta_1 \beta_2 + \beta_1^3}{2\beta_0^4} h_R^2, \quad (3.31)$$

and plot the ratio (Figure 3.6) of the consecutive orders $\frac{\Lambda_R^{(n+1)}}{\Lambda_R^{(n)}}$. There is a qualitative agreement between the ratios presented at Figure 3.6 and our results (see Tables 5-10 in [21]). The influence of truncation, responsible for the differences between different orders and renormalisation schemes, is mostly due to the large value of the effective coupling at considered energies [21]. In fact, as shown in [37], the real value of the coupling constant may be smaller, because of the power correction discussed in the section 3.2. Indeed, according to the OPE analysis the effective coupling constant is modified by a factor

$$\alpha_s \rightarrow \alpha_s \left(1 + \text{const} \cdot \frac{\langle A^2 \rangle}{p^2} \right). \quad (3.32)$$

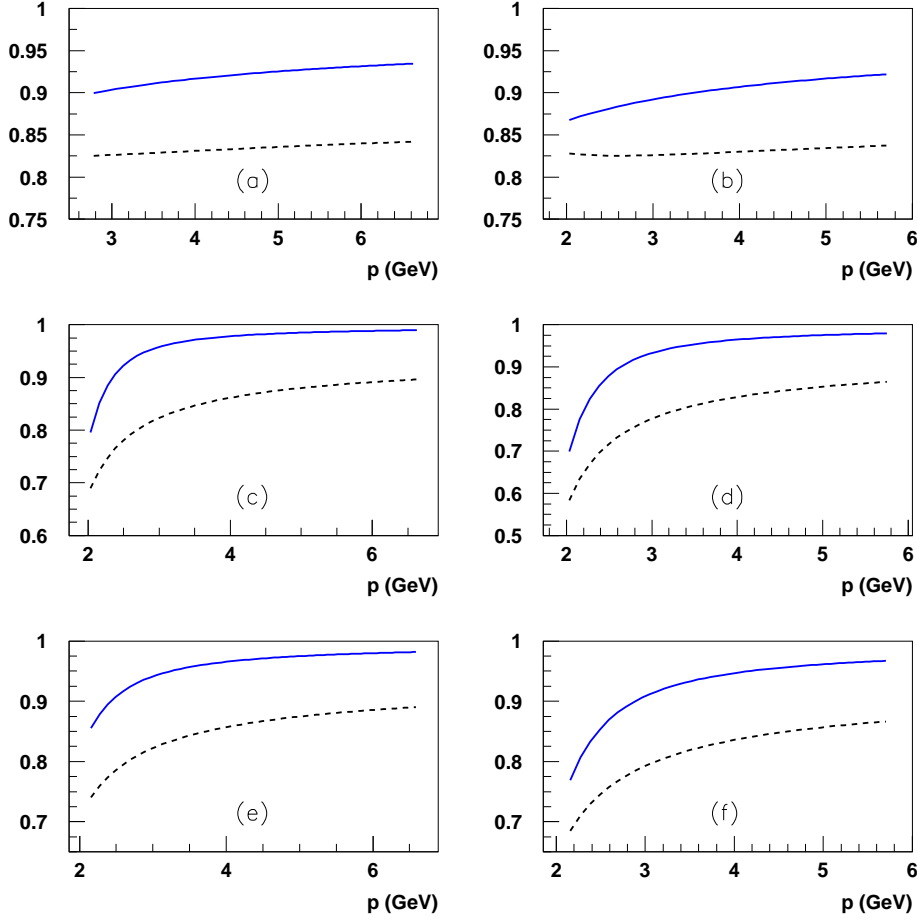


FIG. 3.6 – $\frac{\Lambda_R^{(n+1)}}{\Lambda_R^{(n)}}$ for $n = 2$ (dashed lines) and $n = 3$ (solid lines), for the gluon propagator in the $\overline{\text{MS}}$ scheme (a), $\widetilde{\text{MOM}}$ scheme (c) and $\widetilde{\text{MOM}}_c$ scheme (e), and for the ghost propagator in the $\overline{\text{MS}}$ scheme (b), $\widetilde{\text{MOM}}$ scheme (d) and $\widetilde{\text{MOM}}_c$ scheme (f).

According to the results of the section 3.2, one can eliminate the dominant power correction by considering the ratio of the propagators. In this case one expects a better behaviour of perturbative series at low momenta. We discuss this strategy in the following subsection.

3.3.2 Fit of the ratio

Given that at the leading order the non-perturbative power corrections factorise (3.23),(3.28) and are identical in the case of the ghost and gluon propagators, we can fit the ratio

$$\frac{\widetilde{Z}_3(q^2, \Lambda_R, \langle A^2 \rangle)}{Z_3(q^2, \Lambda_R, \langle A^2 \rangle)} = \frac{\widetilde{Z}_{3,\text{pert}}(q^2, \Lambda_R)}{Z_{3,\text{pert}}(q^2, \Lambda_R)}, \quad (3.33)$$

to the ratio of *perturbative* formulae in scheme R given by (3.8), and then convert Λ_R to $\Lambda_{\overline{\text{MS}}}$ using (3.30). It is interesting to notice that non-perturbative corrections cancel out in this ratio even in the unquenched case with $n_f \neq 0$ flavours of dynamical quarks. The Λ_{QCD} -parameter extracted from this ratio is free from non-perturbative power corrections up to contributions related to the operators of dimension four. In Table 3.6 the best-fit parameters for the three schemes are presented and we plot in Figure 3.7 the lattice data and the $\widetilde{\text{MOM}}$ best-fit curve for the ratio (3.33). In

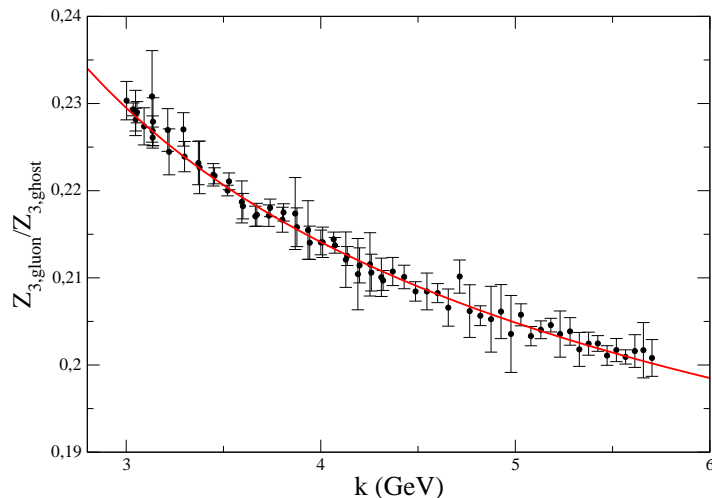


FIG. 3.7 – Plot (in the $\widetilde{\text{MOM}}$ scheme) of the $\frac{Z_3(p^2)}{\widetilde{Z}_3(p^2)}$ for the best fit parameter $\Lambda_{\overline{\text{MS}}} = 269(5)$ MeV.

scheme	$\Lambda_{\overline{\text{MS}}}^{(2)}$	$\chi^2/\text{n.d.f}$	$\Lambda_{\overline{\text{MS}}}^{(3)}$	$\chi^2/\text{n.d.f}$	$\Lambda_{\overline{\text{MS}}}^{4 \text{ loops}}$	$\chi^2/\text{n.d.f}$
$\widetilde{\text{MOM}}$	324(6)	0.33	269(5)	0.34	282(6)	0.34
$\widetilde{\text{MOM}}_c$	351(6)	0.33	273(5)	0.34	291(6)	0.33
$\widetilde{\text{MOM}}_{c0}$	385(7)	0.33	281(5)	0.34	298(6)	0.33

TAB. 3.6 – The best-fitted values of $\Lambda_{\overline{\text{MS}}}$ for the three considered renormalisation schemes. As discussed in the text, $\widetilde{\text{MOM}}_c$ seems to be the one showing the best asymptotic behaviour.

Figure 3.9 we show the evolution of the fitted parameter $\Lambda_{\overline{\text{MS}}}$ when changing the order of perturbation theory used in the fitting formula. One can conclude from Figure 3.9 that the $\widetilde{\text{MOM}}$ scheme at three loops gives the most stable result for $\Lambda_{\overline{\text{MS}}}$. It can also be seen from the ratio of four to three loops contributions (see Figure 3.10) for the perturbative expansion of $\ln Z_3$,

$$\ln Z_3 = r_0 \ln h_R + \sum_{i=1} r_i h_R^i, \quad (3.34)$$

where the coefficients r_i are to be computed from those in equations (3.6-3.10) using the Table 3.1. The same is done for $\ln \widetilde{Z}_3$.

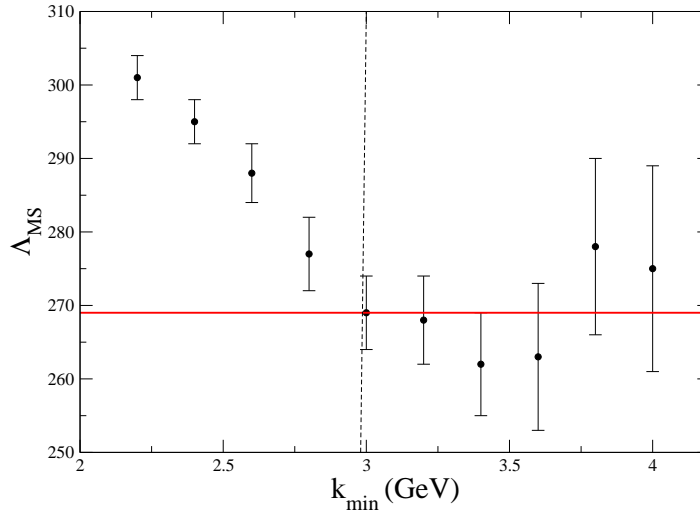


FIG. 3.8 – The determination of the optimal window fit (from 3 GeV to $k_{\max}a \leq \pi/2$) results from the search for some “plateau” of $\Lambda_{\overline{\text{MS}}}$ when one changes the low bound of the fit window. Fits are done in the $\widetilde{\text{MOM}}$ scheme.

According to our analysis, and in agreement with the result of the separate fit, three loops seems to be the optimal order for the asymptoticity³. Indeed, the values of $\Lambda_{\overline{\text{MS}}}$ for the three considered renormalisation schemes practically match each other at three loops (see Figure 3.9). The approximate value

$$\Lambda_{\overline{\text{MS}}} = 269(5)_{-9}^{+12} \quad (3.35)$$

could be presented as the result for the fits of the ratio of dressing functions to perturbative formulae.

The results of the previous subsection and [21] suggest that our present systematic uncertainty may be underestimated (narrowness of the momentum interval, truncation of the perturbative series, etc.), that is why we prefer simply to quote $\Lambda_{\overline{\text{MS}}} \approx 270$ MeV for future reference. This value is pretty smaller than the value of ≈ 330 MeV obtained by independent fits of dressing functions (see Tables 3.4,3.5). In light of our OPE analysis and previous results [44], this argues in favour of presence of low-order non-perturbative corrections to the ghost and gluon propagators in the momentum range [2 GeV, 6 GeV].

3.3.3 Comparing the results

We showed that perturbation theory is quite successful in describing (up to NNNLO) lattice propagators in the momentum range [2 GeV, 6 GeV], yielding compatible values of Λ_{QCD} . The separate fit of the ghost and gluon propagators, and the fit of their ratio favours the existence of $\propto \frac{1}{p^2}$ power corrections and validates the OPE approach in the case of ghost and gluon propagators. The difference with

³Note that the asymptoticity property is better verified in the case of the ratio, see Figure 3.9.

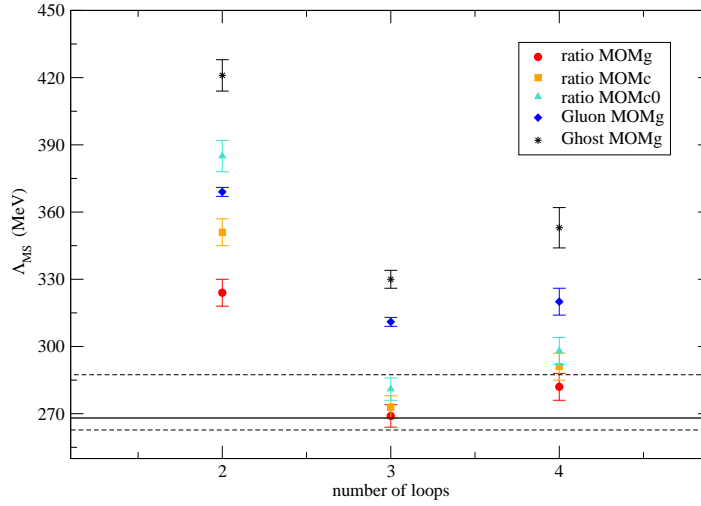


FIG. 3.9 – Evolution of the parameter $\Lambda_{\overline{\text{MS}}}$, extracted from fits of the ratio 3.33 and propagators alone (rhombus and star markers, extracted from Tables 3.4,3.5 [21]) to perturbative formulae, as function of the order of perturbation theory. The solid line corresponds to the value (3.35). Only statistical error is quoted.

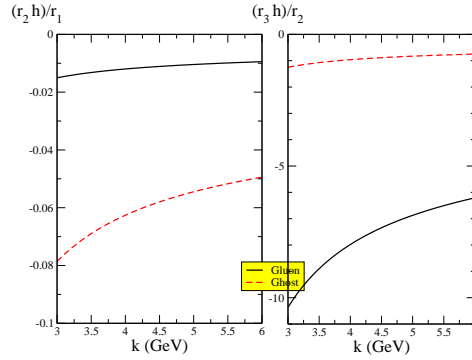


FIG. 3.10 – (b) Ratio of four-loop to three-loop contributions (and of three-loop to two-loops for the sake of comparison) for the perturbative expansion of $\log Z_3$ and $\log \widetilde{Z}_3$ (in $\overline{\text{MOM}}$) in 3.34, plotted versus the momenta inside our fitting window.

previous approaches is that we have not introduced any additional fit parameter, and have only used perturbation theory. Our method can also be used to calculate Λ_{QCD} from propagators alone in the unquenched case. In principle, it can be used to estimate the value of the $\langle A^2 \rangle$ condensate.

The main limitation of the application of perturbation theory to lattice Green functions in the accessible energy interval is the lack of asymptoticity and the truncation of the series. In fact, even the conversion formula (3.29) is not exact at considered momenta. We estimate the accuracy of our results at around 10%. It can be improved by performing the simulations at $\beta = 6.6, 6.8$ on the lattices of sizes $48^4, 64^4$, respectively. The choice of parameters is motivated by the necessity to have the same physical volume of the lattice in order to control the finite-size effects.

Chapitre 4

The infrared behaviour of Green functions

There are compelling reasons to think that confinement is a property of QCD, and does not result from some other theory. One of such indications is a non-zero value of the string tension found in the lattice simulations. As a matter of fact lattice simulations give access to many non-perturbative quantities. We are particularly interested in knowing the Landau gauge Green functions at low momenta, i.e. at energies of order and below than Λ_{QCD} . No free quarks or gluons exist at very small momenta because of confinement. So, a study of gluonic correlation functions in the deep-infrared domain may seem useless. However, in order to study the property of confinement from the first principles one has to understand the change in behaviour of Green functions found at low momenta. Knowing these functions exactly would be a great support for the future development of the theory, because many confinement scenarii (for example the Gribov-Zwanziger scenario) give predictions for low energies momentum dependence of the Green functions in Landau gauge. Lattice simulations allow to test these predictions.

Lattice results for different Green functions of QCD have been successfully tested at large momenta by perturbation theory up to NNNLO (see chapter 3 and [21],[49]). We shall see below that lattice Green functions also satisfy the complete ghost Schwinger-Dyson equation (see Figure 4.2). Thus lattice approach gives consistent results non only in the ultraviolet domain but also in the infrared one. Of course numerical methods could never give us complete Green functions for all possible values of momenta. Nevertheless, lattice gives a *quasi-unique method for testing different analytical approaches*, like study of truncated system of Schwinger-Dyson equations, renormalisation group flow equations and other non-perturbative relations like Slavnov-Taylor identities.

Most of analytical predictions are done for the infrared exponents α_F and α_G that describe power-law deviations from free propagators when $p \rightarrow 0$

$$\begin{aligned}
 p^2 G^{(2)}(p^2) &\equiv G(p^2) \propto \left(\frac{p^2}{\lambda_G^2} \right)^{\alpha_G} \\
 p^2 F^{(2)}(p^2) &\equiv F(p^2) \propto \left(\frac{p^2}{\lambda_F^2} \right)^{\alpha_F} \\
 &\dots
 \end{aligned}
 \tag{4.1}$$

where $\lambda_{G,F}$ are some fixed parameters of dimension one. When p is large, the functions $F(p^2)$ and $G(p^2)$ are logarithmic functions of momentum, and thus $\alpha_{F,G} = 0$. But at low momenta it may not be true. In fact, power-law behaviour is the crudest approximation, allowing to exhibit the most general features of the momentum dependence of the Green functions in the infrared. The real law governing the infrared gluodynamics might be much more complicated. In the following section we review (very briefly) different predictions for the exponents α_G and α_F of, respectively, the gluon and ghost two-point functions. Next we present our analysis of the Slavnov-Taylor identities imposing some limits on these exponents. After this we turn to the study of the ghost Schwinger-Dyson equation and test the widely accepted relation (4.20) between the exponents α_G and α_F . Our conclusion (supported by numerical simulations) is that this relation is not valid. We revisit the usual proof and conclude that either the ghost-gluon vertex behaves unexpectedly in the infrared, or that $\alpha_F = 0$. At the end of the chapter we discuss the results of direct fits of two-point functions, and compare our results with other lattice collaborations.

4.1 Review of today's analytical results

In this section we quote the main analytical results regarding the infrared exponents (4.1). We start with the Zwanziger's prediction obtained for gluonic correlation functions. Next we present the results of other analytical approaches.

4.1.1 Zwanziger's prediction

Zwanziger suggested in [50],[51] that the (Landau gauge) gluon propagator vanishes at zero momentum in the infinite volume limit. The argument is the following. The Faddeev-Popov operator (1.68) is positive definite at a local minimum of the functional (1.60)

$$(\omega, \mathcal{M}_{FP}^{\text{lat}}[U]\omega) \geq 0. \quad (4.2)$$

Choosing a test vector

$$\omega^a(x) = \frac{\exp i \frac{2\pi e_\mu}{L} x}{\sqrt{V}} \chi^a, \quad (4.3)$$

where the normalised colour vector χ^a is an eigenfunction of the "angular momentum" operator $(J^b)_{ac} = if^{abc}$, one obtains from (1.68) and (4.2) the following limit on the mean colour spin

$$\left| \frac{1}{V} \sum_x A_\mu(x) \right| \leq 2 \tan \frac{\pi}{L}. \quad (4.4)$$

Introducing an external colour field H_μ^a source (independent of x), one obtains from (4.4) an estimate for the generating functional

$$\frac{Z(H)}{Z(0)} = \frac{1}{Z(0)} \int [D\mathcal{A}] e^{-S[\mathcal{A}] + H_\mu^a \sum_x A_\mu^a(x)} \leq e^{2V \sum_\mu |H_\mu| \tan \frac{\pi}{L}}. \quad (4.5)$$

The free energy density $w(H) = \frac{1}{V} \log Z[H]$ is convex and bounded from below ($w(0) = 0$), thus one has

$$0 \leq w(H) \leq 2 \sum_{\mu} |H_{\mu}| \tan \frac{\pi}{L}. \quad (4.6)$$

All connected gluonic Green functions can be obtained by calculating the variations of the free energy with respect to the external sources $H_{\mu}^a(x)$. The last inequality suggest that in the infinite volume limit all Green functions vanish at zero momentum. However, the inversion of derivation and thermodynamic limit is not supported by a rigorous proof.

4.1.2 Study of truncated SD and ERG equations

Diverse analytical approaches (study of truncated Schwinger-Dyson equations and of renormalisation group equation, see Table 4.1) agree that the infrared divergence of the ghost propagator is enhanced, i.e. $\alpha_F \leq 0$; while they predict different values for α_G , mostly around $\alpha_G \approx 1.2$. This means that the gluon propagator is suppressed in the infrared. However, some groups obtain $\alpha_G \leq 1$, i.e. an infrared-divergent gluon propagator. Lattice simulations confirmed the prediction for the ghost propagator, whereas the lattice gluon propagator seems to remain finite and non-zero in the infrared, i.e. $\alpha_G = 1$. We discuss this question in details in the section 4.5.

Reference	Method	α_G	α_F
Zwanziger [50]	see subsection 4.1.1	> 1	no
Bloch [52]	SD truncation + perturbation theory	[0.34, 1.06]	[-0.53, -0.17]
von Smekal et al. [53]	SD truncation	1.84	-0.92
Zwanziger [54]	SD truncation + Zwanziger condition	2 or 1.19	-1 or -0.595
Aguilar et al. [55]	SD equation	0.98	-0.04
Kato [56]	ERGE	0.292	-0.146
Pawlowski et al. [57]	ERGE	1.19	-0.595
Fischer et al. [58]	ERGE	1.02	-0.52

TAB. 4.1 – Summary of various analytical predictions

4.2 Constraints on the infrared exponents and the Slavnov-Taylor identity

Let us consider the Slavnov-Taylor identity (1.45) relating the three-gluon vertex $\Gamma_{\lambda\mu\nu}$, the ghost-gluon vertex $\tilde{\Gamma}_{\lambda\mu}(p, q; r)$ and the ghost and gluon propagators :

$$p^{\lambda} \Gamma_{\lambda\mu\nu}(p, q, r) = \frac{F(p^2)}{G(r^2)} (\delta_{\lambda\nu} r^2 - r_{\lambda} r_{\nu}) \tilde{\Gamma}_{\lambda\mu}(r, p; q) - \frac{F(p^2)}{G(q^2)} (\delta_{\lambda\mu} q^2 - q_{\lambda} q_{\mu}) \tilde{\Gamma}_{\lambda\nu}(q, p; r). \quad (4.7)$$

Taking the limit $r \rightarrow 0$ keeping q and p finite, and using the parametrisation $G(r^2) \simeq (r^2)^{\alpha_G}$ valid for $r^2 \ll \Lambda_{\text{QCD}}^2$, one finds the following limits on the infrared exponents

$$\begin{cases} \alpha_G < 1 & \text{gluon propagator } \textit{diverges} \text{ in the infrared, and} \\ \alpha_F \leq 0 & \text{the divergence of the ghost propagator is } \textit{unchanged} \text{ or } \textit{enhanced} \text{ in the infrared} \end{cases} \quad (4.8)$$

Let us discuss in details the origin of the limits (4.8). The ghost-gluon vertex $\tilde{\Gamma}_{\mu\nu}(p, k; q)$ may be parametrised [59] in the most general way as

$$\tilde{\Gamma}_{\mu}^{abc}(p, k; q) = f^{abc}(-ip_\nu) g_0 \tilde{\Gamma}_{\nu\mu}(p, k; q) \quad (4.9)$$

$$= f^{abc}(-ip_\nu) g_0 \cdot [\delta_{\nu\mu} a(p, k; q) - q_\nu k_\mu b(p, k; q) + p_\nu q_\mu c(p, k; q) + q_\nu p_\mu d(p, k; q) + p_\nu p_\mu e(p, k; q)] \quad (4.10)$$

We recall that in this formula $-p$ is the momentum of the outgoing ghost, k is the momentum of the incoming one and $q = -p - k$ the momentum of the gluon (all momenta are taken as entering). For some particular kinematic configurations we use the following dense notations

$$\begin{aligned} a_3(p^2) &= a(-p, p; 0) \\ a_1(p^2) &= a(0, -p; p), \quad b_1(p^2) = b(0, -p; p), \quad d_1(p^2) = d(0, -p; p). \end{aligned} \quad (4.11)$$

The limit $r^2 \rightarrow 0$ leads to an asymmetric kinematic configuration for the three-gluon vertex in the l.h.s. of (4.7). This particular configuration allows a general parametrisation [34]

$$\Gamma_{\mu\nu\rho}(p, -p, 0) = (2\delta_{\mu\nu} p_\rho - \delta_{\mu\rho} p_\nu - \delta_{\rho\nu} p_\mu) T_1(p^2) - \left(\delta_{\mu\nu} - \frac{p_\mu p_\nu}{p^2} \right) p_\rho T_2(p^2) + p_\mu p_\nu p_\rho T_3(p^2). \quad (4.12)$$

with functions $\widehat{T_{1,2,3}}(p^2)$. The scalar function $T_1(p^2)$ is proportional to the gauge coupling in the MOM renormalisation scheme. Now, exhibiting the dominant part of each term in (4.7), we obtain

$$\begin{aligned} & T_1(q^2) (q_\mu q_\nu - q^2 \delta_{\mu\nu}) + q^2 T_3(q^2) q_\mu q_\nu + \eta_{1\mu\nu}(q, r) = \\ & \frac{F((q+r)^2)}{G(r^2)} \left[(a_1(q^2) + r_1(q, r)) (\delta_{\mu\nu} r^2 - r_\mu r_\nu) + (b_1(q^2) + r_2(q, r)) q_\mu (r^2 q_\nu - (q \cdot r) r_\nu) + \right. \\ & \quad \left. + (b_1(q^2) + d_1(q^2) + r_3(q, r)) r_\mu (r^2 q_\nu - (q \cdot r) r_\nu) \right] + \\ & \quad + \frac{F((q+r)^2)}{G(q^2)} \left[a_3(q^2) (q_\mu q_\nu - q^2 \delta_{\mu\nu}) + \eta_{2\mu\nu}(q, r) \right] \end{aligned} \quad (4.13)$$

with $r_{1,2,3}$ and $\eta_{1,2}$ satisfying

$$\begin{aligned} \lim_{r \rightarrow 0} r_1(q, r) &= \lim_{r \rightarrow 0} r_2(q, r) = \lim_{r \rightarrow 0} r_3(q, r) = 0 \\ \lim_{r \rightarrow 0} \eta_{1\mu\nu}(q, r) &= \lim_{r \rightarrow 0} \eta_{2\mu\nu}(q, r) = 0 \end{aligned} \quad (4.14)$$

Identifying the leading terms of the scalar factors multiplying the tensors $q_\mu q_\nu$ and

$(q_\mu q_\nu - q^2 \delta_{\mu\nu})$ we obtain the usual relations ([34]) :

$$\begin{aligned} T_1(q^2) &= \frac{F(q^2)}{G(q^2)} a_3(q^2) \\ T_3(q^2) &= 0. \end{aligned} \quad (4.15)$$

Using these relations in (4.13) we get

$$\lim_{r \rightarrow 0} \frac{F(p^2)}{G(r^2)} \left[a_1(q^2) (r^2 \delta_{\mu\nu} - r_\mu r_\nu) + b_1(q^2) (r^2 q_\mu q_\nu - (r \cdot q) q_\mu r_\nu) \right] = 0. \quad (4.16)$$

Thus one sees that if

$$a_1(q^2) \neq 0 \quad \text{or} \quad b_1 \neq 0 \quad (4.17)$$

then (4.7) can only be compatible with the parametrisation (4.1) if

$$\alpha_G < 1. \quad (4.18)$$

The condition (4.17) is satisfied because at large momentum one has to all orders $a_1(p^2) = 1$ (because of the non-renormalisation theorem [8],[34]).

We can also, instead of letting $r \rightarrow 0$, take the limit $p \rightarrow 0$ of (1.45) as is done in [34]. The dominant part of the l.h.s. of (1.45) is

$$\left(2\delta_{\mu\nu}(p \cdot q) - p_\mu q_\nu - p_\nu q_\mu \right) T_1(q^2) - \left(\delta_{\mu\nu} - \frac{q_\mu q_\nu}{q^2} \right) (p \cdot q) T_2(q^2) + (p \cdot q) q_\mu q_\nu T_3(q^2) \quad (4.19)$$

The r.h.s. is the product of $F(p^2)$ with an expression of at least first order in p . T_1 and T_2 being different from zero we can conclude in this case that $\alpha_F \leq 0$.

Let us repeat here that all these considerations are valid only if all scalar factors of the ghost-ghost-gluon and three-gluons vertices are regular functions when one momentum goes to zero while the others remain finite. Under those quite reasonable hypotheses one obtains important constraints on the gluon and ghost propagators - namely that they are both divergent in the zero momentum limit, and the divergence of the ghost propagator is enhanced.

Let us stress that the limit (4.8) on α_G disagrees with many other analytical predictions quoted in the section 4.1.

4.3 Relation between the infrared exponents

The Schwinger-Dyson equation for the two-point correlation function (and for the quark propagator, but we consider only pure Yang-Mills case here) has the simplest form among other non-perturbative relations between Green functions. It has been used to constrain the the infrared exponents. Even more, there is a commonly accepted relation between the infrared exponents

$$2\alpha_F + \alpha_G = 0. \quad (4.20)$$

which we shall discuss now. The origin of this relation is the dimensional analysis of the Schwinger-Dyson equation for the ghost propagator

$$\frac{1}{F(k)} = 1 + g_0^2 N_c \int \frac{d^4 q}{(2\pi)^4} \left(\frac{F(q^2) G((q-k)^2)}{q^2 (q-k)^2} \left[\frac{(k \cdot q)^2 - k^2 q^2}{k^2 (q-k)^2} \right] H_1(q, k) \right), \quad (4.21)$$

where $H_1(q, k)$ is one of the scalar functions defining the ghost-gluon vertex :

$$q_\nu \tilde{\Gamma}_{\nu\nu}(-q, k; q-k) = q_\nu H_1(q, k) + (q-k)_\nu H_2(q, k), \quad (4.22)$$

where $H_{1,2}$ are functions of the factors a, b, c, d, e (4.9). The large momentum behaviour ([34],[8]) of this vertex depends on the kinematic configuration :

$$\begin{aligned} \frac{p_\mu p_\nu}{p^2} \cdot \tilde{\Gamma}_{\mu\nu}^{\overline{\text{MS}}}(-p, 0; p) &= 1 \quad \text{to all orders} \\ \frac{p_\mu p_\nu}{p^2} \cdot \tilde{\Gamma}_{\mu\nu}^{\overline{\text{MS}}}(-p, p; 0) &= 1 + \frac{9}{16\pi} \alpha_s(p^2) + \dots \end{aligned} \quad (4.23)$$

Note that in the case of the vanishing momentum of the out-going ghost (and only in this case) the non-renormalisation theorem is applicable [8] and hence

$$H_1(q, 0) + H_2(q, 0) = 1. \quad (4.24)$$

Let us now consider two infrared scales $k_1 \equiv k$ and $k_2 \equiv \kappa k$. Calculating the difference of the Schwinger-Dyson equation (4.21) taken at scales k_1 and k_2 and supposing for the moment that $\alpha_F \neq 0$ one obtains

$$\begin{aligned} \frac{1}{F(k)} - \frac{1}{F(\kappa k)} &\propto (1 - \kappa^{-2\alpha_F})(k^2)^{-\alpha_F} = g_0^2 N_c \int \frac{d^4 q}{(2\pi)^4} \left(\frac{F(q^2)}{q^2} \left(\frac{(k \cdot q)^2}{k^2} - q^2 \right) \times \right. \\ &\quad \left. \times \left[\frac{G((q-k)^2) H_1(q, k)}{((q-k)^2)^2} - \frac{G((q-\kappa k)^2) H_1(q, \kappa k)}{((q-\kappa k)^2)^2} \right] \right). \end{aligned} \quad (4.25)$$

This integral equation, as well as the initial equation (4.21), is written in terms of bare Green functions, and the integral may contain ultraviolet divergences. It can be cast into a well-defined renormalised form by multiplying (in (1.38)) $G^{(2)}$ (resp. $F^{(2)}$) by Z_3^{-1} (resp. \tilde{Z}_3^{-1}) and the bare coupling g_0^2 by $Z_g^{-2} = Z_3 \tilde{Z}_3^2$, and finally multiplying the k^2 term by \tilde{Z}_3 . However, in the subtracted equation (4.25) all ultraviolet divergences are cancelled, as well as the $\tilde{Z}_3 k^2$ term. Thus the subtracted Schwinger-Dyson equation holds both in terms of bare and renormalised Green functions without any explicit renormalisation factors.

We now make the hypothesis that there exists a scale q_0 below which the power-law parametrisation is valid

$$G(q^2) \sim (q^2)^{\alpha_G}, \quad F(q^2) \sim (q^2)^{\alpha_F}, \quad \text{for } q^2 \leq q_0^2. \quad (4.26)$$

The equation (4.24) suggests that if *both* functions $H_{1,2}$ are non-singular then one

can suppose $H_1(q, k) \simeq 1$ in (4.25), and (4.20) is straightforward by a dimensional analysis. However, we have a priori no reason to think that the scalar functions $H_1(q, k)$ and $H_2(q, k)$ are *separately* non-singular for all q, k . Writing for example ¹

$$H_1(q, k) \sim (q^2)^{\alpha_\Gamma} h_1 \left(\frac{q \cdot k}{q^2}, \frac{k^2}{q^2} \right), \quad (4.27)$$

with a non-singular function h_1 , we keep all the generality of the argument admitting a singular behaviour of the scalar factor $H_1(q, k)$. Doing the dimensional analysis of the equation (4.25) *without* putting $H_1(q, k) \simeq 1$, we obtain that the relation (4.20) is satisfied if and only if the following triple condition is verified [60] :

$$2\alpha_F + \alpha_G = 0 \quad \longleftrightarrow \quad \begin{cases} \alpha_F \neq 0 \\ \alpha_\Gamma = 0 \\ \alpha_F + \alpha_G < 1 \end{cases} \quad (4.28)$$

All possible cases and limits obtained from the integral convergence conditions are given in Table 4.2. As we shall see the case 2 is excluded by lattice simulations. The case 4 is particularly interesting, it corresponds to the situation when the power-law infrared behaviour of the ghost propagator is the same as in the free case, and no relation between the infrared exponents follows from the Schwinger - Dyson equation. We shall return to this the discussion of this case in the section 4.5.

case	1	2	3	4
	$\alpha_F \neq 0$ $\alpha_F + \alpha_G + \alpha_\Gamma < 1$	$\alpha_F \neq 0$ $\alpha_F + \alpha_G + \alpha_\Gamma \geq 1$	$\alpha_F = 0$ $\alpha_G + \alpha_\Gamma < 1$	$\alpha_F = 0$ $\alpha_G + \alpha_\Gamma \geq 1$
IR convergence conditions	$\alpha_F + \alpha_\Gamma > -2$ $\alpha_G + \alpha_\Gamma > -1$	$\alpha_F + \alpha_\Gamma > -2$ $\alpha_G + \alpha_\Gamma > -1$	$\alpha_\Gamma > -2$ $\alpha_G + \alpha_\Gamma > -1$	$\alpha_\Gamma > -2$ $\alpha_G + \alpha_\Gamma > -1$
SD constraints	$2\alpha_F + \alpha_G + \alpha_\Gamma = 0$	$\alpha_F = -1$	excluded	none

TAB. 4.2 – Summary of the various cases regarding the α coefficients

The first and the last conditions (4.28) are compatible with limits coming from the analysis of the Slavnov-Taylor identity (4.8), and are also consistent with lattice simulations (see section 4.5, [60]). If one of the conditions (4.28) is not verified then, according to the Table 4.2, (4.20) should be replaced by

$$2\alpha_F + \alpha_G + \alpha_\Gamma = 0. \quad (4.29)$$

In the following section we present the results of a numerical test of the relation (4.20), and thus we probe the validity of the condition on α_Γ .

One remark regarding the power-law parametrisation is in order. Suppose for the moment that this parametrisation is exact below the scale q_0 defined in (4.26). Then one can differentiate (4.25) n times with respect to κ , keeping q, k finite. We

¹In fact there are many possible parametrisation. We choose (4.27) in order to illustrate the argument that follows.

obtain

$$\left(k^2\right)^{-2\alpha_F} (-2\alpha_F) \cdot \dots \cdot (-2\alpha_F - n) \kappa^{-2\alpha_F - n} \propto \int d^4q \frac{d^n}{d^n \kappa} \left(\frac{G((q - \kappa k)^2) H_1(q, \kappa k)}{((q - \kappa k)^2)^2} \right). \quad (4.30)$$

The r.h.s of the last equation is not equal to zero for finite k , and thus one immediately has

$$\alpha_F \neq -\frac{n}{2}, \quad n = 1, 2, \dots \quad (4.31)$$

Thus any half-integer predictions for α_F should be considered as an indication of incompleteness of the power-law parametrisation (4.1).

4.4 Lattice study of the ghost Schwinger-Dyson equation

4.4.1 Complete ghost Schwinger-Dyson equation in the lattice formulation

In order to derive the discretized version of the ghost Schwinger-Dyson equation we repeat the same steps as in the continuum case (1.32 - 1.36) but for the lattice version of the Faddeev-Popov operator (1.68). We define the covariant Laplacian

$$\Delta_U^{ab} = \sum_\mu \left(G_\mu^{ab}(x) \left(\delta_{x,y} - \delta_{y,x+e_\mu} \right) - G_\mu^{ab}(x - e_\mu) \left(\delta_{y,x-e_\mu} - \delta_{y,x} \right) \right). \quad (4.32)$$

The appearance of Δ_U in (1.68) is due to the appropriate discretisation of the usual Laplacian operator Δ , dictated by the non-locality of derivatives in the lattice formulation, i.e. replacement of the ∇ operator by its covariant version.

Multiplying (1.68) by $F^{(2)}(x, y)$ from the right, one obtains

$$\begin{aligned} & \frac{1}{N_c^2 - 1} \Delta_U^{ab}(y, z) F_{1\text{conf}}^{(2)ba}(U; z, x) = \delta_{y,x} - \\ & - \frac{f^{abc}}{2(N_c^2 - 1)} \left[A_\mu^c(y) F_{1\text{conf}}^{(2)ba}(U; y + e_\mu, x) - A_\mu^c(y - e_\mu) F_{1\text{conf}}^{(2)ba}(U; y - e_\mu, x) \right]. \end{aligned} \quad (4.33)$$

This is an exact mathematical identity for each gauge configuration U , and thus the consequences that can be derived from this relation are free of any ambiguity originating from the presence of Gribov copies. Performing an averaging $\langle \bullet \rangle$ over the configurations U one gets

$$\begin{aligned} & \frac{1}{N_c^2 - 1} \text{Tr} \left\langle \Delta_U(y, z) F_{1\text{conf}}^{(2)}(z, x) \right\rangle = \delta_{y,x} - \\ & - \frac{f^{abc}}{2(N_c^2 - 1)} \left\langle A_\mu^c(y) F_{1\text{conf}}^{(2)ba}(U, y + e_\mu, x) - A_\mu^c(y - e_\mu) F_{1\text{conf}}^{(2)ba}(U, y - e_\mu, x) \right\rangle \end{aligned} \quad (4.34)$$

This averaging procedure depends on the way chosen to treat the Gribov problem : the particular set of configurations over which it is performed depends on the pres-

cription which is adopted (fc/bc procedures on the lattice, restriction to the fundamental modular region ; see the subsection 2.4.2 for details). Consequently, the Green functions may vary but they must in any case satisfy the above equation, even when the volume of the lattice is finite.

Like in the continuum case, we perform a Fourier transform and obtain :

$$\frac{1}{N_c^2 - 1} \text{Tr} \sum_x e^{ip \cdot x} \left\langle \Delta_U(0, z) F_{1\text{conf}}^{(2)}(U, z, x) \right\rangle = 1 - i \sin(p_\mu) \frac{f^{abc}}{(N_c^2 - 1)} \left\langle A_\mu^c(0) \tilde{F}_{1\text{conf}}^{(2)ba}(U, p) \right\rangle \quad (4.35)$$

Although the equations (4.33) and (4.34) have to be exactly verified by lattice data, the relation (4.35) does only approximately (within statistical errors) since it relies on translational invariance, which could be guaranteed only if we used an infinite number of Monte-Carlo configurations.

The presence of Δ_U in the last equation is due to non-zero lattice spacing effects. Indeed, lattice perturbation theory possesses an infinite number of ghost-gluon vertices depending on the lattice spacing a , giving tadpole contributions like the one presented at the Figure 4.1. Such tadpole contributions may be estimated by a mean

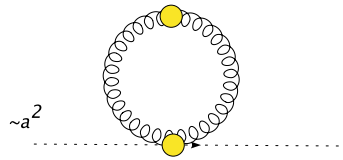


FIG. 4.1 – Example of the terms in the Schwinger-Dyson equation on the lattice.

field method [61]. Using the average plaquette $\langle P \rangle$ (for $\beta = 6.0$ $\langle P \rangle \simeq 0.5937$) one predicts a tadpole correction factor $\propto \langle P \rangle^{-(1/4)} \simeq 1.14$. These terms disappear in the continuum limit, but they do so only very slowly : the tadpole corrections (1 - plaquette) vanish only as an inverse logarithm with the lattice spacing. This is to be contrasted with the corrections arising in the r.h.s which are expected to be of order a^2 . Our lattice calculation [60] gives

$$\Delta_U \simeq \Delta / (1.16 \pm 0.01), \quad (4.36)$$

almost independently of the momentum. This is in good agreement with the correction factor 1.14 quoted above.

We see from Figure 4.2 that the lattice Green functions match pretty well the SD equation (4.35) in both the ultraviolet and infrared regions. Lattice propagators were successfully checked by the perturbation theory at large momentum, and they satisfy the ghost Schwinger-Dyson equation. This means that lattice approach gives consistent results also in the infrared.

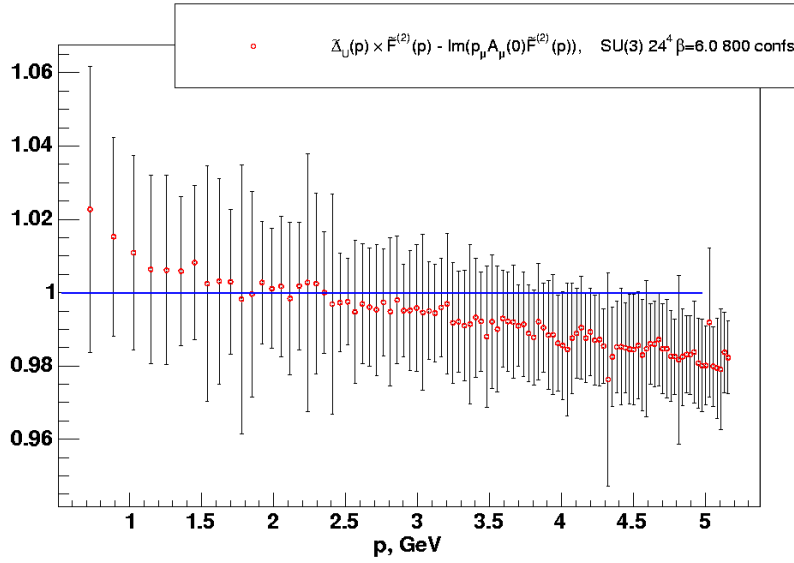


FIG. 4.2 – Checking that lattice Green functions satisfy the ghost SD equation (4.35). We plot $\frac{1}{1.16} \tilde{F}(p^2) - 80 \frac{p_\mu}{N_c^2 - 1} f^{abc} \langle A_\mu^c(0) \tilde{F}_{1conf}^{(2)ba}(\mathcal{A}, p) \rangle$ compared to 1.

4.4.2 Checking the validity of the tree-level approximation for the ghost-gluon vertex

The simplest approximation (used by many authors, see section 4.1) of the ghost Schwinger - Dyson equation (4.21) corresponds to the case

$$H_1(q, k) = 1 \quad \forall q, k, \quad (4.37)$$

an approximation motivated by the non-renormalisation theorem (4.24) valid for the sum $H_1(q, k) + H_2(q, k)$ when $k = 0$. This gives

$$\frac{1}{F(k)} = 1 + \frac{g_0^2 N_c}{k^2} \int \frac{d^4 q}{(2\pi)^4} \left(\frac{F(q^2) G((k-q)^2)}{q^2 (k-q)^2} \frac{(k \cdot q)^2 - k^2 q^2}{(q-k)^2} \cdot 1 \right). \quad (4.38)$$

Strictly speaking this equation, written in this way, is meaningless since it involves UV-divergent quantities. However it is well defined at fixed ultraviolet cut-off.

We want to check whether lattice propagators satisfy it. According to perturbation theory, it should be approximately true at large k . Lattice propagators are discrete functions of momentum and thus one has to handle the problem of the numerical evaluation of the loop integral I in (4.38). Let us express the integrand solely in terms of q^2 and $(k-q)^2$

$$I = \int \frac{d^4 q}{(2\pi)^4} \frac{F^2(q) G(k-q)}{q^2 (k-q)^2} \left[\frac{(k-q)^2}{4} + \frac{(k^2)^2 + (q^2)^2 - 2k^2 q^2}{4(k-q)^2} - \frac{q^2 + k^2}{2} \right]. \quad (4.39)$$

Then we write

$$I = I_1 + I_2 + I_3 + I_4 + I_5 + I_6, \quad (4.40)$$

each I_i corresponds to one term in (4.39). All these integrals have the form

$$I_i = C_i(k) \int \frac{d^4q}{(2\pi)^4} f_i(q) h_i(k - q). \quad (4.41)$$

The convolution in the r.h.s. is just the Fourier transform of the product at the same point in configuration space :

$$\int \frac{d^4q}{(2\pi)^4} f_i(q) h_i(k - q) = F_+ \left(F_-(f_i)[x] F_-(h_i)[x] \right) (k), \quad (4.42)$$

where $F_-(\hat{f})(x)$ is an inverse and $F_+(f)(k)$ a direct Fourier transform. Thus, in order to calculate the integral I from discrete lattice propagators one proceeds as follows :

1. calculate $\{f_i\}(p)$ and $\{h_i\}(p)$ as functions of $F(p), G(p), p^2$ for all i
2. apply the inverse Fourier transform F_- to all these functions and get $f_i(x)$ and $h_i(x)$
3. compute the product at the same point $f_i(x) \cdot h_i(x)$
4. apply the direct Fourier transform F_+ to $f_i(x) \cdot h_i(x)$

The integrands in (4.39) depend only on the squared norms q^2 and $(k - q)^2$, and thus the angular part may be integrated out, giving the four-dimensional Hankel transformation

$$\begin{aligned} \widehat{f(|x|)}[p] &= \frac{1}{|p|} \int_0^\infty J_1(|p|r) r^2 f(r) dr \\ f(r) &= \frac{1}{(2\pi)^2} \frac{1}{r} \int_0^\infty J_1(\rho r) \rho^2 \widehat{f(|x|)}[\rho] d\rho. \end{aligned} \quad (4.43)$$

These integrals are evaluated numerically by means of the Riemann sum

$$f(r) = (2\pi)^{-2} |r|^{-1} \sum_{i=1}^N J_1(r\rho_i) \rho_i^2 \frac{\hat{f}[\rho_i] + \hat{f}[\rho_{i-1}]}{2} (\rho_i - \rho_{i-1}), \quad \rho_0 = 0, \quad (4.44)$$

where N is the number of data points. The inverse transformation is done in the similar way. In practice, because of the lattice artifacts (see subsection 2.3.2) which become important at large ρ the summation has to be restricted to $\rho < \rho_{max} \simeq 2.2$ instead of the maximal value 2π .

Now we are ready to check the approximate equation (4.38) on the lattice. We still have to face the same problem we have already encountered in the previous subsection, namely that the lattice Faddeev-Popov operator involves the non trivial discretisation Δ_U of the Laplacian operator. This is taken into account by means of the substitution of $\widetilde{\Delta_U}(p^2)/p^2$ to the “1” term in the l.h.s of equation (4.38) We present on Figure 4.3 the result of the numerical integration described above. We have chosen for this purpose the data set from the simulation with the gauge group $SU(3)$ at $\beta = 6.4, V = 32^4, a^{-1} \approx 3.6$ GeV. One sees that the equality is achieved at large momenta, but in the infrared the naive approximation of the ghost Schwinger-Dyson equation fails. The errors on Figure 4.3 include statistical Monte-Carlo errors

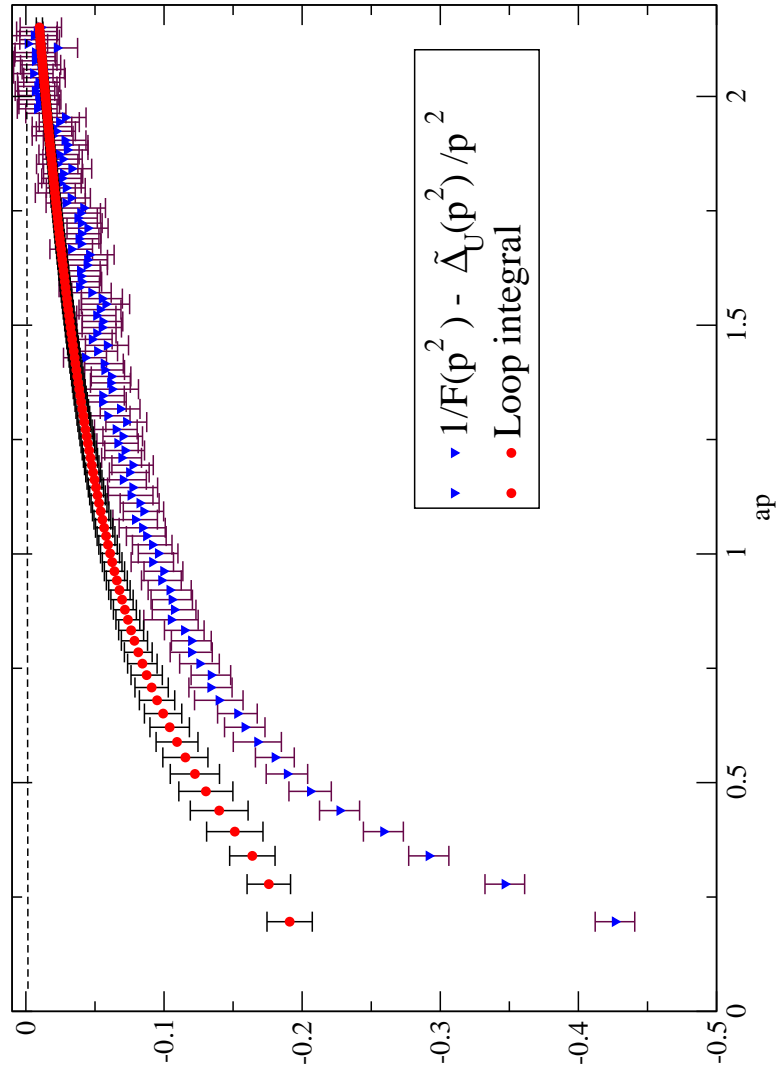


FIG. 4.3 – Checking whether lattice Green functions satisfy the ghost SD equation (4.21) with an assumption $H_1(q, k) = 1$. The upper line (circles) correspond to the loop integral in (4.21), and the down line (triangles) corresponds to $1/F(p^2) - 1$. In this plot $a^{-1} \approx 3.6$ GeV.

for $F(q^2)$ and $G(q^2)$ and the bias coming from the UV cut-off of the integral I .

We see that at small momenta (below ≈ 3 GeV) the ghost Schwinger-Dyson equation with the assumption $H_1(q, k) = 1$ is not satisfied. However, it is quite difficult to establish whether this disagreement is due to the infrared or ultraviolet dependencies of $H_1(q, k)$. To check this one has to know $H_1(q, k)$ for all values of q, k . Unfortunately this information is not available. Thus the main conclusion of the present subsection is that the scalar function $H_1(q, k)$ plays an important role in the infrared gluodynamics, and it cannot be set to one.

4.5 Direct fits of infrared exponents

We have seen in the previous section that lattice simulations give consistent results for the Green functions at all momenta. Another interesting feature that we have established is the important role of the scalar factor $H_1(q, k)$ coming from the complete ghost-gluon vertex (4.22). In this section we present numerical results allowing to check the relation (4.20). After this we present our results for direct fits of the exponents α_F and α_G , and compare them to the results of other lattice collaborations.

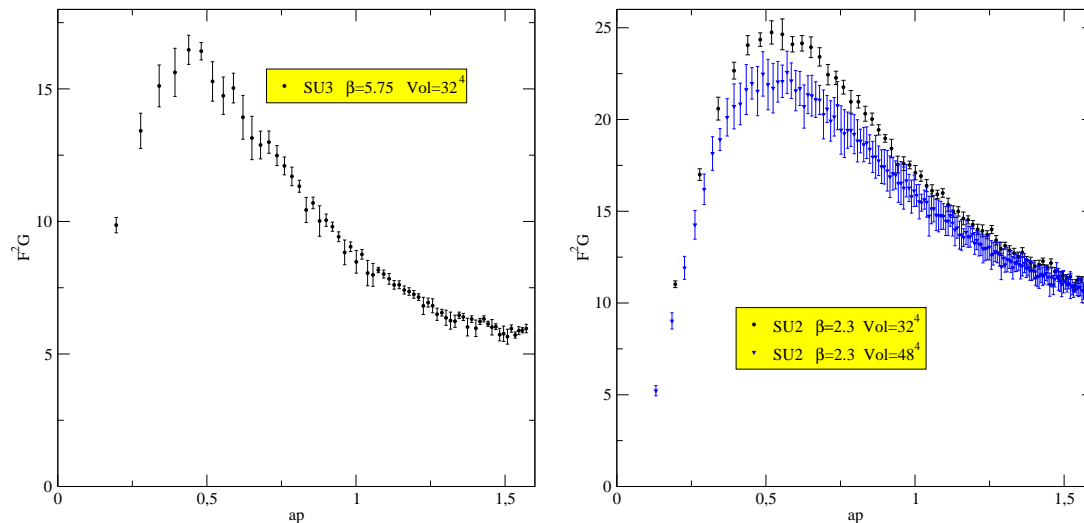


FIG. 4.4 – Direct test of the relation $2\alpha_F + \alpha_G = 0$. If the last is true $F^2 G$ has to be constant in the infrared. We see that it is clearly not the case. In these plots $a^{-1} \approx 1.2$ GeV, so the peak is located at ≈ 600 MeV.

4.5.1 Testing the relation $2\alpha_F + \alpha_G = 0$.

In order to test the relation (4.20) we plot at Figure 4.4 the quantity $F^2(p^2)G(p^2)$. If all the conditions (4.28) are satisfied this quantity should be constant in the infrared (or slightly varying). We see from Figure 4.4 that in the infrared (below ≈ 600 MeV) the quantity $F^2 G$ is not constant, and thus one of the conditions (4.28) is not verified. We have seen that the conditions $\alpha_F \neq 0$ and $\alpha_F + \alpha_G < 1$ are consistent with the limits (4.8) from the Slavnov-Taylor identity (4.7). We have also seen (cf. Figures 4.2 and 4.3) that neglecting the momentum dependence of the vertex is not possible in the infrared, because in this case the ghost Schwinger-Dyson equation is no longer satisfied by lattice propagators. Thus the only possibility is to admit that $H_1(q, k)$ plays an important role, and that the relation (4.20) is not verified. If $\alpha_F \neq 0$ then the modified form (4.29) that takes in account the singularity of $H_1(q, k)$ should be considered (according to Fig.4.3), with $\alpha_F < 0$ in our parametrisation. This singularity is probably related to the non-perturbative power corrections to the vertex discussed in the subsection 3.2.3.

Another reason to think that the relation (4.20) is not exact is the dependence of α_F and α_G on the choice of the Gribov copy. We have seen in the section 2.4 that the

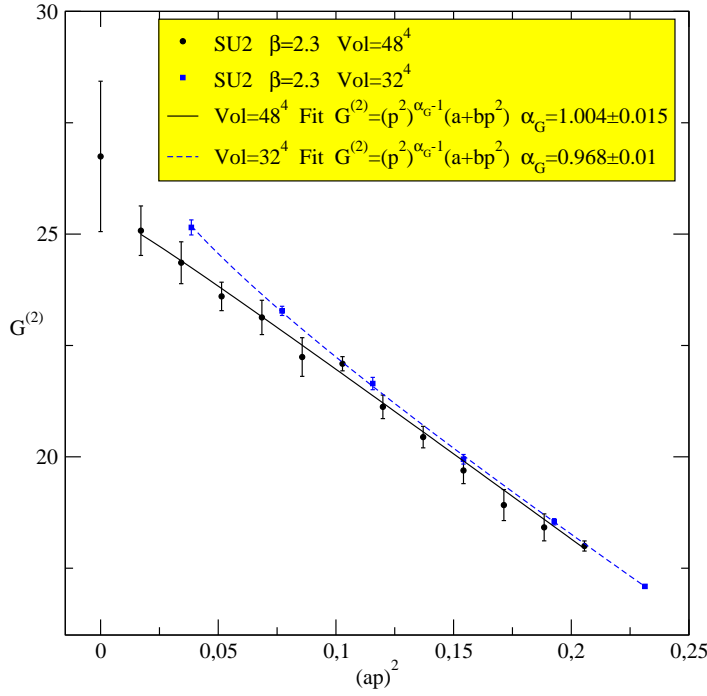


FIG. 4.5 – $G^{(2)}(p^2)$ from lattice simulation for $SU(2)$ (left). $\beta_{SU(2)} = 2.3$ and $\beta_{SU(3)} = 5.75$. The volumes are 32^4 and 48^4 for $SU(2)$. In these plots $a^{-1} \approx 1.2$ GeV.

low-momentum dependence of the gluon propagator is not sensitive to the bc/fc choice while the infrared behaviour of the ghost propagator depends on it. But the Schwinger - Dyson equation for the ghost propagator is independent of the choice of the copy, because it is valid exactly for every gauge configuration, even on a finite lattice (see equations (1.36) and (4.34)). Hence if there is a relation between the infrared exponents α_F and α_G resulting from the ghost Schwinger - Dyson equation then it could not depend on the choice of the copy. Thus it is not possible to have a relation with α_F and α_G alone. This above argument is not directly applicable in the case $\alpha_F = 0$.

According to the analysis performed in the section 4.3, and given (see next subsection) that the case 2 of the Table 4.2 is excluded by lattice simulations the following explanations of the non-validity of the relation $2\alpha_F + \alpha_G = 0$ are possible :

1. The ghost-gluon vertex contains scalar factors that are singular in the infrared, i.e. $\alpha_\Gamma \neq 0$ in the equation 4.27.
2. The case 4 of the Table 4.2 is realised [62] and hence there exists *no* relation between the infrared exponents. Let us recall that in the above case one has $\alpha_F = 0$ and $\alpha_G + \alpha_\Gamma \geq 1$. If the ghost-gluon vertex is regular in the infrared then one has

$$\begin{cases} \alpha_F = 0 \\ \alpha_G \geq 1. \end{cases} \quad (4.45)$$

4.5.2 Lattice fits for α_F and α_G .

Let us now discuss the direct fits for the infrared exponents α_G and α_F . The examples of such fits of lattice data are presented on Figure 4.5. The errors are quite large, leading to an instability in the fit results. That is why we fit both propagators in the infrared to the formula

$$(q^2)^\alpha (\lambda + \mu q^2) \quad (4.46)$$

where we added an additional term of the form μq^2 in order to describe a situation like the one at Figure 4.5(left) where $G^{(2)}(p^2)$ seems to go to a finite limit when p goes to zero. The obtained values for $\alpha_{F,G}$ are summarised in Table 4.3. For $SU(2)$

Group	Volume	β	α_G	α_F
$SU(2)$	48^4	2.3	1.004(15)	-0.087(15)
$SU(2)$	32^4	2.3	0.968(11)	-0.109(14)

TAB. 4.3 – Summary of the fit results for the F and G functions

and the larger lattice volume the value obtained for α_G is compatible with 1. We also take into account our experience from previous studies of the gluon propagator where we have always observed that the gluon propagator goes continuously to a finite limit in the infrared region (see Figure 4.6). However, the fits are quite instable,

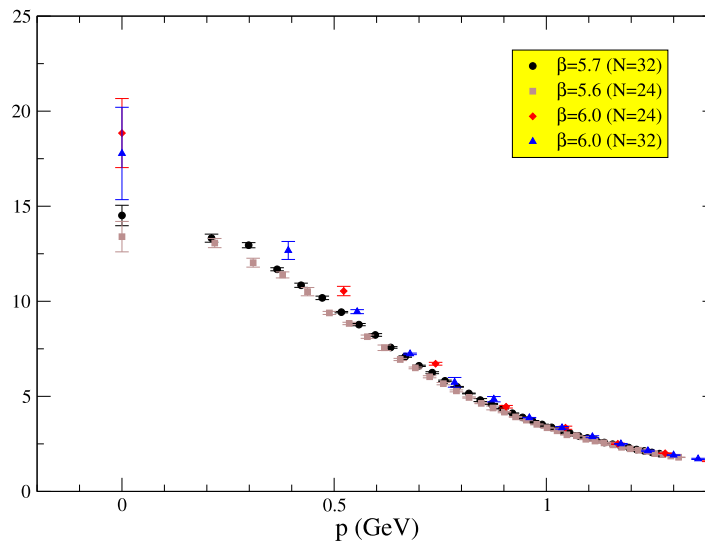


FIG. 4.6 – The continuity of the lattice gluon propagator in the infrared.

and depend a lot on the choice of the fit formula that can considerably change the result. The main problem is the lack of data points at low momenta.

Regarding the gluon propagator another strategy may be taken. It consists in extrapolating the available data to the infinite volume limit. A very detailed study of the gluon dressing function and specially of its volume dependence at $k = 0$ has

already been performed in [63]. This study shows that a value $\alpha_G = 1$ is compatible with the data (the dressing function shows no signal of discontinuity in the neighbourhood of zero) and that no pathology shows up as the volume goes to infinity. Let us compare all available lattice results for the point $G^{(2)}(0)$ and check whether there is an agreement between the data. Following [63] we renormalise the gluon propagator in the MOM scheme at 4 GeV and use the suggested extrapolation formula

$$G_R^{(2)}(0, \mu = 4 \text{ GeV}) = G_{R\infty}^{(2)}(0, \mu = 4 \text{ GeV}) + \frac{c}{V}. \quad (4.47)$$

We compare the results of [63],[64] and our data from the Table 4.4. The results for the fit parameters $G_{R\infty}^{(2)}(0)$ and c are presented in the Table 4.5. We are aware that not

β	V in units of a	bare propagator $G^{(2)}(p)$	$1/aL$ in GeV
5.7	16^4	16.81 ± 0.13	0.0672
5.7	24^4	15.06 ± 0.29	0.0448
5.8	16^4	19.12 ± 0.16	0.0841
5.9	24^4	18.12 ± 0.30	0.0685
6.0	32^4	17.70 ± 0.59	0.0615
6.0	24^4	19.67 ± 0.35	0.0821

TAB. 4.4 – Physical lattice sizes and raw data for the gluon propagator at zero momentum $G^{(2)}(p)$ from our old data.

reference	$G_R^{(2)}(0, \mu = 4 \text{ GeV})$ in GeV^{-2}	c in $\text{GeV}^{-2} \text{ fm}^4$	max vol in fm^4
[63]	7.95 ± 0.13	245 ± 22	2000
Table 4.4	9.1 ± 0.3	140 ± 50	90
[64]	10.9 – 11.3	47 – 65	110s

TAB. 4.5 – Summary of the infinite volume zero momentum propagator and its slope in terms of $1/V$ for three different simulations. The largest volume used in the fit is also indicated. The statistical error is not quoted in [64].

all systematic errors are taken into account : $O(a)$ effects, effect due to different lattice shape, insufficiently large volumes (for the second and third lines), uncertainty in the estimate of the lattice spacing in physical units, etc. However, it seems that not only there is a clear indication in favour of a finite non vanishing zero momentum gluon propagator, but that different lattice collaborations agree on the value. Of course a more extensive study is necessary to check this statement. The other free parameter of the fit - the slope c - is clearly different, but still all the values are in agreement in the order of magnitude.

We conclude [65] thus that all available numerical results point towards a finite non-vanishing and zero momentum renormalised lattice gluon propagator in the infinite volume limit. This suggests that $\alpha_G = 1$. An additional study at much larger lattices is needed to get a reliable result for this infrared exponent.

This last result is in conflict with the limits found from the study of the Slavnov - Taylor identity (4.8), and contradicts the Zwanzigers's prediction that the gluon

propagator is infrared suppressed. However, it is very close to the results presented in [55].

Let us finally discuss the gauge-dependence of the parameter α_G . This is still an open question. However, the results of works [66],[67] suggest that the value of α_G does not change drastically (see Figure 4.8) when changing the gauge parameter ξ . This question deserves a separate study.

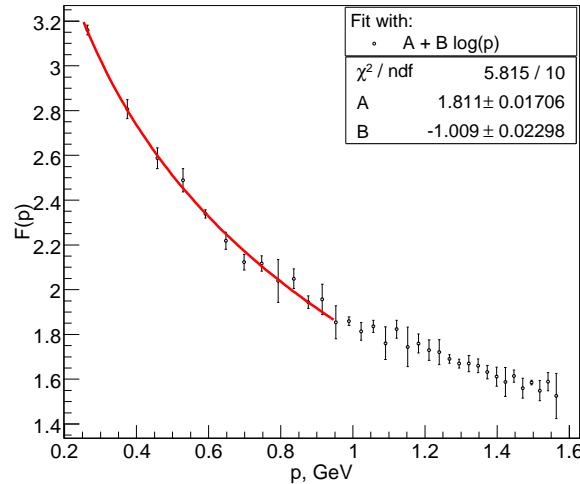


FIG. 4.7 – The fit of the ghost scalar factor $F(p)$ to the formula $A + B \log p$. It suggests that the infrared divergence of $F(p)$ is very slow. Hence α_F is close to zero [62]. The simulations were performed on a $V = 32^4$ lattice at $\beta = 5.8$. The Landau gauge was fixed using the f.c. choice for the Gribov copies.

To finish this chapter, let us summarise the lattice results. We have found that α_F is very close to 0 (see Figure 4.7), α_G is close to 1 and the widely used relation $2\alpha_F + \alpha_G = 0$ is not true. Going back to the possibilities given in the Table 4.2 we find that the cases 2 and 3 are not realised. We are left with the cases 1 and 4, and for the moment lattice simulations cannot say which possibility is true. However, all numerical results are better explained by the possibility (4.45) corresponding to the case 4 of the Table 4.2 supplied with an hypothesis of the regularity of the scalar factors entering the ghost-gluon vertex. We recall that in this case one has :

$$\left\{ \begin{array}{l} \alpha_F = 0 \\ \alpha_G \geq 1. \\ \text{no relation between } \alpha_F \text{ and } \alpha_G \text{ follows from the ghost SD equation.} \end{array} \right. \quad (4.48)$$

Note that it is still in conflict with the constraints coming from the Slavnov - Taylor identity (4.8). Thus the essential question today is to understand whether $\alpha_F = 0$ or not [62]. And, of course, a study on larger lattices is necessary to perform better fits of the infrared exponents.

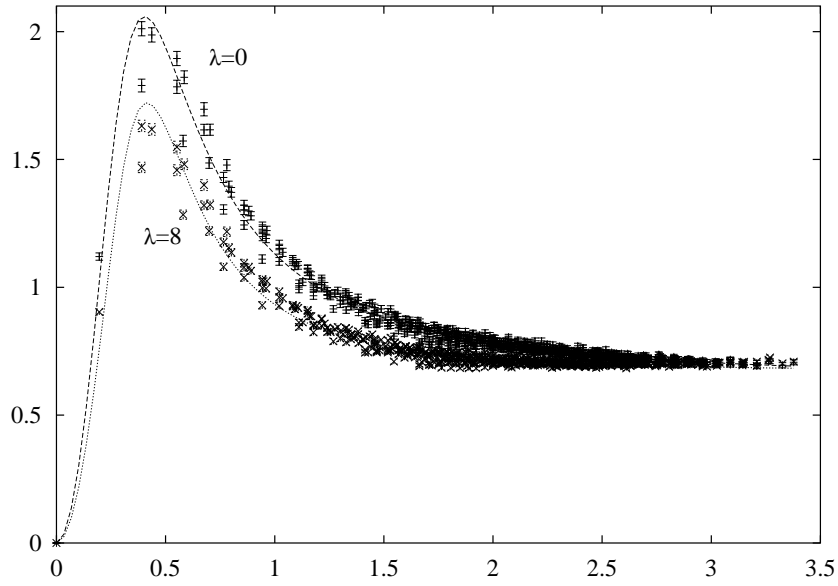


FIG. 4.8 – Transverse part of the gluon propagator $p^2 G^{(2)}(p)$ in covariant gauges as a function of p . The two sets of data refer to $(\xi = \lambda)$ $\xi = 0$ (Landau gauge) and $\xi = 8$, 221 thermalized $SU(3)$ configurations at $\beta = 6.0$ with a volume $V \times T = 16^3 \times 32$. Extracted from [66].

Chapitre 5

Conclusions

In this chapter we discuss the conclusions of the present dissertation. Lattice simulations is a great tool to study the non-perturbative effects in QCD. The main goal of this dissertation is to exhibit how these effects influence the momentum behaviour of different Green functions in Landau gauge. Our hope is that the knowledge of the change in momentum behaviour at low momenta can help in the understanding of one of the most difficult puzzles of QCD - the mechanism of confinement.

In the chapter 3 the large momentum behaviour of the ghost and the gluon propagator of a pure Yang-Mills theory in Landau gauge is investigated. The main parameter under study is the scale Λ_{QCD} . We show that the values of Λ_{QCD} fitted from the ghost and the gluon propagator are consistent. However, the available momentum range (from ≈ 2 to ≈ 6.5 GeV) is situated in the zone where non-perturbative effects cannot be neglected. So at first glance the agreement between Λ_{QCD} extracted from different Green function may seem strange. An explanation of this fact comes from the OPE analysis allowing to estimate the influence of dominant non-perturbative power corrections. We found that these corrections are the same in the case of the ghost and gluon propagators, that is why the values of Λ_{QCD} are compatible. According to the OPE calculation, the value of Λ_{QCD} that is extracted from the propagators is modified by the non-perturbative effects. We used the fact that the equivalence of the leading power corrections implies that their ratio is free of power corrections at the considered order. Thus the ratio of the ghost and gluon propagators is a quantity which is better described by perturbation theory in the considered energy interval than the propagators themselves. Indeed, our analysis of the lattice data showed that the fit of the ratio gives a smaller value for Λ_{QCD} (≈ 270 MeV in the $\overline{\text{MS}}$ renormalisation scheme) compared to the value obtained from the separate fits of the propagators ($\Lambda_{\overline{\text{MS}}} \approx 330$ MeV). Both fits are performed on the same data samples. This speaks in favour of a presence of non-perturbative power corrections in the interval $[2 \text{ GeV}, 6.5 \text{ GeV}]$, in agreement with the OPE predictions and the results of previous investigations.

One can use the Slavnov - Taylor identities in order to find other relations between the Wilson coefficients in different Green functions. For example we found that the dominant $\propto \frac{1}{p^2}$ power corrections are the same in the case of the three gluon vertex and the ghost-gluon vertex in asymmetric kinematic configurations (with the

gluon momentum set to zero). We have also shown that the power correction to the ghost-gluon vertex with vanishing momentum of the entering ghost is equal to zero (in Landau gauge). However, this is not true if the momentum of the entering ghost is not *exactly* equal to zero. In this case the vertex has an $\propto \frac{1}{p^2}$ power correction that becomes quite important at low momenta.

As a partial conclusion we stress the attention of the reader on the fact that lattice simulations are very successful in describing the Green functions at large momentum, the results are consistent with the predictions of perturbation theory, completed with the OPE calculation of the power corrections, up to NNNLO.

In the chapter 4 we turn to the study of very low momentum behaviour (of order and below Λ_{QCD}) of the Green functions. One of the very interesting puzzles in the infrared is the problem of the Gribov ambiguity. The lattice method has an advantage to explicitly perform the Gribov quantisation. However, the gauge is not fixed in a unique way and there are Gribov copies on the lattice. We showed that the probability to find a secondary Gribov copy possess the property of scaling. This probability increases significantly when the physical volume of the lattice exceeds some critical volume (of around $(2.75/\sqrt{\sigma})^4$ in the case of $SU(2)$ gauge theory). Our conclusion is that in order to study the non-perturbative effects one has to work at lattices with physical volume larger than the critical one that we found.

Our first step in the study of low-momentum behaviour of Green functions is to check that lattice simulations can give reliable results in the infrared. For this purpose we verified (numerically, see Figure 4.2) that lattice Green functions satisfy the complete ghost Schwinger - Dyson equation (1.38) for all considered momenta. These tests allow us to conclude that numerical simulation on the lattice give relevant results not only in the ultraviolet domain, but also in the infrared one.

The quantitative parameters we are interested in are the infrared exponents α_F and α_G describing the power-law deviation (this is a crudest approximation) from free propagators (ghost and gluon respectively) in the deep infrared. Our analysis of the Slavnov-Taylor identity relating the three-gluon vertex, the ghost-gluon vertex and the propagators showed that the power-law infrared divergence of the ghost propagator is unchanged or enhanced in the infrared (compared to the free case), and that the gluon propagator must diverge in the infrared. The latter limit is in conflict with today's lattice results yielding a finite non-zero gluon propagator at zero momentum, and with most present analytical estimations that we quote in the section 4.1, that support a vanishing gluon propagator in the infrared.

Another analytical relation imposing constraints on the infrared exponents is the ghost Schwinger-Dyson equation. We revisited the commonly accepted relation (4.20) between these exponents saying that $2\alpha_F + \alpha_G = 0$. According to our analysis this relation is true only if the ghost-gluon vertex contains no singularity, in none of the scalar functions defining the vertex. Our numerical studies showed that the relation in question is not valid, because F^2G is infrared suppressed, and hence $2\alpha_F + \alpha_G > 0$. This statement is supported by the fact that lattice propagators do not match the reduced Schwinger - Dyson equation (see Figure 4.3), whereas the complete one is perfectly verified, Figure 4.2. There are even more reasons to think that the relation (4.20) is not true. First, we have seen that the non-perturbative ghost-

gluon vertex contains singular contributions from the $\langle A^2 \rangle$ condensate for most kinematic configurations. However, it is difficult to estimate the role of such contributions at very low momenta. Second, we have seen that the infrared behaviour of the ghost and gluon propagator seem to vary differently with the choice of the Gribov copy (bc or fc). We have seen that the form of the complete ghost Schwinger - Dyson equation does not depend on the choice of the Gribov copy. If $\alpha_F \neq 0$ and it depends on the choice of the copy, it is impossible to have an exact relation between α_F and α_G alone, and to satisfy the condition of independence of the choice of the copy.

The direct fit of the propagators in the infrared supports the prediction that the infrared behaviour of the ghost propagator is enhanced in the infrared. But this enhancement is very slight. The gluon propagator is found to be infrared finite. This last result is in conflict with the limit found from the analysis of the Slavnov - Taylor identity. For the moment we have no explanation regarding this disagreement.

Summarising the numerical results, we found that the gluon propagator is finite in the infrared ($\alpha_G \approx 1$), that the infrared divergence of the ghost propagator is almost the same as in the free case ($\alpha_F \approx 0$) and that the commonly accepted relation $2\alpha_F + \alpha_G = 0$ is not true. Going back to the analysis of the ghost Schwinger - Dyson equation (see Table 4.2), two solutions are possible :

1. The infrared exponent of the ghost propagator α_F is *strictly* equal to zero, i.e. the power-law infrared dependence is the same as at large momenta. This implies that *no* relation between α_F and α_G follows from the ghost Schwinger - Dyson equation. If we now suppose that the ghost-gluon vertex contains no (infrared) singular components then all our lattice results are perfectly described.
2. The infrared exponent of the ghost propagator $\alpha_F \neq 0$, then there is a relation between α_F , α_G and α_Γ following from the ghost Schwinger - Dyson equation. The fact that the relation $2\alpha_F + \alpha_G = 0$ is not verified on the lattice suggests that there is a singularity in one of the scalar factors defining the ghost-gluon vertex i.e. $\alpha_\Gamma \neq 0$.

The today's lattice results speak in favour of the first possibility, but calculations at larger lattices are necessary in order to conclude.

Bibliographie

- [1] V. N. Gribov. Quantization of non-abelian gauge theories. *Nucl. Phys.*, B139 :1, 1978.
- [2] Axel Maas. On the spectrum of the Faddeev-Popov operator in topological background fields. 2005, hep-th/0511307.
- [3] M. Semenov-Tyan-Shanskii and V. Franke. All gauge orbits and some Gribov copies encompassed by the Gribov horizon. *Zap. Nauch. Sem. Leningrad. Otdeleniya Matematicheskogo Instituta im. V. A. Steklova, AN SSSR*, vol. 120 :159, 1982. (English translation :New York, Plenum Press 1986).
- [4] Pierre van Baal. More (thoughts on) Gribov copies. *Nucl. Phys.*, B369 :259–275, 1992.
- [5] Daniel Zwanziger. Non-perturbative Faddeev-Popov formula and infrared limit of QCD. *Phys. Rev.*, D69 :016002, 2004, hep-ph/0303028.
- [6] Reinhard Alkofer and Lorenz von Smekal. The infrared behavior of QCD Green's functions : Confinement, dynamical symmetry breaking, and hadrons as relativistic bound states. *Phys. Rept.*, 353 :281, 2001, hep-ph/0007355.
- [7] A. A. Slavnov. Ward identities in gauge theories. *Theor. Math. Phys.*, 10 :99–107, 1972.
- [8] J. C. Taylor. Ward identities and charge renormalization of the Yang-Mills field. *Nucl. Phys.*, B33 :436–444, 1971.
- [9] J. C. Taylor. Gauge theories of weak interactions. Cambridge 1976, 167p.
- [10] C. Bagnuls and C. Bervillier. Exact renormalization group equations : An introductory review. *Phys. Rept.*, 348 :91, 2001, hep-th/0002034.
- [11] Ulrich Ellwanger, Manfred Hirsch, and Axel Weber. The heavy quark potential from Wilson's exact renormalization group. *Eur. Phys. J.*, C1 :563–578, 1998, hep-ph/9606468.
- [12] Kenneth G. Wilson. Confinement of quarks. *Phys. Rev.*, D10 :2445–2459, 1974.
- [13] I. Montvay and G. Munster. Quantum fields on a lattice. Cambridge, UK : Univ. Pr. (1994) 491 p. (Cambridge monographs on mathematical physics).
- [14] J. Smit. Introduction to Quantum Fields on a lattice : A robust mate. *Cambridge Lect. Notes Phys.*, 15 :1–271, 2002.
- [15] K. Osterwalder and E. Seiler. Gauge field theories on the lattice. *Ann. Phys.*, 110 :440, 1978.
- [16] C. Itzykson, Michael E. Peskin, and J. B. Zuber. Roughening of Wilson's surface. *Phys. Lett.*, B95 :259, 1980.

- [17] Stephen L. Adler. Overrelaxation algorithms for lattice field theories. *Phys. Rev.*, D37 :458, 1988.
- [18] A. Y. Lokhov, O. Pene, and C. Roiesnel. Scaling properties of the probability distribution of lattice Gribov copies. 2005, hep-lat/0511049.
- [19] P. Boucaud, J. P. Leroy, J. Micheli, O. Pene, and C. Roiesnel. Lattice calculation of $\alpha(s)$ in momentum scheme. *JHEP*, 10 :017, 1998, hep-ph/9810322.
- [20] B. Alles et al. α_s from the nonperturbatively renormalised lattice three gluon vertex. *Nucl. Phys.*, B502 :325–342, 1997, hep-lat/9605033.
- [21] Ph. Boucaud et al. Large momentum behavior of the ghost propagator in SU(3) lattice gauge theory. *Phys. Rev.*, D72 :114503, 2005, hep-lat/0506031.
- [22] Yousef Saad. Iterative methods for sparse linear systems. PWS Publishing, New York, 1996.
- [23] B. Efron. Bootstrap methods : Another look at the jackknife. *The Annals of Statistics*, 7 :1–26, 1979.
- [24] A. C. Davison and D. V. Hinkley. Bootstrap methods and their applications. *Monographs on Statistics and Applied Probability 57*, Chapman and Hall/CRC, (1994).
- [25] A. Sternbeck, E. M. Ilgenfritz, and M. Mueller-Preussker. Spectral properties of the Landau gauge Faddeev-Popov operator in lattice gluodynamics. *Phys. Rev.*, D73 (2006) 014502, hep-lat/0510109.
- [26] Jacques C. R. Bloch, Attilio Cucchieri, Kurt Langfeld, and Tereza Mendes. Propagators and running coupling from SU(2) lattice gauge theory. *Nucl. Phys.*, B687 :76–100, 2004, hep-lat/0312036.
- [27] J. Fingberg, Urs M. Heller, and F. Karsch. Scaling and asymptotic scaling in the SU(2) gauge theory. *Nucl. Phys.*, B392 :493–517, 1993, hep-lat/9208012.
- [28] Attilio Cucchieri. Gribov copies in the Minimal Landau gauge : The influence on gluon and ghost propagators. *Nucl. Phys.*, B508 :353–370, 1997, hep-lat/9705005.
- [29] T. D. Bakeev, Ernst-Michael Ilgenfritz, V. K. Mitryushkin, and M. Mueller-Preussker. On practical problems to compute the ghost propagator in SU(2) lattice gauge theory. *Phys. Rev.*, D69 :074507, 2004, hep-lat/0311041.
- [30] A. Sternbeck, E. M. Ilgenfritz, M. Muller-Preussker, and A. Schiller. The influence of Gribov copies on the gluon and ghost propagator. *AIP Conf. Proc.*, 756 :284–286, 2005, hep-lat/0412011.
- [31] A. Sternbeck, E. M. Ilgenfritz, M. Muller-Preussker, and A. Schiller. The gluon and ghost propagator and the influence of Gribov copies. *Nucl. Phys. Proc. Suppl.*, 140 :653–655, 2005, hep-lat/0409125.
- [32] P. J. Silva and O. Oliveira. Gribov copies, lattice QCD and the gluon propagator. *Nucl. Phys.*, B690 :177–198, 2004, hep-lat/0403026.
- [33] A. Sternbeck, E. M. Ilgenfritz, M. Mueller-Preussker, and A. Schiller. Towards the infrared limit in SU(3) Landau gauge lattice gluodynamics. *Phys. Rev.*, D72 :014507, 2005, hep-lat/0506007.
- [34] K. G. Chetyrkin and A. Retey. Three-loop three-linear vertices and four-loop mom beta functions in massless QCD. 2000, hep-ph/0007088.

- [35] K. G. Chetyrkin. Four-loop renormalization of QCD : Full set of renormalization constants and anomalous dimensions. *Nucl. Phys.*, B710 :499–510, 2005, hep-ph/0405193.
- [36] T. van Ritbergen, J. A. M. Vermaseren, and S. A. Larin. The four-loop beta function in Quantum chromodynamics. *Phys. Lett.*, B400 :379–384, 1997, hep-ph/9701390.
- [37] P. Boucaud et al. Lattice calculation of $1/p^2$ corrections to α_S and of Λ_{QCD} in the $\widetilde{\text{MOM}}$ scheme. *JHEP*, 04 :006, 2000, hep-ph/0003020.
- [38] P. Boucaud et al. Preliminary calculation of α_S from Green functions with dynamical quarks. *JHEP*, 01 :046, 2002, hep-ph/0107278.
- [39] Kenneth G. Wilson. Nonlagrangian models of current algebra. *Phys. Rev.*, 179 :1499–1512, 1969.
- [40] B. L. Ioffe. Condensates in Quantum chromodynamics. *Phys. Atom. Nucl.*, 66 :30–43, 2003, hep-ph/0207191.
- [41] Martin Lavelle and Michael Oleszczuk. The Operator Product Expansion of the QCD propagators. *Mod. Phys. Lett.*, A7 :3617–3630, 1992.
- [42] Jorg Ahlback, Martin Lavelle, Martin Schaden, and Andreas Streibl. Propagators and four-dimensional condensates in pure QCD. *Phys. Lett.*, B275 :124–128, 1992.
- [43] P. Boucaud et al. Consistent OPE description of gluon two point and three point green function ? *Phys. Lett.*, B493 :315–324, 2000, hep-ph/0008043.
- [44] Ph. Boucaud et al. Testing Landau gauge ope on the lattice with a condensate. *Phys. Rev.*, D63 :114003, 2001, hep-ph/0101302.
- [45] P. Boucaud et al. A transparent expression of the $\langle A^2 \rangle$ -condensate’s renormalization. *Phys. Rev.*, D67 :074027, 2003, hep-ph/0208008.
- [46] Gunnar S. Bali and Klaus Schilling. Running coupling and the lambda parameter from SU(3) lattice simulations. *Phys. Rev.*, D47 :661–672, 1993, hep-lat/9208028.
- [47] William Celmaster and Richard J. Gonsalves. The renormalization prescription dependence of the QCD coupling constant. *Phys. Rev.*, D20 :1420, 1979.
- [48] D. Becirevic et al. Asymptotic scaling of the gluon propagator on the lattice. *Phys. Rev.*, D61 :114508, 2000, hep-ph/9910204.
- [49] Ph. Boucaud et al. Non-perturbative power corrections to ghost and gluon propagators. *JHEP*, 01 :037, 2006, hep-lat/0507005.
- [50] Daniel Zwanziger. Vanishing color magnetization in lattice Landau and Coulomb gauges. *Phys. Lett.*, B257 :168–172, 1991.
- [51] D. Zwanziger. Vanishing of zero momentum lattice gluon propagator and color confinement. *Nucl. Phys.*, B364 :127–161, 1991.
- [52] J. C. R. Bloch. Two-loop improved truncation of the ghost-gluon Dyson-Schwinger equations : Multiplicatively renormalizable propagators and non-perturbative running coupling. *Few Body Syst.*, 33 :111–152, 2003, hep-ph/0303125.

- [53] Lorenz von Smekal, Andreas Hauck, and Reinhard Alkofer. A solution to coupled Dyson-Schwinger equations for gluons and ghosts in Landau gauge. *Ann. Phys.*, 267 :1, 1998, hep-ph/9707327.
- [54] Daniel Zwanziger. Non-perturbative Landau gauge and infrared critical exponents in QCD. *Phys. Rev.*, D65 :094039, 2002, hep-th/0109224.
- [55] A. C. Aguilar and A. A. Natale. A dynamical gluon mass solution in a coupled system of the Schwinger-Dyson equations. *JHEP*, 08 :057, 2004, hep-ph/0408254.
- [56] Junya Kato. Infrared non-perturbative propagators of gluon and ghost via exact renormalization group. 2004, hep-th/0401068.
- [57] Jan M. Pawłowski, Daniel F. Litim, Sergei Nedelko, and Lorenz von Smekal. Infrared behaviour and fixed points in Landau gauge QCD. *Phys. Rev. Lett.*, 93 :152002, 2004, hep-th/0312324.
- [58] Christian S. Fischer and Holger Gies. Renormalization flow of Yang-Mills propagators. *JHEP*, 10 :048, 2004, hep-ph/0408089.
- [59] James S. Ball and Ting-Wai Chiu. Analytic properties of the vertex function in gauge theories. 2. *Phys. Rev.*, D22 :2550, 1980.
- [60] Ph. Boucaud et al. The infrared behaviour of the pure Yang-Mills Green functions. 2005, hep-ph/0507104.
- [61] G. Peter Lepage and Paul B. Mackenzie. On the viability of lattice perturbation theory. *Phys. Rev.*, D48 :2250–2264, 1993, hep-lat/9209022.
- [62] J.P. Leroy A. Le Yaouanc A.Y. Lokhov J. Micheli O. Pene J. Rodriguez-Quintero Ph. Boucaud, Th. Bruntjen. Is the QCD ghost dressing function finite at zero momentum ? *JHEP* 0606, 001 (2006), hep-ph/0604056.
- [63] Frederic D. R. Bonnet, Patrick O. Bowman, Derek B. Leinweber, Anthony G. Williams, and James M. Zanotti. Infinite volume and continuum limits of the Landau-gauge gluon propagator. *Phys. Rev.*, D64 :034501, 2001, hep-lat/0101013.
- [64] Orlando Oliveira and Paulo J. Silva. Finite volume effects in the gluon propagator. *PoS, LAT2005* :287, 2005, hep-lat/0509037.
- [65] Ph. Boucaud et al. Short comment about the lattice gluon propagator at vanishing momentum. 2006, hep-lat/0602006.
- [66] L. Giusti, M. L. Paciello, S. Petrarca, C. Rebbi, and B. Taglienti. Results on the gluon propagator in lattice covariant gauges. *Nucl. Phys. Proc. Suppl.*, 94 :805–808, 2001, hep-lat/0010080.
- [67] L. Giusti, M. L. Paciello, S. Petrarca, B. Taglienti, and N. Tantalo. Quark and gluon propagators in covariant gauges. *Nucl. Phys. Proc. Suppl.*, 106 :995–997, 2002, hep-lat/0110040.